Imperial College London
Department of Mathematics

Sparse spectral methods for integral equations and equilibrium measures

Timon Salar Gutleb

Presented for the degree of Doctor of Philosophy
in Mathematics of the Imperial College London, July 2022

Abstract

In this thesis, we introduce new numerical approaches to two important types of integral equation problems using sparse spectral methods. First, linear as well as nonlinear Volterra integral and integro-differential equations and second, power-law integral equations on d-dimensional balls involved in the solution of equilibrium measure problems.

These methods are based on ultraspherical spectral methods and share key properties and advantages as a result of their joint starting point: By working in appropriately weighted orthogonal Jacobi polynomial bases, we obtain recursively generated banded operators allowing us to obtain high precision solutions at low computational cost.

This thesis consists of three chapters in which the background of the above-mentioned problems and methods are respectively introduced in the context of their mathematical theory and applications, the necessary results to construct the operators and obtain solutions are proved and the method's applicability and efficiency are showcased by comparing them with current state-of-the-art approaches and analytic results where available.

The first chapter gives a general scope introduction to sparse spectral methods using Jacobi polynomials in one and higher dimensions.

The second chapter concerns the numerical solution of Volterra integral equations. The introduced method achieves exponential convergence and works for general kernels, a major advantage over comparable methods which are limited to convolution kernels.

The third chapter introduces an approximately banded method to solve power law kernel equilibrium measures in arbitrary dimensional balls. This choice of domain is suggested by the radial symmetry of the problem and analytic results on the supports of the resulting measures. For our method, we obtain the crucial property of computational cost independent of the dimension of the domain, a major contrast to particle simulations which are the current standard approach to these problems and scale extremely poorly with both the dimension and the number of particles.

Copyright Declaration

Statement of Originality

I hereby confirm that the content of this thesis presented for the award of a PhD degree, including all figures and tables, is the result of my own research and that all external sources have been explicitly cited.

Acknowledgements

I wish to thank Sheehan Olver for introducing me to the expansive world of computational orthogonal polynomials and for his overall excellent supervision. Sheehan was always available to provide insightful comments and feedback, even during the latter half of my project in the midst of a pandemic.

I also wish to thank José A. Carrillo for our productive joint discussions on fractional differential equations and for providing much appreciated guidance through the forest of literature on equilibrium measures and Riesz potentials.

Furthermore, I want to thank Norbert J. Mauser, for setting me on the path of computational mathematics and making it possible for me to participate in the research group at the Wolfgang Pauli Institute at the University of Vienna, as well as collaboration on physics related projects.

I also wish to thank my long-time friends and colleagues Markus Rademacher, Jakob Möller, Peter Allmer and Arkadij Bojko for enjoyable and productive discussions of both my own and their research projects as well as their friendship and Matthew Colbrook with whom I co-organized a number of Cambridge-Imperial seminars for PhD students in computational mathematics which were a personal highlight of my time in London.

I also wish to thank my parents Aida Gutleb and Bernhard Gutleb, my grandparents Bernhardine and Adolf Gutleb as well as my sister Daria Dubičanac and brother-in-law Marko Dubičanac for their immense support and patience throughout all of my studies including this PhD project.

Finally, I want to express my deepest gratitude to Emily Mia Gutleb, my wife and partner throughout this journey, for her gracious support of my ambitions and work.

Contents

List of Tables

List of Figures

Chapter 1

Banded spectral methods

The general notation adopted throughout this thesis will largely follow that of the NIST Digital Library of Mathematical Functions (DLMF) [73]. We provide references for more specialized notation where appropriate.

1.1 Orthogonal polynomials and spectral methods

1.1.1 Introduction

Broadly the label *spectral method* refers to any method used to obtain numerical solutions to mathematical problems which involves the expansion and approximation of functions in simpler basis function spaces. The most widely known representatives of this class of methods make use of Fourier series, in which case the basis functions are the sinusoids appearing in the series representation. Another widely known but numerically significantly less well-behaved approach is the expansion of functions as a Taylor series, in which case the basis functions are simply the monomials $\{1, x, x^2, x^3 ...\}$. The present thesis concerns itself with spectral methods whose basis functions are orthogonal polynomials, specifically Jacobi polynomials. In what follows, we give an overview of the general aspects of approximation theory using orthogonal polynomials as required for the discussion of such spectral methods and give an introduction to sparse computation with Jacobi polynomial bases.

1.1.2 Jacobi polynomial bases

The Jacobi polynomials, named after mathematician Carl Gustav Jacob Jacobi, are a two parameter family of ordered complete sets of classical orthogonal polynomials on the interval $(-1, 1)$, orthogonal with respect to the Jacobi weight

$$w^{(a,b)}(x) = (1-x)^a(1+x)^b,$$

with $a, b > -1$. The n-th degree Jacobi polynomial with basis parameters a and b is typically denoted $P_n^{(a,b)}$ and satisfies the orthogonality condition [73, 18.3]

$$\int_{-1}^{1} (1-x)^a(1+x)^b P_n^{(a,b)}(x) P_m^{(a,b)}(x)\, dx = \frac{2^{a+b+1}\Gamma(n+a+1)\Gamma(n+b+1)}{(2n+a+b+1)\Gamma(n+1)\,\Gamma(n+a+b+1)}\delta_{nm}, \tag{1.1}$$

where δ_{nm} denotes the Kronecker delta and $\Gamma(\cdot)$ the Gamma function, as well as the following second order homogeneous linear differential equation [73, 18.8.1]:

$$\left(1-x^2\right) f''(x) + (b-a-(a+b+2)x) f'(x) + n(n+a+b+1) f(x) = 0.$$

Alongside the above, there are many equivalent ways of defining the Jacobi polynomials – other popular ways include the use of Rodrigues' formula [73, 18.5.1]

$$P_n^{(a,b)}(x) := \frac{(-1)^n}{2^n n!}(1-z)^{-a}(1+z)^{-b}\frac{d^n}{dx^n}\left\{(1-x)^a(1+x)^b\left(1-x^2\right)^n\right\},$$

and the explicit series representation [73, 18.5.7]

$$P_n^{(a,b)}(x) := \frac{\Gamma(a+n+1)}{n!\,\Gamma(a+b+n+1)}\sum_{m=0}^{n}\binom{n}{m}\frac{\Gamma(a+b+n+m+1)}{\Gamma(a+m+1)}\left(\frac{x-1}{2}\right)^m.$$

involving gamma functions $\Gamma(\cdot)$ and binomial coefficients.

The above series representation can easily be seen to be of the form of a finite hypergeometric series, cf. [73, 15.2.2], which allows one to concisely define the Jacobi polynomials using only a Gaussian hypergeometric ${}_2F_1$ function and the Pochhammer symbol (or rising factorial) denoted $(\cdot)_n$ [73, 18.5.7]:

$$P_n^{(a,b)}(x) := \frac{(a+1)_n}{n!}\,{}_2F_1\left(-n, 1+a+b+n, a+1, \frac{1-x}{2}\right). \tag{1.2}$$

This last definition of the Jacobi polynomials will be the most useful to us in this thesis, in particular when discussing equilibrium measures in Chapter 3. We provide additional details on the hypergeometric function and some of its properties in Section 1.4.

As is generally true for orthogonal polynomials, the choice of normalization constants as seen in Equation (1.1) is somewhat arbitrary. Appropriately dividing by these constants yields *orthonormal* Jacobi polynomials, but throughout this thesis we will be working with the canonical (and *not* orthonormal) normalization used in all of the above definitions.

Being orthogonal polynomials the Jacobi polynomials satisfy a characteristic three term recurrence relationship [73, 18.2(iv),18.9.2], specifically

$$P_{n+1}^{(a,b)}(x) = (\kappa_1 x + \kappa_2)P_n^{(a,b)}(x) + \kappa_3 P_{n-1}^{(a,b)}(x), \tag{1.3}$$

with constants independent of x but depending on n, a, b:

$$\begin{aligned}
\kappa_1 &= \frac{(2n+a+b+1)(2n+a+b+2)}{2(n+1)(n+a+b+1)},\\
\kappa_2 &= \frac{(a^2-b^2)(2n+a+b+1)}{2(n+1)(n+a+b+1)(2n+a+b)},\\
\kappa_3 &= -\frac{(n+a)(n+b)(2n+a+b+2)}{(n+1)(n+a+b+1)(2n+a+b)}.
\end{aligned}$$

There are many more recurrence relationships for the Jacobi polynomials which may for example be obtained from their hypergeometric function representation by use of more general contiguous and recurrence relationships for said functions, cf. [73, 18.9]. We now list

a non-exhaustive selection of additional properties with significance in applications including the methods introduced in this thesis.

Sign inversion and parameter exchange 'symmetry' [73, 18.6.1]:

$$P_n^{(a,b)}(-x) = (-1)^n P_n^{(b,a)}(x). \tag{1.4}$$

Endpoint evaluation [73, 18.6.1]:

$$P_n^{(a,b)}(1) = \frac{(a+1)_n}{n!}. \tag{1.5}$$

Indefinite integration [73, 18.17.1]:

$$\int (1-x)^a (1+x)^b P_n^{(a,b)}(x)\mathrm{d}x = -\frac{(1-x)^{a+1}(1+x)^{b+1}}{2n} P_{n-1}^{(a+1,b+1)}(x) + \text{const.} \tag{1.6}$$

Derivative [73, 18.9.15]:

$$\frac{\mathrm{d}}{\mathrm{d}x} P_n^{(a,b)}(x) = \frac{(n+a+b+1)}{2} P_{n-1}^{(a+1,b+1)}(x). \tag{1.7}$$

Weighted derivative [73, 18.9.16]:

$$\frac{\mathrm{d}}{\mathrm{d}x}\left((1-x)^a(1+x)^b P_n^{(a,b)}(x)\right) = -2(n+1)(1-x)^{a-1}(1+x)^{b-1} P_{n+1}^{(a-1,b-1)}(x). \tag{1.8}$$

Lowering the second parameter via weight multiplication [73, 18.9.6]:

$$(n+\tfrac{a}{2}+\tfrac{b}{2}+1)(1+x)P_n^{(a,b+1)}(x) = (n+1)P_{n+1}^{(a,b)}(x) + (n+b+1)P_n^{(a,b)}(x). \tag{1.9}$$

Raising the second parameter [73, 18.9.5]:

$$(2n+a+b+1)P_n^{(a,b)}(x) = (n+a+b+1)P_n^{(a,b+1)}(x) + (n+a)P_{n-1}^{(a,b+1)}(x). \tag{1.10}$$

We refer to the DLMF [73], as well as the formula collections by Prudnikov, Brychkov and Marichev [86, 87] for a vast collection of further relationships and properties.

1.1.3 Shifted Jacobi polynomial bases

The previous section defined the Jacobi polynomials on their canonical domain $(-1, 1)$. In this section we briefly discuss how simple variable transformations allow us to use the Jacobi polynomials on any single interval domain. We also introduce so-called radial or radially shifted Jacobi polynomials which are related but distinct from the shifted polynomials and have applications in ball domains in higher dimensions.

To obtain Jacobi polynomials shifted from $x \in (-1, 1)$ to the interval (l_1, l_2) with arbitrary non-degenerate boundary points

$$l_1 < l_2, \quad l_1, l_2 \in \mathbb{R}$$

one uses the well-known change of variables

$$t = \frac{(l_2 + l_1)}{2} + \frac{(l_2 - l_1)}{2} x. \tag{1.11}$$

The change of variables must be applied consistently, i.e. to the polynomials themselves but also to the weight in order to retain orthogonality on the new domain (l_1, l_2). For the general variable change above, the orthogonality weight on the new interval domain becomes

$$w^{(a,b)}_{(l_1,l_2)}(t) = (l_2 - t)^a (t - l_1)^b . \tag{1.12}$$

We furthermore introduce the notation $\tilde{P}^{(a,b)}_n(x)$ for the shifted Jacobi polynomials to the domain $x \in (0, 1) = (l_1, l_2)$, with orthogonality weight

$$w^{(a,b)}_{(0,1)}(x) = \tilde{w}^{(a,b)}(x) = (1 - x)^a x^b.$$

These polynomials frequently appear in applications to simplify notation, including those we discuss in Chapter 2 for Volterra integral equations.

The radial or radially shifted Jacobi polynomials $\tilde{P}_n^{(a,b)}(r^2) = P_n^{(a,b)}(2r^2 - 1)$ are obtained by means of a quadratic as opposed to linear shift in the variable resulting in a polynomial basis orthogonal on $r \in (0, 1)$. These polynomials are widely used in higher dimensional domains such as disks and balls, where their orthogonality property is natural with respect to the symmetry of the domain. We will discuss the higher dimensional uses of the radial Jacobi polynomials in more detail in Section 1.3.3.

1.1.4 Ultraspherical polynomial bases

The ultraspherical or Gegenbauer polynomials, denoted $\{C_n^{(\lambda)}(x)\}_{n\geqslant 0}$ with $0 \neq \lambda > -\frac{1}{2}$, are a complete set of classical orthogonal polynomials orthogonal on $(-1, 1)$ with respect to the ultraspherical weight

$$w^{(\lambda)}(x) = (1 - x^2)^{\lambda - \frac{1}{2}} = (1 - x)^{\lambda - \frac{1}{2}}(1 + x)^{\lambda - \frac{1}{2}},$$

and thus satisfy the orthogonality condition

$$\int_{-1}^{1} (1 - x^2)^{\lambda - \frac{1}{2}} C_n^{(\lambda)}(x) C_m^{(\lambda)}(x)\, dx = \frac{2^{1-2\lambda}\pi\Gamma(n + 2\lambda)}{\Gamma(n + 1)(n + \lambda)(\Gamma(\lambda))^2}\delta_{nm}.$$

As can be deduced from the form of the ultraspherical weight the ultraspherical polynomials arise out of the Jacobi polynomials $P_n^{(a,b)}$ in the special case when $a = b$, albeit with slightly different normalization. Both the ultraspherical and the Jacobi polynomials may be considered a generalization of the Legendre polynomials typically denoted $P_n(x)$ which are orthogonal with respect to the uniform weight $w(x) = 1$ and correspond to $a = b = 0$ or $\lambda = \frac{1}{2}$.

The following describes the relationship between the two canonical normalizations of the Jacobi and ultraspherical polynomials [73, 18.7.1,18.7.2]:

$$C_n^{(\lambda)}(x) = \frac{(2\lambda)_n}{(\lambda+\frac{1}{2})_n} P_n^{(\lambda-\frac{1}{2},\lambda-\frac{1}{2})}(x), \tag{1.13}$$

$$P_n^{(\alpha,\alpha)}(x) = \frac{(\alpha+1)_n}{(2\alpha+1)_n} C_n^{(\alpha+\frac{1}{2})}(x). \tag{1.14}$$

Using these relationships one can readily obtain analogous versions of the above-stated definitions and properties of the Jacobi polynomials for the ultraspherical polynomials, e.g.:
Classical recurrence relationship [73, 18.9.1]:

$$C_{n+1}^{(\lambda)}(x) = \frac{2(n+\lambda)}{(n+1)} x C_n^{(\lambda)}(x) - \frac{(n+2\lambda-1)}{(n+1)} C_{n-1}^{(\lambda)}(x). \tag{1.15}$$

In what follows we explicitly collect a selection of these properties which will be useful.
Hypergeometric representation [73, 18.5.9]

$$C_n^{(\lambda)}(x) := \frac{(2\lambda)_n}{n!} {}_2F_1\left(-n, n+2\lambda, \lambda+\frac{1}{2}; \frac{1-x}{2}\right). \tag{1.16}$$

Indefinite integration [73, 18.17.1]:

$$\int (1-x^2)^{\lambda-\frac{1}{2}} C_n^{(\lambda)}(x)\mathrm{d}x = -\frac{2\lambda(1-x^2)^{\lambda+\frac{1}{2}}}{n^2+2\lambda n} C_{n-1}^{(\lambda+1)}(x) + \text{const.} \tag{1.17}$$

Orthogonality condition, special case where $m = 0$:

$$\int_{-1}^{1} (1-x^2)^{\lambda-\frac{1}{2}} C_n^{(\lambda)}(x)\mathrm{d}x = \frac{2^{1-2\lambda}\pi\Gamma(n+2\lambda)}{n!(n+\lambda)(\Gamma(\lambda))^2}\delta_{n0}. \tag{1.18}$$

Derivative [73, 18.9.19]:

$$\frac{\mathrm{d}}{\mathrm{d}x} C_n^{(\lambda)}(x) = 2\lambda C_{n-1}^{(\lambda+1)}(x). \tag{1.19}$$

Weighted derivative [73, 18.9.20]:

$$\frac{\mathrm{d}}{\mathrm{d}x}\left((1-x^2)^{\lambda-\frac{1}{2}}C_n^{(\lambda)}(x)\right) = -\frac{(n+1)(n+2\lambda-1)}{2(\lambda-1)}(1-x^2)^{\lambda-\frac{3}{2}}C_{n+1}^{(\lambda-1)}(x)\,. \tag{1.20}$$

Lowering recurrence via weight multiplication [73, 18.9.8]:

$$(1-x^2)C_n^{(\lambda+1)}(x) = \frac{(n+2\lambda)(n+2\lambda+1)}{4\lambda(n+\lambda+1)}C_n^{(\lambda)}(x) - \frac{(n+1)(n+2)}{4\lambda(n+\lambda+1)}C_{n+2}^{(\lambda)}(x). \tag{1.21}$$

Raising the basis parameter [73, 18.9.7]:

$$(n+\lambda)C_n^{(\lambda)}(x) = \lambda\left(C_n^{(\lambda+1)}(x) - C_{n-2}^{(\lambda+1)}(x)\right). \tag{1.22}$$

As with the Jacobi polynomials, we refer to the DLMF [73], as well as the formula collections by Prudnikov, Brychkov and Marichev [86, 87] for a large collection of properties of the ultraspherical polynomials.

1.1.5 Function approximation and sparse operators

While we will focus on methods involving Jacobi polynomials, most of the concepts discussed in this section readily translate to other orthogonal polynomials, as e.g., seen in the recently published detailed overview in [76], so we keep the notation generic in this section.

The fundamental idea underlying orthogonal polynomial spectral methods is the classical result that any sufficiently well-behaved function $f(x)$ may be expanded in a complete basis of polynomials $\{p_j(x)\}_{j\geqslant 0}$ with coefficients f_j:

$$f(x) = \sum_{j=0}^{\infty} p_j(x) f_j.$$

For orthogonal polynomials $p_j(x)$ with respect to a weight $w(x)$ the unique scalar coefficients of this expansion are given by

$$f_j = \frac{1}{h_j} \int_\Omega w(x) p_j(x) w(x) f(x) \mathrm{d}x,$$
$$h_j = \int_\Omega w(x) (p_j(x))^2 \mathrm{d}x.$$

We note that Slevinsky recently developed and implemented an open source, stable and multi-threaded C library called FastTransforms [4] which allows the efficient computation of these coefficients along with an associated Julia package FastTransforms.jl [5]. We refer to the papers [97, 98, 66] which discuss the methods used in these packages in detail.
Collecting the basis elements $p_j(x)$ and the coefficients f_j into infinite dimensional vectors

$$\mathbf{p}(x) = \begin{pmatrix} p_0(x) & p_1(x) & \dots \end{pmatrix}, \quad \mathbf{f} = \begin{pmatrix} f_0 \\ f_1 \\ \vdots \end{pmatrix}$$

we may instead choose to write the above series expansions as

$$f(x) = \mathbf{p}(x)\mathbf{f}.$$

We may also adopt the viewpoint of quasimatrices for the object $\mathbf{p}(x)$: Instead of thinking of it as an infinite-dimensional vector of functions, we can think of $\mathbf{p}(x)$ as being a two-dimensional array of values with one discrete index for the degree of the polynomial and one continuous index $x \in \Omega$ with Ω the domain of the given set of polynomials. This quasimatrix viewpoint reduces many common operations in the resulting spectral methods to straightforward classical linear algebra analogies and thus makes numerical approximations natural both in written notation and in code. A computer implementation of the above ideas may for example be found in the Julia language [16] package ecosystem around ContinuumArrays.jl [3], QuasiArrays.jl [7] and ClassicalOrthogonalPolynomials.jl [2].
Thinking of functions in terms of their respective coefficient column vectors in an orthogonal polynomial basis means that operators become (infinite dimensional) matrices. For example, the multiplication-by-x operator acts as

$$xf(x) = x\mathbf{p}(x)\mathbf{f} = \mathbf{p}(x)\mathrm{X}\mathbf{f},$$

where the entries of the infinite dimensional operator X can be obtained from the three term recurrence of the given polynomial basis, which also immediately demonstrates that multiplication-by-x is tridiagonal:

$$\mathrm{X} = \begin{pmatrix} a_0 & c_0 & & \\ b_0 & a_1 & c_1 & \\ & b_1 & a_2 & \ddots \\ & & \ddots & \ddots \end{pmatrix}. \tag{1.23}$$

Explicit forms of the constants a_j, b_j and c_j are straightforwardly obtained by rearranging

the classical recurrence relationship in Eq. (1.3). If the underlying orthogonal polynomial basis is orthonormal, the multiplication-by-x operator is also symmetric [41, 1.3.14]. The takeaway from this is that instead of having to re-expand $xf(x)$ we can efficiently and accurately compute them via $\mathbf{X}\mathbf{f}$ from the known coefficicents of $f(x)$. Similar banded matrix forms can be obtained for differentiation, integration, basis changes and more, based on various recurrence relationships – some of which we have listed above for Jacobi and ultraspherical polynomials.

An important part of Chapter 2 and Chapter 3 will be proofs that the infinite matrix forms of the Volterra integro-differential operators and power law integral operators respectively are banded and approximately banded in appropriate Jacobi polynomial bases.

1.2 Function evaluation using Clenshaw's algorithm

While there are straightforward ways to evaluate functions given as coefficient vectors in some orthogonal polynomial basis, i.e. the evaluation of $\sum_{j=0}^{\infty} p_j(x) f_j$ at a given point, Clenshaw's algorithm [30] allows one to reduce this evaluation to the solution of an upper triangular linear system, solved via backwards substitution. Among other benefits, Clenshaw's algorithm is thus far more memory optimized than a naive evaluation approach for approximated functions, cf. [77]. Furthermore, the sparse spectral method for Volterra integral equations we derive in Chapter 2 relies on an operator-valued modification of Clenshaw's algorithm.

In what follows we write $\mathbf{e}_0$ for the first standard basis vector of appropriate length, i.e. the vector with 1 in its first component, and $x_* \in (-1, 1)$ for an arbitrary point at which we wish to evaluate the approximated function. The classical three term recurrence relationship of the Jacobi polynomials can be used to write

$$\mathcal{L}_N(x_*)\mathbf{P}_N^{(a,b)}(x_*)^{\mathsf{T}} = \mathbf{e}_0, \tag{1.24}$$

where $\mathbf{P}_N^{(a,b)}(x)$ collects the polynomials up to order N and the operator $\mathcal{L}_N(x_*)$ is defined as

$$\mathcal{L}_N(x_*) = \begin{pmatrix} 1 & & & & \\ a_0 - x_* & b_0 & & & \\ c_0 & a_1 - x_* & b_1 & & \\ & \ddots & \ddots & \ddots & \\ & & c_{N-2} & a_{N-1} - x_* & b_{N-1} \end{pmatrix},$$

with the constants a_j, b_j and c_j corresponding with the notation used for the multiplication-by-x operator in Eq. (1.23). Solving the lower triangular system in (1.24) via forward substitution provides a way to recursively evaluate each element of the basis $\mathbf{P}^{(a,b)}(x)$ and thus also an approximated function if the coefficients of $f(x)$ in this basis are known. Clenshaw's algorithm proceeds similarly but instead uses backward substitution on the upper triangular system

$$f(x_*) = \mathbf{P}_N^{(a,b)}(x_*)\mathbf{f} = \mathbf{e}_0^\mathsf{T}\mathcal{L}_N(x_*)^{-\mathsf{T}}\mathbf{f}. \tag{1.25}$$

1.3 Multivariate orthogonal polynomials

The previous sections discussed the use of single variable, i.e. univariate, polynomials to approximate univariate functions. Analogous ideas allow one to approximate functions of multiple variables in higher dimensional domains using multivariate polynomials. In recent years, substantial advances have been made in the use of multivariate orthogonal polynomials for sparse spectral methods on triangles [77, 78], disks [108], trapeziums [99], wedges [79], surfaces of revolution [80] as well as quadratic and cubic curves [38, 81]. Dunkl and Xu's recent book [35] on orthogonal polynomials in several variables provides an excellent survey of bases on various classical arbitary dimensional domains such as cubes, balls and simplices. Preliminary support for multivariate orthogonal polynomials on triangles and disks is available in the MultivariateOrthogonalPolynomials.jl [6] Julia package.

1.3.1 From univariate to bivariate spectral methods

A bivariate function $f(x, y)$ may be expanded in a complete set of orthogonal polynomials $\{p_{n,k}(x, y)\}_{n,k\geqslant 0}$ with unique coefficients $f_{n,k}$ via

$$f(x, y) = \sum_{n=0}^{\infty} \sum_{k=0}^{n} p_{n,k}(x, y) f_{n,k} = \mathbf{p}(x, y)\mathbf{f}, \tag{1.26}$$

where we have used the following notation analogous to that in Section 1.1.5:

$$\mathbf{f} = \begin{pmatrix} \mathbf{f}_0 \\ \mathbf{f}_1 \\ \mathbf{f}_2 \\ \vdots \end{pmatrix}, \qquad \mathbf{f_n} = \begin{pmatrix} f_{n,0} \\ f_{n,1} \\ \vdots \\ f_{n,n} \end{pmatrix}, \tag{1.27}$$

$$\mathbf{p}(x, y) = \begin{pmatrix} \mathbf{p}_0(x, y) & \mathbf{p}_1(x, y) & \dots \end{pmatrix}, \tag{1.28}$$

$$\mathbf{p}_n(x, y) = \begin{pmatrix} p_{n,0}(x, y) & p_{n,1}(x, y) & \dots & p_{n,n}(x, y) \end{pmatrix}, \tag{1.29}$$

that is, the vectors $\mathbf{p}(x, y)$ and $\mathbf{f}$ collect their respective elements in lexicographic order. One may contruct versions with more than two variables in analogous fashion.

1.3.2 Proriol polynomials on the triangle

The Proriol polynomials, denoted $\{P_{n,k}^{(a,b,c)}(x, y)\}_{n,k\geqslant 0}$ are a three parameter family of complete orthogonal polynomials on the triangle $T^2 = \{(x, y) \in \mathbb{R}^2, 0 \leqslant x, 0 \leqslant y \leqslant 1 - x\}$ with respect to the weight

$$w^{(a,b,c)}(x) = x^a y^b (1 - x - y)^c, \tag{1.30}$$

meaning that they satisfy

$$\int_0^1 \int_0^{1-x} x^a y^b (1-x-y)^c P_{n,k}^{(a,b,c)}(x,y) P_{m,j}^{(a,b,c)}(x,y) \mathrm{d}x\mathrm{d}y = \kappa_{n,m,j,k} \delta_{n,m} \delta_{k,j}, \tag{1.31}$$

where we refer to [35, 2.4] for the explicit constant of orthogonality. Due to their close relationship with the one-dimensional Jacobi polynomials as defined in Section 1.1.2 they are also sometimes referred to as Jacobi polynomials on the triangle or simply orthogonal polynomials on the triangle [35, 77, 49, 73] without further specification:

$$P_{n,k}^{(a,b,c)}(x,y) = (1-x)^k P_{n-k}^{(2k+b+c+1,a)}(2x-1) P_k^{(c,b)}\left(\frac{2y}{1-x} - 1\right). \tag{1.32}$$

Versions of this basis for other orientations of the triangle are straightforward to obtain via variable transformations, cf. [73, 18.37(ii)] and [35, 2.4]. We will use the Proriol polynomials in Chapter 2 to construct sparse spectral methods for Volterra integro-differential equations with general kernels. The following alternative representation in terms of the shifted Jacobi polynomials as defined in Section 1.1.3 will be more convenient for that purpose:

$$P_{n,k}^{(a,b,c)}(x,y) = (1-x)^k \tilde{P}_{n-k}^{(2k+b+c+1,a)}(x) \tilde{P}_k^{(c,b)}\left(\frac{y}{1-x}\right). \tag{1.33}$$

The history of orthogonal polynomials on triangles appears to begin with Proriol in 1957 [84] who this family of polynomials were subsequently named after. They were later picked up and discussed by Koornwinder in a 1975 survey [56], see also [37] for a loosely contemporary discussion of biorthogonal triangle polynomials. While Munschy and Pluvinage [67] used the uniform weight special case to obtain approximate solutions to Schrödinger-type equations in 1957, the Proriol polynomials' first use in numerical methods in the modern sense appears to have been due to Dubiner in 1991 who used them in a spectral element scheme [34]. Following Dunkl and Xu's inclusion of triangle and simplex polynomials in their book on multivariate orthogonal polynomials [35], Olver, Townsend and Vasil [77, 78] derived explicit recurrence relationships and ladder operators along with producing an efficient implementation. Their

research laid the groundwork for the sparse spectral methods for Volterra integral equations research discussed in Chapter 2, based on [45, 49]. More general orthogonal polynomials on arbitrary dimensional simplex domains were also discussed in [35].

As in the 1-dimensional case we can define infinite dimensional sparse multiplication matrices X and Y which respectively act as

$$\mathbf{P}^{(a,b,c)}(x,y)\mathrm{X}\mathbf{f}_{\triangle} = xf(x,y),$$
$$\mathbf{P}^{(a,b,c)}(x,y)\mathrm{Y}\mathbf{f}_{\triangle} = yf(x,y).$$

Note that since we will often be discussing approximations on the triangle simultaneously with those on the real line as well as conversion operators between them in Chapter 2, we will denote coefficient vectors with respect to the Proriol polynomials with a subscript $\triangle$ symbol throughout this thesis to avoid ambiguity. Unlike in the 1-dimensional case these matrices are now block tridiagonal instead of tridiagonal for the Proriol polynomials, cf. [77]:

$$\mathrm{X}^{\mathsf{T}} = \begin{pmatrix} A_0^x & B_0^x & & \\ C_0^x & A_1^x & B_1^x & \\ & C_1^x & A_2^x & \ddots \\ & & \ddots & \ddots \end{pmatrix}, \quad \mathrm{Y}^{\mathsf{T}} = \begin{pmatrix} A_0^y & B_0^y & & \\ C_0^y & A_1^y & B_1^y & \\ & C_1^y & A_2^y & \ddots \\ & & \ddots & \ddots \end{pmatrix}, \tag{1.34}$$

where $A_n^x, A_n^y \in \mathbb{R}^{(n+1)\times(n+1)}$, $B_n^x, B_n^y \in \mathbb{R}^{(n+1)\times(n+2)}$ and $C_n^x, C_n^y \in \mathbb{R}^{(n+2)\times(n+1)}$. Raising and lowering as well as other kinds of useful operators discussed for the one dimensional case may also be constructed for the Proriol polynomials, see [78, 77].

Finally, we describe a generalization of Clenshaw's algorithm as discussed in Section 1.2 to the Proriol polynomials. This efficient way of evaluating functions expanded in Proriol polynomials was recently discussed in [77]. Analogous to the move from tridiagonal to block tridiagonal for the multiplication operators, Clenshaw's algorithm for the Proriol polynomi-

als involves solving a block triangular system to evaluate at (x_*, y_*) instead, namely:

$$\mathcal{L}_N(x_*, y_*)\mathbf{P}_N^{(a,b,c)}(x_*, y_*)^\mathsf{T} = \begin{pmatrix} I_1 & & & \\ A_0^x - x_* I_1 & B_0^x & & \\ A_0^y - y_* I_1 & B_0^y & & \\ C_0^x & A_1^x - x_* I_2 & B_1^x & \\ C_0^y & A_1^y - y_* I_2 & B_1^y & \\ & \ddots & \ddots & \ddots \end{pmatrix} \mathbf{P}_N^{(a,b,c)}(x_*, y_*)^\mathsf{T} = \mathbf{e}_0,$$

where we have denoted the $k \times k$ identity matrix by I_k. As this system is not triangular but block triangular, we must first apply a preconditioner to be able to use forward or backward substitution methods:

$$\begin{pmatrix} 1 & & & \\ & B_0^+ & & \\ & & B_1^+ & \\ & & & \ddots \end{pmatrix} \mathcal{L}_N(x_*, y_*) = \tilde{\mathcal{L}}_N(x_*, y_*).$$

After appropriate preconditioning, the matrix $\tilde{\mathcal{L}}_N(x_*, y_*)$ should then be lower triangular, allowing the evaluation of functions expanded in the Proriol polynomials recursively via forward substitution. Choosing left-inverses to the following blocks satisfies our preconditioning requirements:

$$B_n = \begin{pmatrix} B_n^x \\ B_n^y \end{pmatrix}.$$

That is, we choose B_n^+ such that $B_n^+ B_n = I_n$. The analogue of Clenshaw's algorithm for the Proriol polynomials then reads

$$f(x_*, y_*) = \mathbf{P}_N^{(a,b,c)}(x_*, y_*)\mathbf{f}_\triangle = \mathbf{e}_0^\mathsf{T} \tilde{\mathcal{L}}_N(x_*, y_*)^{-\mathsf{T}} \mathbf{f}_\triangle.$$

Using backward substitution to solve this allows for function evaluation in optimal $O(N^2)$ complexity, cf. [77].

1.3.3 Radial Jacobi polynomials on arbitrary dimensional balls

The Zernike polynomials, herein denoted $Z_n^{(0,m,2)}(r,\phi)$, are a widely known and used complete orthogonal polynomials on the disk $\mathbb{D} = \{\mathbf{x} \in \mathbb{R}^2, |\mathbf{x}| = r \leqslant 1\}$, i.e. the ball in two dimensions. They are polynomials in the x and y coordinate variables but are more commonly written in their polar coordinate form which decays into a product of angular and radial components:

$$Z_n^{(0,m,2)}(r,\phi) = U^{(m)}(\phi) R_n^{(0,m,2)}(r), \tag{1.35}$$

where the radial part inherits its orthogonality directly from its relationship to the one-dimensional Jacobi polynomials:

$$R_n^{(0,m,2)}(r) := r^m \tilde{P}_n^{(0,m)}(r^2), \tag{1.36}$$

and the angular part is given by

$$U^{(m)}(\phi) = \begin{cases} \cos(m\phi), & \text{for } m \geqslant 0, \\ \sin(m\phi), & \text{else.} \end{cases}$$

The motivation for the chosen notation is a natural generalization which we discuss below. The Zernike polynomials have a long-standing history of use in pure mathematics as well as applications and engineering focused fields going back to [117, 118]. Nowadays they are mostly known in the optics literature for their uses in describing various optical effects on lenses, cf. [101, 63, 89], but have also seen recent use in other applications such as impact crater models [112] and atmospheric science [90, 72]. As a result of their history and interdisciplinary applications one finds a large number of conflicting notations and

ordering schemes for the Zernike polynomials present in the literature – we will avoid most of this confusion by relying on their Fourier and Jacobi representations instead, which are straightforward.

Various generalizations of the Zernike polynomials have been described, see e.g. [115, 8, 105, 11, 69], which among other potential generalizations allow the definition of a family of polynomials orthogonal with respect to the weight

$$w_{\bullet}^{(k)}(r) = (1 - r^2)^k, \tag{1.37}$$

which are sometimes referred to simply as *generalized* Zernike polynomials. The angular part of the generalized Zernike polynomials remains unchanged while the radial part becomes

$$R_n^{(k,m,2)}(r) := r^m \tilde{P}_n^{(k,m)}(r^2). \tag{1.38}$$

The idea of combining spherical harmonics with a radial Jacobi polynomial basis can further be expanded to d-dimensional balls. We will use a special case of the above on arbitrary dimensional balls in Chapter 3: the restriction to the $m = 0$ (angle-independent) mode, which can be used for radially symmetric functions on balls, with the corresponding radial part being:

$$R_n^{(k,0,d)}(r) = \tilde{P}_n^{\left(k,\frac{d-2}{2}\right)}(r^2). \tag{1.39}$$

As this basis is restricted to the $m = 0$ mode and thus no longer includes an angular component, we will refer to this simply as a radial Jacobi polynomial basis. Just like the generalized Zernike polynomials in two dimensions, the radial Jacobi polynomials in arbitrary dimensions are orthogonal with respect to the weight in Eq. (1.37).

Finally, we include a list of basic properties for the radial Jacobi polynomials $\tilde{P}_n^{(a,b)}(|\mathbf{x}|^2)$ which are direct consequences of the respective properties of the Jacobi polynomials [73, 18.9]:

Classical recurrence relationship:

$$\tilde{P}_{n+1}^{(a,b)}(|\mathbf{x}|^2) = (2A_n|x|^2 + (B_n - A_n))\tilde{P}_n^{(a,b)}(|\mathbf{x}|^2) - C_n\tilde{P}_{n-1}^{(a,b)}(|\mathbf{x}|^2), \tag{1.40}$$

with constants independent of x but dependent on n, a, b:

$$\begin{aligned} A_n &= \tfrac{(2n+a+b+1)(2n+a+b+2)}{2(n+1)(n+a+b+1)}, \\ B_n &= \tfrac{(a^2-b^2)(2n+a+b+1)}{2(n+1)(n+a+b+1)(2n+a+b)}, \\ C_n &= \tfrac{(n+a)(n+b)(2n+a+b+2)}{(n+1)(n+a+b+1)(2n+a+b)}. \end{aligned}$$

Explicit representations:

$$\tilde{P}_n^{(a,b)}\left(|x|^2\right) = \sum_{k=0}^{n}(-1)^{n+k}\tfrac{(n+a+b+1)_k(b+k+1)_{n-k}}{k!\,(n-k)!}|\mathbf{x}|^{2k}, \tag{1.41}$$

$$= \tfrac{\Gamma(a+n+1)}{n!\,\Gamma(a+b+n+1)}\sum_{k=0}^{n}(-1)^k\binom{n}{k}\tfrac{\Gamma(a+b+n+k+1)}{\Gamma(a+k+1)}\left(1-|\mathbf{x}|^2\right)^k, \tag{1.42}$$

$$= \frac{(a+1)_n}{n!}{}_2F_1\left(\begin{matrix}-n, & n+a+b+1 \\ & a+1\end{matrix}; 1-|\mathbf{x}|^2\right)$$

$$= (-1)^n\frac{(b+1)_n}{n!}{}_2F_1\left(\begin{matrix}-n, & n+a+b+1 \\ & b+1\end{matrix}; |\mathbf{x}|^2\right). \tag{1.43}$$

Symmetry:

$$P_n^{(a,b)}(1-2|\mathbf{x}|^2) = (-1)^n P_n^{(b,a)}(2|\mathbf{x}|^2-1). \tag{1.44}$$

Various basis conversions:

$$\tilde{P}_n^{(a,b)}\left(|\mathbf{x}|^2\right) = \tfrac{(n+a+b+1)}{(2n+a+b+1)}\tilde{P}_n^{(a+1,b)}\left(|\mathbf{x}|^2\right) - \tfrac{(n+b)}{(2n+a+b+1)}\tilde{P}_{n-1}^{(a+1,b)}\left(|\mathbf{x}|^2\right), \tag{1.45}$$

$$\tilde{P}_n^{(a,b)}\left(|\mathbf{x}|^2\right) = \tfrac{(n+a+b+1)}{(2n+a+b+1)}\tilde{P}_n^{(a,b+1)}\left(|\mathbf{x}|^2\right) + \tfrac{(n+a)}{(2n+a+b+1)}\tilde{P}_{n-1}^{(a,b+1)}\left(|\mathbf{x}|^2\right).$$

$$|\mathbf{x}|^2 \tilde{P}_n^{(a,b+1)}\left(|\mathbf{x}|^2\right) = K_n \tilde{P}_{n+1}^{(a,b)}\left(|\mathbf{x}|^2\right) + \tfrac{(n+b+1)}{2(n+\frac{a}{2}+\frac{b}{2}+1)} \tilde{P}_n^{(a,b)}\left(|\mathbf{x}|^2\right), \tag{1.46}$$

$$(|\mathbf{x}|^2-1)\tilde{P}_n^{(a+1,b)}\left(|\mathbf{x}|^2\right) = K_n \tilde{P}_{n+1}^{(a,b)}\left(|\mathbf{x}|^2\right) - \tfrac{(n+a+1)}{2(n+\frac{a}{2}+\frac{b}{2}+1)} \tilde{P}_n^{(a,b)}\left(|\mathbf{x}|^2\right),$$

with $K_n = \frac{(n+1)}{2(n+\frac{a}{2}+\frac{b}{2}+1)}$.

1.4 Notes on hypergeometric and Meijer-G functions

Hypergeometric functions are a large class of functions which include many familiar functions as special cases, including the above-discussed polynomials as for example seen in Eq. (1.2). The most commonly used hypergeometric function is the so-called Gaussian hypergeometric function denoted ${}_2F_1$. The more general hypergeometric function ${}_pF_q$ as well as the even more general class of hypergeometric functions known as Meijer-G functions satisfy various known properties including reductions to simpler forms, symmetries, various recurrence relationships and more.

Definition 1.1. *Let $a_1, a_2, ..., a_p$ and $b_1, b_2, ..., b_q$ be real or complex, $m \in [0, q]$ and $n \in [0, p]$ be integers and let none of $a_k - b_j$ be positive for $1 \leqslant k \leqslant n$ and $1 \leqslant j \leqslant m$. Then the Meijer-G function is defined via the following Mellin-Barnes integral:*

$$G_{p,q}^{m,n}\left(\begin{matrix} a_1, \ldots, a_p \\ b_1, \ldots, b_q \end{matrix}; z\right) = \frac{1}{2\pi \mathrm{i}} \int_L \frac{\prod_{\ell=1}^{m} \Gamma\left(b_\ell - s\right) \prod_{\ell=1}^{n} \Gamma\left(1 - a_\ell + s\right)}{\left(\prod_{\ell=m}^{q-1} \Gamma\left(1 - b_{\ell+1} + s\right) \prod_{\ell=n}^{p-1} \Gamma\left(a_{\ell+1} - s\right)\right)} z^s \mathrm{d}s.$$

The integration path L has to be chosen such that it separates the poles of the $\Gamma(b_\ell - s)$ from the poles of the $\Gamma(1 - a_\ell + s)$ factors. For details on how to choose L, we refer to [73, 16.17.1].

As these functions satisfy far too many interesting properties to provide an exhaustive list here, we will make no such attempt – entire books collecting formulae have been written for these functions, see e.g. the excellent collections in [73, 85, 87]. Instead, in what follows we

will include the specific properties we make of use in this thesis and include references or comments on how they may be obtained.

The hypergeometric functions as special case Meijer-G functions:[73, 16.18.1]:

$$
\begin{aligned}
{}_pF_q\left(\begin{matrix}a_1,\ldots,a_p\\ b_1,\ldots,b_q\end{matrix};z\right) &= \left(\frac{\prod_{k=1}^{q}\Gamma\left(b_k\right)}{\prod_{k=1}^{p}\Gamma\left(a_k\right)}\right)G^{1,p}_{p,q+1}\left(\begin{matrix}1-a_1,\ldots,1-a_p\\ 0,1-b_1,\ldots,1-b_q\end{matrix};-z\right)\\
&= \left(\frac{\prod_{k=1}^{q}\Gamma\left(b_k\right)}{\prod_{k=1}^{p}\Gamma\left(a_k\right)}\right)G^{p,1}_{q+1,p}\left(\begin{matrix}1,b_1,\ldots,b_q\\ a_1,\ldots,a_p\end{matrix};-\frac{1}{z}\right).
\end{aligned}
$$

Explicit series representation:

The Meijer-G function has the explicit series representation [73, 16.17.2]:

$$
G^{m,n}_{p,q}\left(\begin{matrix}a_1,\ldots,a_p\\ b_1,\ldots,b_q\end{matrix};z\right) = \sum_{k=1}^{m}A^{m,n}_{p,q,k}(z)\,{}_pF_{q-1}\left(\begin{matrix}1+b_k-a_1,\ldots,1+b_k-a_p\\ 1+b_k-b_1,\ldots *\ldots,1+b_k-b_q\end{matrix};(-1)^{p-m-n}z\right),
$$

where $*$ on the right-hand side indicates that the entry $1+b_k-b_k$ is not included and

$$
A^{m,n}_{p,q,k}(z) = \frac{\prod_{\substack{\ell=1\\ \ell\neq k}}^{m}\Gamma\left(b_\ell-b_k\right)\prod_{\ell=1}^{n}\Gamma\left(1+b_k-a_\ell\right)z^{b_k}}{\prod_{\ell=m}^{q-1}\Gamma\left(1+b_k-b_{\ell+1}\right)\prod_{\ell=n}^{p-1}\Gamma\left(a_{\ell+1}-b_k\right)}.
$$

This series representation only holds when certain conditions on p, q, a_j and b_j are satisfied, see [73, 16.17] for details. We also note the following series representations of the ${}_pF_q$ and ${}_2F_1$ hypergeometric functions [73, 16.2.1,]:

$$
{}_pF_q\left(\begin{matrix}a_1,\ldots,a_p\\ b_1,\ldots,b_q\end{matrix};z\right) = \sum_{k=0}^{\infty}\frac{\left(a_1\right)_k\cdots\left(a_p\right)_k}{\left(b_1\right)_k\cdots\left(b_q\right)_k}\frac{z^k}{k!}, \tag{1.47}
$$

$$
{}_2F_1\left(a,b;c;z\right) = \sum_{k=0}^{\infty}\frac{(a)_k(b)_k}{(c)_k}\frac{z^k}{k!} = \frac{\Gamma\left(c\right)}{\Gamma\left(a\right)\Gamma\left(b\right)}\sum_{k=0}^{\infty}\frac{\Gamma\left(a+k\right)\Gamma\left(b+k\right)}{\Gamma\left(c+k\right)}\frac{z^k}{k!}. \tag{1.48}
$$

Parameter symmetries:

The Meijer-G function is invariant with respect to permutations of its upper or lower parameters respectively and the same holds for hypergeometric ${}_pF_q$ functions. Furthermore, the following properties hold [73, 16.19.1–16.19.2]:

$$G_{p,q}^{m,n}\left(\begin{matrix}a_1,\dots,a_p\\ b_1,\dots,b_q\end{matrix};\frac{1}{z}\right)=G_{q,p}^{n,m}\left(\begin{matrix}1-b_1,\dots,1-b_q\\ 1-a_1,\dots,1-a_p\end{matrix};z\right), \tag{1.49}$$

$$z^{\mu}G_{p,q}^{m,n}\left(\begin{matrix}a_1,\dots,a_p\\ b_1,\dots,b_q\end{matrix};z\right)=G_{p,q}^{m,n}\left(\begin{matrix}a_1+\mu,\dots,a_p+\mu\\ b_1+\mu,\dots,b_q+\mu\end{matrix};z\right). \tag{1.50}$$

Parameter cancellation and reduction to lower order functions:

The general Meijer-G function satisfies the following reduction rules, cf. [36, Eq. 21–22] and [73]:

$$G_{p+1,q+1}^{m,n+1}\left(\begin{matrix}a_0,\dots,a_p\\ b_1,\dots,b_q,a_0\end{matrix};z\right)=G_{p,q}^{m,n}\left(\begin{matrix}a_1,\dots,a_p\\ b_1,\dots,b_q\end{matrix};z\right), \tag{1.51}$$

By the respective symmetry properties for permutations of upper and lower parameters as well as (1.49-1.50) many similar reduction properties may be derived from the one above. As ${}_pF_q$ hypergeometric functions are a special case of Meijer-G functions, such cancellation rules also hold for them. An explicit example of such a cancellation which we will use in Chapter 3 is the reduction of ${}_3F_2$ to ${}_2F_1$ functions:

$${}_3F_2\left(\begin{matrix}a_1, & a_2, & a_3\\ & c_1, & a_3\end{matrix};z\right)={}_2F_1\left(\begin{matrix}a_1, & a_2\\ & c_1\end{matrix};z\right). \tag{1.52}$$

Finite sums of general hypergeometric functions:

Certain finite sums of hypergemeotric functions may be collapsed to a single hypergemeotric function via the following expression contained in the works of Prudnikov, Brychkov and

Marichev [87, 5.3.6.3]:

$$\sum_{k=0}^{n}(-1)^k\binom{n}{k}\frac{(1-\mathfrak{b})_k}{(1-\mathfrak{a})_k}{}_{p+m}F_q\left(\begin{matrix}\mathbf{a}_p, & \Delta(m,\mathfrak{a}-k)\\ & \mathbf{b}_q\end{matrix};x\right)$$
$$=\frac{(\mathfrak{b}-\mathfrak{a})_n}{(1-\mathfrak{a})_n}{}_{p+2m}F_{q+m}\left(\begin{matrix}\mathbf{a}_p, & \Delta(m,\mathfrak{a}-\mathfrak{b}+1), & \Delta(m,\mathfrak{a}-n)\\ & \mathbf{b}_q, & \Delta(m,\mathfrak{a}-\mathfrak{b}-n+1)\end{matrix};x\right)$$

where $\Delta(k,\mathfrak{a}) := \frac{\mathfrak{a}}{k}, \frac{\mathfrak{a}+1}{k}, ..., \frac{\mathfrak{a}+k-1}{k}$, cf [87, p.798]. In Chapter 3 we will make use of the $p = q = m = 1$ special case which reduces certain finite sums of ${}_2F_1$ functions to the ${}_3F_2$ function:

$$\sum_{k=0}^{n}(-1)^k\binom{n}{k}\frac{(1-\mathfrak{b})_k}{(1-\mathfrak{a})_k}{}_2F_1\left(\begin{matrix}a_1, & \mathfrak{a}-k\\ & b_1\end{matrix};x\right) \tag{1.53}$$
$$=\frac{(\mathfrak{b}-\mathfrak{a})_n}{(1-\mathfrak{a})_n}{}_3F_2\left(\begin{matrix}a_1, & \mathfrak{a}-\mathfrak{b}+1, & \mathfrak{a}-n\\ b_1, & \mathfrak{a}-\mathfrak{b}-n+1\end{matrix};x\right).$$

A class of contiguous recurrence relationships:

Gaussian hypergeometric functions of general form

$${}_2F_1\left(\begin{matrix}a+\epsilon_1 n, & b+\epsilon_2 n\\ & c+\epsilon_3 n\end{matrix};z\right)$$

where $\epsilon_i \in \{-1,0,1\}$ satisfy numerous recurrence relationships. Many of these can be obtained by appropriately combining the so-called contiguous relationships for hypergeometric functions, which are e.g. listed in [73, 15.5.11–15.5.18]. One such recurrence which we use

in Chapter 3 and may be obtained in this way is the following two-term recurrence:

$$
\begin{aligned}
{}_2F_1\left(\begin{matrix} a+1, & b-1 \\ & c \end{matrix}; z\right) =& \frac{(a-b)\left(z\left((a-b)^2-1\right)+2ab-ac-bc+c\right)}{a(a-b-1)(b-c)}\,{}_2F_1\left(\begin{matrix} a, & b \\ & c \end{matrix}; z\right) \\
&- \frac{b(a-b+1)(a-c)}{a(a-b-1)(b-c)}\,{}_2F_1\left(\begin{matrix} a-1, & b+1 \\ & c \end{matrix}; z\right). \qquad (1.54)
\end{aligned}
$$

Chapter 2

Sparse spectral methods for Volterra integro-differential equations

The content of this chapter is based on research published in [49] and [45]. For the purposes of this thesis, the content of the papers has been rewritten and merged into one coherent chapter. Furthermore, all appearing figures for the numerical experiments included in this chapter are original and were generated exclusively for this thesis.

2.1 Introduction to Volterra integral equations (VIEs)

Definition 2.1 (Volterra integral operator)**.** *For a given kernel $K(x, y)$, we define the Volterra integral operator with respect to $K(x, y)$ as:*

$$(\mathcal{V}_K u)(x) := \int_0^{\ell(x)} K(x, y)u(y)\mathrm{d}y.$$

In what follows we will discuss limits of integration options $\ell(x) = x$ and $\ell(x) = 1 - x$, as the former is the traditional definition of Volterra integrals and the latter variant arises naturally in our derivation.

Volterra integral *equations* (VIEs) then, are equations in which the unknown function is acted upon by a Volterra integral operator as defined above, whereas Volterra integro-differential equations also involve derivatives. One furthermore distinguishes different so-called *kinds* of these equations, of particular relevance to us are *first* and *second* kind

equations for which we will explicitly construct a banded spectral method. Denoting the unknown by u and the right-hand side function as g, first-kind Volterra integro-differential equations have the general form

Definition 2.2 (Volterra integral equations of the first-kind)**.**

$$\mathcal{V}_K u = g.$$

Second kind equations arise out of first-kind equations by the addition of an identity operator I to the Volterra integral term

Definition 2.3 (Volterra integral equations of the second-kind)**.**

$$(\lambda I - \mathcal{V}_K)u = g.$$

The above definitions are for the *linear* varieties of these equations. We will discuss nonlinear and integro-differential generalizations in Section 2.6. It should be noted that the name third-kind equation is also used in the literature, see e.g. [100, 9, 10], but its specific meaning is less standardized. While our method also has applications for some of these third-kind equations, we will only sparingly mention them in numerical examples in Section 2.8.

Due to their common occurrence in natural science and finance applications, cf. [21, 113], there is a rich literature on numerical algorithms for Volterra integral and integro-differential equations, including numerical methods approaching half a century in age [19]. Some recent notable numerical schemes developed for Volterra integral and integro-differential equations include the convolution kernel, i.e. $K(x, y) = K(x - y)$, approach due to Loureiro and Xu in [116, 62] which generalizes an ultraspherical spectral method for convolution kernel problems developed by Hale and Townsend in [52, 53] as well as collocation methods [20, 32] and wavelet based approaches [59, 96, 54]. The significance of the method we propose in

this chapter is that it achieves competitive accuracy and efficiency comparable to that of the ultraspherical spectral method due to Hale [52] while not being restricted to convolution kernels.

While superficially first and second-kind Volterra integral equations may appear similar, important mathematical properties of the respective operators are different. Of particular importance for our context is that first-kind operators are compact in certain function spaces, meaning that straightforward convergence properties from finite section theory are not applicable. As we will see in Section 2.7, at least for the linear case second-kind operators are readily found to be more well-behaved. For similar reasons the difference between first and second-kind equations will come into play again when we discuss preconditioning for equilibrium measure problems in Chapter 3.

The remainder of this chapter is organized as follows: In Section 2.2 we briefly discuss the above-mentioned spectral method for Volterra integral equations with convolution kernels due to Hale and Townsend. In Section 2.3 we derive banded representations of the Volterra integral operator on selected Jacobi polynomial bases. In Section 2.5 we detail the resulting sparse spectral method algorithm for the linear equations. In Section 2.6 we describe a generalization of the method to integro-differential and nonlinear equations. Convergence proofs for the linear case for first and second-kind equations are given in Section 2.7. We close with several numerical experiments and validations in Section 2.8 and an overview of the results in Section 2.9.

2.2 The Hale-Townsend method for convolution kernel Volterra integral equations

In this section we state the known result due to Hale and Townsend [52, 53] that Volterra integro-differential equations of convolution type, i.e. $K(x, y) = K(x - y)$, may be solved using banded operators in a Legendre polynomial basis. As mentioned in Chapter 1, the Legendre polynomials $P_n(x) = P_n^{(0,0)}(x)$ correspond to the special case $a = b = 0$ of the

Jacobi polynomials. This section serves to describe the context of the method we introduce in this chapter which holds for more general kernels.

We reproduce the main results underlying the banded spectral method for Volterra integro-differential equations introduced by Hale and Townsend in [52, 53] in the following theorem:

Theorem 2.1. *We denote the shifted and scaled Legendre polynomial basis with $x \in (0,1)$ by $\tilde{\mathbf{P}}(x)$ and a polynomial of degree m by $K(x) = \tilde{\mathbf{P}}(x)\mathbf{K}$, where $\mathbf{K}$ is an infinite dimensional coefficient vector with m nonzero entries. Then the convolution Volterra integral operator*

$$(\mathcal{V}_K u)(x) = \int_0^x K(x-y)u(y)y, \quad 0 \leqslant x \leqslant 1,$$

corresponds to an $(m+2)$-banded infinite dimensional matrix V_K such that

$$(\mathcal{V}_K u)(x) = \tilde{\mathbf{P}}(x)\mathrm{V}_K\mathbf{u}.$$

Furthermore, the entries of V_K may be computed using the following recurrence relationship:

$$(\mathrm{V}_K)_{j,n+1} = (\mathrm{V}_K)_{j,n-1} - \frac{2n+1}{2j+3}(\mathrm{V}_K)_{j+1,n} + \frac{2n+1}{2j-1}(\mathrm{V}_K)_{j-1,n},$$

with the following starting values:

$$(\mathrm{V}_K)_{j,0} = \begin{cases} \frac{1}{2}\left(\frac{K_{j-1}}{2j-1} - \frac{K_{j+1}}{2j+3}\right), & j \neq 0 \\ \frac{1}{2}\left(K_0 - \frac{K_1}{3}\right), & j = 0, \end{cases}$$

$$(\mathrm{V}_K)_{j,1} = \begin{cases} \frac{(\mathrm{V}_K)_{j-1,0}}{2j-1} - (\mathrm{V}_K)_{j,0} - \frac{(\mathrm{V}_K)_{j+1,0}}{2j+3}, & j \neq 0 \\ -\frac{(\mathrm{V}_K)_{1,0}}{3}, & j = 0, \end{cases}$$

$$(\mathrm{V}_K)_{0,n} = \frac{(-1)^n(\mathrm{V}_K)_{n,0}}{2n+1}, \qquad n \geqslant 0.$$

Proof. The proof that the Volterra operator corresponds to an $(m+2)$-banded infinite dimensional matrix can be found in [52, Proposition 3.1], while the proof of the recurrence

relationship is given in [53, Theorem 4.1]. □

Hale and Townsend's results allow one to solve Volterra integral equations for sufficiently smooth convolution kernels K and solutions u with spectral accuracy and linear complexity. By appending appropriate evaluation operators one can also use these results to solve Volterra integro-differential equations with convolution kernels, cf. [52]. We delay the discussion of this procedure resulting in almost banded linear systems for integro-differential equations to Section 2.6, as it similarly applies for our general kernel method. Finally, we note that while Hale and Townsend's result uses Legendre polynomials, Xu and Loureiro proved generalizations for other orthogonal polynomial bases such as Jacobi polynomials, cf. [116, 62].

In the section which follows we derive a general kernel banded spectral method by using properties of the Proriol polyomials on the triangle, retaining the attractive features of spectral accuracy and linear complexity of Hale and Townsend's approach.

2.3 Banded Volterra operators in Jacobi bases

Before we derive the banded structure of the Volterra integral operator, we describe the general strategy and define some of the auxiliary operators we will require. The first stepping stone is to rewrite the following integral over a general bivariate function $f(x, y)$ as a product of operators acting on the coefficient vectors of this function in a basis of Proriol polynomials on the triangle as introduced in Section 1.3.2:

$$\int_0^{1-x} f(x, y)\mathrm{d}y = \tilde{\mathbf{P}}(x)\mathrm{W}\mathrm{Q}_y\mathbf{f}_\triangle. \tag{2.1}$$

In the above, we have introduced the two infinite-dimensional matrices W and Q_y, which respectively act as weight and integration operators. Note that integrating over one variable, in this case y, still leaves us with a univariate function and thus the result of $\mathrm{W}\mathrm{Q}_y\mathbf{f}_\triangle$ is as a coefficient vector of the integrated function in univariate shifted Jacobi polynomials on

the univariate interval $(0, 1)$. We delay the explicit entry-wise characterization of these two matrices to a later point, as they will make more sense when the full strategy is understood. The next step is to define an extension operator E_y, which has the property of mapping a univariate function expanded in univariate Jacobi polynomials to a bivariate function on the triangle expanded in Proriol polynomials, i.e.:

$$\tilde{\mathbf{P}}(x)\mathbf{f} = \mathbf{P}(x, y)\mathrm{E}_y\mathbf{f}. \tag{2.2}$$

The resulting bivariate function defined by the coefficient vector $\mathbf{f}_\triangle = \mathrm{E}_y\mathbf{f}$ is independent of y and the extension operation can thus be thought of as extending the univariate function across the triangle domain. Putting the two previous steps together allows us to write an integration of a univariate function expanded in some Jacobi polynomial basis as

$$\int_0^{1-x} f(x, y)\mathrm{d}y = \tilde{\mathbf{P}}(x)\mathrm{W}\mathrm{Q}_y\mathrm{E}_y\mathbf{f}. \tag{2.3}$$

The most straightforward way of changing the limits of integration to $\ell(x) = x$ is to define a reflection operator R based on the equivalent of the symmetry property in Eq. 1.4 for the shifted Jacobi polynomials on $(0, 1)$:

$$\tilde{\mathbf{P}}(x)\mathrm{R}\mathbf{f} = f(1 - x). \tag{2.4}$$

It turns out that the above-defined operators satisfy nice commutation relationships with the multiplication by x and y operators on the Proriol polynomials as defined in Eq.(1.34). To remove ambiguity, we denote the multiplication-by-x operator on the real interval using $\bar{\mathrm{X}}$ in the following relationships:

$$\mathrm{Q}_y\mathrm{X}\mathbf{f}_\triangle = \bar{\mathrm{X}}\mathrm{Q}_y\mathbf{f}_\triangle, \tag{2.5}$$

$$\mathrm{Y}\mathrm{E}_y\mathbf{f} = \mathrm{E}_y\bar{\mathrm{X}}\mathbf{f}. \tag{2.6}$$

Having made the above observations, we now move on to deriving the explicit form of the operators. First, we have so far deliberately suppressed the basis parameters for the shifted Jacobi and the Proriol polynomials but to derive an explicit element-wise construction we have to choose concrete bases. We make the choice $(a, b, c) = (0, 0, 0)$ for the Proriol polynomials, as this leads to a particularly simple form. The natural choice for the corresponding univariate basis then becomes $\tilde{\mathbf{P}}^{(1,0)}(x)$ as the following first steps towards the entries of Q_y show:

$$\begin{aligned}\tilde{\mathbf{P}}^{(1,0)}(x)\mathrm{W}\mathrm{Q}_y\mathbf{f}_{\triangle} &= \int_0^{1-x} f(x,y)\mathrm{d}y = \int_0^{1-x} \sum_{n=0}^{\infty}\sum_{k=0}^{n} P_{n,k}^{(0,0,0)}(x,y) f_{n,k}\mathrm{d}y \\ &= \sum_{n=0}^{\infty}\sum_{k=0}^{n} f_{n,k}(1-x)^k \tilde{P}_{n-k}^{(2k+1,0)}(x) \int_0^{1-x} \tilde{P}_k^{(0,0)}\left(\frac{y}{1-x}\right)\mathrm{d}y \\ &= \sum_{n=0}^{\infty}\sum_{k=0}^{n} f_{n,k}(1-x)^{k+1} \tilde{P}_{n-k}^{(2k+1,0)}(x) \int_0^{1} \tilde{P}_k^{(0,0)}(s)\,\mathrm{d}s.\end{aligned}$$

In the above computation, the first line is simply an expansion of the function $f(x, y)$ in the Proriol basis $\mathbf{P}^{(0,0,0)}(x, y)$. The second line then uses the definition of the Proriol polynomials in terms of shifted Jacobi polynomials as described in Eq. (1.33). The final step makes the variable substitution $\frac{y}{1-x} \to s$. Continuing from the final line of the above computation, we make the observation that $\int_0^1 \tilde{P}_k^{(0,0)}(s)\,\mathrm{d}s$ vanishes for all $k > 0$ due to the orthogonality of the shifted Jacobi – or in this case specifically Legendre – polynomials. Since furthermore we have $\int_0^1 \tilde{P}_0^{(0,0)}(s)\,\mathrm{d}s = 1$ this results in the following simplification:

$$\tilde{\mathbf{P}}^{(1,0)}(x)\mathrm{W}\mathrm{Q}_y\mathbf{f}_{\triangle} = \int_0^{1-x} f(x,y)\mathrm{d}y = \sum_{n=0}^{\infty} f_{n,0}(1-x)\tilde{P}_n^{(1,0)}(x) \tag{2.7}$$

with limits of integration from 0 to $1 - x$. Using the reflection operator, i.e. the symmetry property in Eq. (1.4), we obtain a version valid for integration limits from 0 to x as an immediate corollary. Setting $W = (I - \mathrm{X})$ on the basis of (2.7), we find that we can write Q_y as a block matrix with the n-th diagonal block being given by an n-dimensional row

vector with 1 as the first element and 0 as the remaining elements, i.e.:

$$\mathrm{Q}_y = \begin{pmatrix} 1 & & & & \\ & 1 & 0 & & \\ & & 1 & 0 & 0 \\ & & & \ddots & \ddots & \ddots & \ddots \end{pmatrix}.$$

The expansion operator from the univariate Jacobi polynomials to the triangle has a straightforward block matrix form

$$\mathrm{E}_y = \begin{pmatrix} \times & & \\ & \times & \\ & \times & \\ & & \ddots \\ & & \ddots \\ & & \ddots \end{pmatrix},$$

whose entries depend on the basis parameters used in the univariate and triangle bases. For the basis choices made above, that is $\tilde{\mathbf{P}}^{(1,0)}(x)$ for the univariate basis and $\mathbf{P}^{(0,0,0)}(x,y)$ for the triangle, the n-th diagonal block, which is an n-dimensional column vector, has j-th entry $\frac{(-1)^{j+n}(2j-1)}{n}$.

Finally, we point out that due to the block structure of the expansion and integration operators, multiplication of Q_y and E_y yields a diagonal matrix D whose entries are analytically known and thus can be directly generated, i.e. without the need for matrix multiplication:

$$(\mathrm{Q}_y\mathrm{E}_y)_{n,n} = (\mathrm{D})_{n,n} = \frac{(-1)^{n+1}}{n}.$$

2.4 An operator-valued version of Clenshaw's algorithm

The operators defined in the previous section allow for the efficient computation of integrals of the form $\int_0^x f(y)\mathrm{d}y$, which corresponds to a Volterra integral with trivial kernel $K(x,y) =$

1. In this section we describe how a modification of Clenshaw's algorithm discussed above in Section 1.2 can be used to extend this approach to general kernels. First, we note that if we had access to the kernel multiplication operator $K(\mathrm{X},\mathrm{Y})$, with X and Y being the multiplication operators defined in Section 1.3.2 on the Proriol polynomial basis, we could naively simply compute

$$\int_0^{1-x} K(x,y)f(y)\mathrm{d}y = \tilde{\mathbf{P}}^{(1,0)}(x)(I-\bar{\mathrm{X}})\mathrm{Q}_y K(\mathrm{X},\mathrm{Y})\mathrm{E}_y\mathbf{f}.$$

To obtain the kernel multiplication operator we could for example use a variant of Clenshaw's method, as was recently discussed in [77]. While this turns out to be computationally wasteful for the computation of Volterra integrals, which is our primary concern in this chapter, it is still the method of choice when the multiplication operators themselves are required and we thus briefly describe it before explaining how to improve upon it for Volterra integrals. The kernel multiplication operator $K(\mathrm{X},\mathrm{Y})$ can be written in an operator Clenshaw approach, cf. Section 1.2, as

$$K(\mathrm{X},\mathrm{Y}) = (\mathbf{e}_0 \otimes I)\mathcal{L}^{-\mathsf{T}}\mathbf{K}_{\triangle}, \tag{2.8}$$

where $\otimes$ denotes the Kronecker product, $\mathbf{K}_{\triangle}$ represents the Proriol polynomial coefficients of the bivariate kernel function and $\mathcal{L}$ is defined to be

$$\mathcal{L} = \begin{pmatrix} (I_1\otimes I) & & & & \\ (A_0^x\otimes I)-(I_1\otimes \mathrm{X}) & (B_0^x\otimes I) & & & \\ (A_0^y\otimes I)-(I_1\otimes \mathrm{Y}) & (B_0^y\otimes I) & & & \\ (C_0^x\otimes I) & (A_1^x\otimes I)-(I_2\otimes \mathrm{X}) & (B_1^x\otimes I) & & \\ (C_0^y\otimes I) & (A_1^x\otimes I)-(I_2\otimes \mathrm{Y}) & (B_1^y\otimes I) & & \\ & \ddots & & \ddots & \ddots \end{pmatrix}.$$

When we introduced the Clenshaw method on the triangle in Section 1.3.2, we noted that these systems require preconditioning in order to use backward substitution. A preconditioner satisfying our requirements is

$$\begin{pmatrix} (I_1 \otimes I) & & & \\ & (B_0^+ \otimes I) & & \\ & & (B_1^+ \otimes I) & \\ & & & \ddots \end{pmatrix} \mathcal{L} = \tilde{\mathcal{L}},$$

where the blocks B_n^+ are defined exactly as in Section 1.3.2, cf. [77].

While the above approach allows us to compute the kernel multiplication operator effectively using an operator valued Clenshaw method, there are still substantial improvements we can make to our algorithm if the ultimate goal is to compute the Volterra integral operator. It is instructive to illustrate the general idea of these improvements the simpler context of monomial expansions first. Given a monomial expansion of a general kernel function $K(x,y) = \sum_{n=0}^{\infty}\sum_{j=0}^{n} k_{nj} x^{n-j} y^j$ we can write the Volterra integral operator in the following way using the results of the previous section:

$$\begin{aligned} \int_0^{1-x} K(x,y) f(y) \mathrm{d}y &= \tilde{\mathbf{P}}^{(1,0)}(x)(I - \bar{\mathrm{X}})\mathrm{Q}_y K(\mathrm{X},\mathrm{Y})\mathrm{E}_y \mathbf{f} \\ &= \tilde{\mathbf{P}}^{(1,0)}(x)(I - \bar{\mathrm{X}})\mathrm{Q}_y \left(\sum_{n=0}^{\infty}\sum_{j=0}^{n} k_{nj} \mathrm{X}^{n-j}\mathrm{Y}^j \right) \mathrm{E}_y \mathbf{f} \\ &= \tilde{\mathbf{P}}^{(1,0)}(x)(I - \bar{\mathrm{X}}) \sum_{n=0}^{\infty}\sum_{j=0}^{n} k_{nj} \bar{\mathrm{X}}^{n-j}\mathrm{Q}_y\mathrm{E}_y \bar{\mathrm{X}}^j \mathbf{f} \\ &= \tilde{\mathbf{P}}^{(1,0)}(x)(I - \bar{\mathrm{X}}) \sum_{n=0}^{\infty}\sum_{j=0}^{n} k_{nj} \bar{\mathrm{X}}^{n-j} D \bar{\mathrm{X}}^j \mathbf{f}, \end{aligned}$$

where again we note that the multiplication-by-x operator on the real interval is denoted by $\bar{\mathrm{X}}$ to avoid ambiguity with the triangle basis multiplication-by-x operator denoted X. Note that the second to last step used the commutation relationships in (2.5–2.6). The above derivation shows that instead of the very costly approach of generating the kernel multi-

plication operator (either via a direct expansion or operator valued Clenshaw algorithm) on the triangle and then multiplying it with all of the required operators one by one, we can instead generate the entire Volterra integral operator in the kernel computation step while making use of the diagonal nature of integration in these bases. Simultaneously we only require the use of the tridiagonal multiplication-by-x operators associated with the univariate Jacobi polynomials as opposed to the more involved multiplication operators on the triangle domain.

As stated, the monomial example was merely for illustrative purposes – in practice we will use this idea of using the commutation relationships to generate the Volterra integral operator during the kernel computation step but expand in the kernel in an orthogonal polynomial (Proriol) basis for substantially improved efficiency and convergence.

By replacing $\mathbf{K}_\triangle$ with $(\mathbf{K}_\triangle \otimes \mathrm{Q}_y\mathrm{E}_y)$ in (2.8) and using the commutation relationships (2.5–2.6) we find that all the X operators can be replaced by left multiplication by $\bar{\mathrm{X}}$ and all Y operators with right multiplication by $\bar{\mathrm{X}}$ respectively – we will denote this using $\diamond$ on the respective sides. The system to solve is then

$$\begin{aligned}\mathrm{Q}_y K(\mathrm{X},\mathrm{Y})\mathrm{E}_y &= (\mathbf{e}_0 \otimes I)\mathcal{L}_V^{-\mathsf{T}}(\mathbf{K}_\triangle \otimes \mathrm{Q}_y\mathrm{E}_y)\\ &= (\mathbf{e}_0 \otimes I)\mathcal{L}_V^{-\mathsf{T}}(\mathbf{K}_\triangle \otimes D),\end{aligned}$$

where we have

$$\mathcal{L}_V = \begin{pmatrix} (I_1 \otimes I) & & & & \\ (A_0^x \otimes I) - (I_1 \otimes \bar{\mathrm{X}}\diamond) & (B_0^x \otimes I) & & & \\ (A_0^y \otimes I) - (I_1 \otimes \diamond\bar{\mathrm{X}}) & (B_0^y \otimes I) & & & \\ (C_0^x \otimes I) & (A_1^x \otimes I) - (I_2 \otimes \bar{\mathrm{X}}\diamond) & (B_1^x \otimes I) & & \\ (C_0^y \otimes I) & (A_1^x \otimes I) - (I_2 \otimes \diamond\bar{\mathrm{X}}) & (B_1^y \otimes I) & & \\ & \ddots & & \ddots & \ddots \end{pmatrix}.$$

After preconditioning, as described above and in Section 1.2, this allows for efficient computation of $\mathrm{Q}_y K(\mathrm{X},\mathrm{Y})\mathrm{E}_y$ by taking advantage of the diagonality of $D = \mathrm{Q}_y\mathrm{E}_y$. Note that the weight $I - \bar{\mathrm{X}}$ was not included in this computation and thus must still be applied to this operator to obtain the full Volterra integral operator.

As the final part of this section we briefly mention how the described approach must be modified if we instead wish to integrate from 0 to x; there are two mathematically equivalent approaches: First, we may replace all the left multiplications with $\bar{\mathrm{X}}$ by left multiplications with $(I-\bar{\mathrm{X}})$ while the right multiplications remain as they are since they correspond to multiplications by y. The second option is to simply supply the function $H(x,y) = K(1-x,y)$ to the algorithm instead, avoiding the need for a separate implementation entirely.

2.5 Sparse spectral method for linear Volterra integral equations

This section details the sparse solution algorithms for linear Volterra integral equations of first and second-kind, as presented in Algorithm 1 and 2 on the basis of the results derived in the previous sections.

We begin with Volterra integral equations of second-kind, that is equations of the form

$$u(x) = g(x) + \int_0^x K(x,y)u(y)\mathrm{d}y,$$

where $g(x)$ and $K(x,y)$ are given. We have seen in the previous section that we can obtain the $\mathrm{Q}_y K(I-\mathrm{X},\mathrm{Y})\mathrm{E}_y$ part of the Volterra operator using a recursive operator-valued Clenshaw method but are left with a missing multiplication of $(I-\mathrm{X})$. An elegant quasimatrix version of the full equation may be found by introducing the weighted lowering operator $\mathrm{L}_{(1,0)}^{(0,0)}$, whose entries are found using the recurrence relationships in (1.9) and which maps from $\tilde{\mathbf{P}}^{(1,0)}(x)$ to $\tilde{\mathbf{P}}^{(0,0)}(x)$ while simultaneously multiplying by $(1-x)$. After an application of the reflection operator discussed in (2.4), we use the raising operator $\mathrm{S}_{(0,0)}^{(1,0)}$, whose entries

are given by the recurrence relationships (1.10), to return to our original basis of $\tilde{\mathbf{P}}^{(1,0)}(x)$. In summary, we can write the Volterra integral equations of the second-kind as

$$\tilde{\mathbf{P}}^{(1,0)}(x)\mathbf{u} = \tilde{\mathbf{P}}^{(1,0)}(x)\left(I - \mathrm{S}^{(1,0)}_{(0,0)}\mathrm{RL}^{(0,0)}_{(1,0)}\mathrm{Q}_y K(I - \mathrm{X}, \mathrm{Y})\mathrm{E}_y\right)^{-1}\mathbf{g},$$

which means that we can obtain $\mathbf{u}$ by solving a banded linear system, as all of the operators appearing in the above equation are banded. The reason we lower, reflect, then raise instead of just multiplying $(I - \mathrm{X})$ and then reflecting, is that the reflection operator acting on $\tilde{\mathbf{P}}^{(1,0)}(x)$ would move us to $\tilde{\mathbf{P}}^{(0,1)}(x)$ and thus an incompatible basis, whereas $\tilde{\mathbf{P}}^{(0,0)}(x)$ is mapped to $\tilde{\mathbf{P}}^{(0,0)}(x)$ due to the parameter symmetry. Consequently, if we instead intend to solve a second-kind Volterra integral equation with limits of integration 0 to $1 - x$, i.e. without the need for reflection, we instead obtain the slightly simpler form

$$\tilde{\mathbf{P}}^{(1,0)}(x)\mathbf{u} = \tilde{\mathbf{P}}^{(1,0)}(x)\left(I - (I - \bar{\mathrm{X}})\mathrm{Q}_y K(\mathrm{X}, \mathrm{Y})\mathrm{E}_y\right)^{-1}\mathbf{g}.$$

This procedure is summarized in Algorithm 2.

Next we briefly discuss the ways in which solving Volterra integral equations of first-kind differs from the method introduced for second-kind equations. First, it is evident from the symmetries of the first-kind equation that we will not require any reflections – this is because, in general if $u(x)$ solves

$$u(x) = \int_0^x K(x, y)u(y)\mathrm{d}y,$$

then clearly $u(1 - x)$ solves

$$u(1 - x) = \int_0^{1-x} K(1 - x, y)u(y)\mathrm{d}y,$$

and vice versa. In general this symmetry does not hold for second-kind equations. For technical reasons, the discussion of which we delay to the convergence analysis in Section 2.7,

the equation must furthermore first be divided by $(1-x)$ on both sides before expanding the functions in the appropriate bases. This means that the Clenshaw obtained term $\mathrm{Q}_y K(I - \mathrm{X}, \mathrm{Y})\mathrm{E}_y$ is already the to-be-inverted operator, i.e.:

$$\tilde{\mathbf{P}}^{(1,0)}(x)\mathbf{u} = \tilde{\mathbf{P}}^{(1,0)}(x)\left(\mathrm{Q}_y K(I - \mathrm{X}, \mathrm{Y})\mathrm{E}_y\right)^{-1}\mathbf{q},$$

where $q(x) = \frac{g(1-x)}{1-x}$. We summarize the full procedure in Algorithm 1.

Algorithm 1 Linear Volterra integral equations of first-kind

$$\int_0^x K(x,y)u(y)\mathrm{d}y = g(x).$$

1. Expand $q(x) = \frac{g(1-x)}{1-x}$ in $\tilde{\mathbf{P}}^{(1,0)}(x)$, obtaining $\mathbf{q}$.
2. Generate $\mathrm{Q}_y K(I - \mathrm{X}, \mathrm{Y})\mathrm{E}_y$ via operator-valued Clenshaw method.
3. Solve the banded linear system $\mathrm{Q}_y K(I - \mathrm{X}, \mathrm{Y})\mathrm{E}_y\mathbf{u} = \mathbf{q}$ for $\mathbf{u}$.
4. The solution is $\tilde{\mathbf{P}}^{(1,0)}(x)\mathbf{u}$.

Algorithm 2 Linear Volterra integral equations of second-kind

$$u(x) - \int_0^x K(x,y)u(y)\mathrm{d}y = g(x).$$

1. Expand $g(x)$ in $\tilde{\mathbf{P}}^{(1,0)}(x)$, obtaining $\mathbf{g}$.
2. Generate $\mathrm{Q}_y K(I - \mathrm{X}, \mathrm{Y})\mathrm{E}_y$ recursively via an operator-valued Clenshaw method.
3. Solve the banded linear system $\left(I - \mathrm{S}^{(1,0)}_{(0,0)}\mathrm{RL}^{(0,0)}_{(1,0)}\mathrm{Q}_y K(I - \mathrm{X}, \mathrm{Y})\mathrm{E}_y\right)\mathbf{u} = \mathbf{g}$ for $\mathbf{u}$.
4. The solution is $\tilde{\mathbf{P}}^{(1,0)}(x)\mathbf{u}$.

2.6 Integro-differential and nonlinear generalization

In this section we extend the above methods to integro-differential Volterra equations (VIDEs), nonlinear Volterra integral equations as well as simultaneously nonlinear and integro-differential Volterra equations. We begin with linear integro-differential Volterra equations, a for our purposes sufficiently general form of which is

$$\sum_{k=0}^{m} \lambda_k \frac{\mathrm{d}^k u}{\mathrm{d}x^k} = g(x) + \int_0^{\ell(x)} K(x,y)u(y)\mathrm{d}y, \tag{2.9}$$

for some $m \in \mathbb{N}_0$ and $\lambda_k \in \mathbb{R}$. As may be inferred from the derivative recurrence relationships for the univariate Jacobi polynomials in (1.7), the introduction of derivative operators of various orders needs to be treated with some care in order to maintain a consistent polynomial basis. First, we define the operator which acts on the coefficient space of $\tilde{\mathbf{P}}^{(1,0)}(x)$ to obtain the derivative as

$$f'(x) = \tilde{\mathbf{P}}^{(2,1)}(x)\mathcal{D}^{(1,0)}\mathbf{f},$$

where the entries are obtained via the recurrence in (1.7). Note the basis shift, which similarly holds in the general basis case, i.e.

$$f'(x) = \tilde{\mathbf{P}}^{(2+k,1+k)}(x)\mathcal{D}^{(1+k,k)}\mathbf{f}_{(1+k,k)},$$

where to avoid ambiguity we have labeled the coefficient vector $\mathbf{f}_{(1+k,k)}$ with a subscript indicating that it is an expansion in the basis $\tilde{\mathbf{P}}^{(1+k,k)}(x)$. Where we write no subscript in this chapter, we mean the coefficient vector with respect to $\tilde{\mathbf{P}}^{(1,0)}(x)$ as discussed above but when multiple bases are involved in an expression we will also make this basis explicit to avoid ambiguity.

Importantly, since first order derivatives cause a basis parameter shift, higher order derivatives are not obtained by simply re-applying the first order derivative operator. Instead,

they are comprised of consecutive applications of higher basis parameter versions of first order derivatives. We will thus denote the order of our derivative operatars by subscript, e.g. for the second order derivative we write

$$f''(x) = \tilde{\mathbf{P}}^{(3+k,2+k)}(x)\mathcal{D}^{(2+k,1+k)}\mathcal{D}^{(1+k,k)}\mathbf{f}_{(1+k,k)} = \tilde{\mathbf{P}}^{(3+k,2+k)}(x)\mathcal{D}_2^{(1+k,k)}\mathbf{f}_{(1+k,k)}.$$

Note that we choose the superscript on the second order operator such that it indicates what basis it *acts* on, as opposed to the basis it maps to, consistent with our above notation for the first order derivatives. In general we thus observe that the m-th order derivative operators act as

$$f^{(m)}(x) = \tilde{\mathbf{P}}^{(1+k+m,k+m)}(x)\mathcal{D}_m^{(1+k,k)}\mathbf{f}_{(1+k,k)}.$$

There are a number of reasons why the above discussion on its own is still insufficient to invert a sum of derivative operators and the Volterra integral operator. First and foremost, we will have to apply consistent raising operators to both the Volterra integral operator and all derivative operators which are not of the highest appearing order, for the resulting basis to be consistent with the shift caused by the highest order derivative operator. Second, the inverse of an operator mapping from basis $\tilde{\mathbf{P}}^{(1,0)}(x)$ to the some other basis $\tilde{\mathbf{P}}^{(1+m,m)}(x)$ also reverses this mapping, meaning that the function $g(x)$ should initially be expanded in the basis consistent with the highest order derivative, i.e. $\tilde{\mathbf{P}}^{(1+m,1+m)}(x)$ – in principle we could also compute an expansion in $\tilde{\mathbf{P}}^{(1,0)}(x)$ and apply a raising operator but this is computationally wasteful. The final piece we are missing is that differential equations are ill-posed without supplementary constraints on the solution, such as boundary conditions. In fact for a differential equation with highest appearing derivative order m, we in general require m boundary conditions, e.g.

$$\left.\frac{\mathrm{d}^k u}{\mathrm{d}x^k}\right|_{x=0} = c_k,$$

where $k = 0...m-1$ and $c_k \in \mathbb{R}$. Boundary conditions are enforced on coefficients by appending evaluation operators (which take the form of row vectors) as well as the initial conditions to the system. These evaluation operators in general lead to a loss of true bandedness of the operator, as they fill in the top m rows – we explore the structure of these operators further in the numerical experiments section. However, the resulting almost banded systems remain highly efficient to solve. We summarize the resulting procedure for linear VIDEs in Algorithm 3. Note that the entries of the evaluation operators, which we denote $\mathcal{E}_0$ may be obtained via the Jacobi polynomial properties in (1.4) and (1.5).

To solve nonlinear Volterra integral equations we use an iterative approach, meaning that we leverage the linear method along with a root search algorithm (such as Newton's method). We summarize the steps of the resulting nonlinear integral equation method in Algorithm 4. The same idea also allows us to solve integro-differential equations based on the linear VIDE solver we derived above – with Algorithm 5 detailing the steps.

2.7 Convergence proofs for the linear VIEs

In practice, computers cannot use the full analytic infinite-dimensional versions of the methods discussed in previous sections. Instead, as sketched in Section 1.1.5, we terminate the polynomial approximation of the appearing functions at some finite degree $N \in \mathbb{N}$. As a result, we also only ever have to compute $N \times N$ blocks of the infinite-dimensional banded operators.

In this section we prove convergence of the obtained truncated solution coefficient vectors $\mathbf{u}_N$ to the true solution $\mathbf{u}$ as $N \to \infty$, given appropriate assumptions. For this purpose we first define some useful operators.

Algorithm 3 Linear integro-differential Volterra equations (linear VIDEs)

$$\left(\sum_{k=0}^{m} \lambda_k \frac{\mathrm{d}^k u}{\mathrm{d}x^k}\right) - \int_0^x K(x,y)u(y)\mathrm{d}y = g(x), \quad \lambda_k \in \mathbb{R}; m \in \mathbb{N}$$

$$\left.\frac{\mathrm{d}^k u}{\mathrm{d}x^k}\right|_{x=0} = c_k, \quad k = 0...m-1 \text{ and } c_k \in \mathbb{R}.$$

1. Expand $g(x)$ in $\tilde{\mathbf{P}}^{(1+m,m)}(x)$.
2. Generate $\mathrm{Q}_y K(I - \mathrm{X}, \mathrm{Y})\mathrm{E}_y$ recursively via operator-valued Clenshaw method.
3. Generate the banded operator $\left(\sum_{k=0}^{m} \lambda_k \mathrm{S}^{(1+m,m)}_{(1+k,k)} \mathcal{D}^{(1,0)}_k - \mathrm{S}^{(1+m,m)}_{(0,0)} \mathrm{RL}^{(0,0)}_{(1,0)} \mathrm{Q}_y K(I - \mathrm{X}, \mathrm{Y})\mathrm{E}_y\right)$.
4. Append evaluation operators $(\mathcal{E}_0, \mathcal{E}_0\mathcal{D}^{(1,0)}, ...)$ to the top rows of the computed operator and append corresponding initial conditions $(c_0, c_1, ...)$ to the top of $\mathbf{g}_{(1+m,m)}$.
5. Solve the now almost banded linear system:
$$\begin{pmatrix} \mathcal{E}_0 \\ \mathcal{E}_0\mathcal{D}^{(1,0)} \\ \vdots \\ \mathcal{E}_0\mathcal{D}^{(m,m-1)}_{m-1} \\ \sum_{k=0}^{m} \lambda_k \mathrm{S}^{(1+m,m)}_{(1+k,k)} \mathcal{D}^{(1,0)}_k - \mathrm{S}^{(1+m,m)}_{(0,0)} \mathrm{RL}^{(0,0)}_{(1,0)} \mathrm{Q}_y K(I - \mathrm{X}, \mathrm{Y})\mathrm{E}_y \end{pmatrix} \mathbf{u}_{(1,0)} = \begin{pmatrix} c_0 \\ c_1 \\ \vdots \\ c_{m-1} \\ \mathbf{g}_{(1+m,m)} \end{pmatrix}$$
6. The approximate solution is $\tilde{\mathbf{P}}^{(1,0)}(x)\mathbf{u}_{(1,0)}$.

Algorithm 4 Non-linear Volterra integral equations

$$u(x) = g(x) + \int_0^x K(x,y) f(y, u(y)) \mathrm{d}y.$$

1. Expand $g(x)$ in $\tilde{\mathbf{P}}^{(1,0)}(x)$.
2. Generate $\mathrm{Q}_y K(I - \mathrm{X}, \mathrm{Y})\mathrm{E}_y$ recursively via operator-valued Clenshaw method.
3. Generate the operator $\left(I - \mathrm{S}_{(0,0)}^{(1,0)} \mathrm{RL}_{(1,0)}^{(0,0)} \mathrm{V}_K\right)$.
4. Use a simultaneous root-search algorithm (e.g. Newton method) for the elements of the objective function $F(\mathbf{u}) = \left(I - \mathrm{S}_{(0,0)}^{(1,0)} \mathrm{RL}_{(1,0)}^{(0,0)} \mathrm{V}_K\right) \mathbf{f}(y, \mathbf{u}) - \mathbf{g}$.
5. The approximate solution is given by the obtained root $\tilde{\mathbf{P}}^{(1,0)}(x)^{\mathsf{T}}\mathbf{u}$.

Definition 2.4 (Analysis and synthesis operators)**.** *We define the analysis operator*

$$\mathcal{E} : L^2(0,1) \to \ell^2$$

as the inclusion of a square integrable function into the infinite-dimensional Banach sequence space ℓ^2 of normalized shifted Legendre polynomials $\tilde{\mathbf{P}}(x)$. Furthermore, we define the synthesis operator as the inverse of the analysis operator:

$$\mathcal{E}^{-1} : \ell^2 \to L^2(0,1).$$

The terminology ('analysis' and 'synthesis') are borrowed from frame theory [29]. We note as an important property of the above defined operators that they are both *bounded*. We furthermore note a distinction between the bases used in our descriptions of the algorithms and the proofs we present in this section: In these proofs we will use the fact that the basis obtained for the linear Volterra integral equations is of the form $(1-x)\mathbf{P}^{(1,0)}(x)$, meaning that it is possible to use conversion operators to transform our method into one which uses only normalized Legendre polynomials via the weighted lowering relationships in (1.9).

Algorithm 5 Non-linear integro-differential Volterra equations

$$\left(\sum_{k=0}^{m} \lambda_k \frac{\mathrm{d}^k u}{\mathrm{d}x^k}\right) - \int_0^x K(x,y) f(y,u(y)) \mathrm{d}y = g(x), \quad \lambda_k \in \mathbb{R}; m \in \mathbb{N}$$

$$\left.\frac{\mathrm{d}^k u}{\mathrm{d}x^k}\right|_{x=0} = c_k, \quad k = 0...m-1 \text{ and } c_k \in \mathbb{R}.$$

1. Expand $g(x)$ in $\tilde{\mathbf{P}}^{(1+m,m)}(x)$.
2. Generate $\mathrm{Q}_y K(I - \mathrm{X}, \mathrm{Y})\mathrm{E}_y$ recursively via operator-valued Clenshaw method.
3. Generate the banded operator $\left(\sum_{k=0}^{m} \lambda_k \mathrm{S}^{(1+m,m)}_{(1+k,k)} \mathcal{D}^{(1,0)}_k - \mathrm{S}^{(1+m,m)}_{(0,0)} \mathrm{RL}^{(0,0)}_{(1,0)} \mathrm{Q}_y K(I - \mathrm{X}, \mathrm{Y})\mathrm{E}_y\right)$.
4. Append evaluation operators $(\mathcal{E}_0, \mathcal{E}_0\mathcal{D}^{(1,0)}, ...)$ as the first row of the operator and append corresponding initial conditions $(c_0, c_1, ...)$ to the top of $\mathbf{g}_{(1+m,m)}$.
5. Use a simultaneous root-search algorithm (e.g. Newton method) for the elements of the objective function
$$F(\mathbf{u}) = \begin{pmatrix} \mathcal{E}_0\mathbf{u} - c_0 \\ \mathcal{E}_0\mathcal{D}^{(1,0)}\mathbf{u} - c_1 \\ \vdots \\ \mathcal{E}_0\mathcal{D}^{(m,m-1)}_{m-1}\mathbf{u} - c_{m-1} \\ \left(\sum_{k=0}^{m} \lambda_m \mathrm{S}^{(1+m,m)}_{(1+k,k)} \mathcal{D}^{(1,0)}_k - \mathrm{S}^{(1+m,m)}_{(0,0)} \mathrm{RL}^{(0,0)}_{(1,0)} \mathrm{Q}_y K(I - \mathrm{X}, \mathrm{Y})\mathrm{E}_y\right) \mathbf{f}(y,\mathbf{u}) - \mathbf{g}_{(1+m,m)} \end{pmatrix}.$$
6. The approximate solution is given by the obtained root $\tilde{\mathbf{P}}^{(1,0)}(x)^{\mathsf{T}}\mathbf{u}$.

Definition 2.5 (Truncation projection operator)**.** *We define the truncation projection operators $\mathcal{P}_n : \ell^2 \to \ell^2$ to map an infinite coefficient vector to a truncated version with zeros after a cutoff point given by n, that is:*

$$\mathcal{P}_n \begin{pmatrix} u_1 \\ \vdots \\ u_n \\ u_{n+1} \\ \vdots \end{pmatrix} = \begin{pmatrix} u_1 \\ \vdots \\ u_n \\ 0 \\ \vdots \end{pmatrix}.$$

We now mention two classical results on the existence of solutions to the analytic Volterra integral equations in certain well-behaved special cases. For our numerical approach we will always assume that the problems we wish to solve have unique solutions; analytic topics such as uniqueness and existence of solutions to these types of equations have been discussed at length in the literature and we refer to e.g. [21, 88, 113] for details.

Theorem 2.2. *Let $I = [0, T]$, let $\mathcal{V} : C(I) \to C(I)$ denote the linear Volterra integral operator*

$$(\mathcal{V}u)(t) := \int_0^t K(t, s)u(s)\mathrm{d}s, \quad t \in I,$$

with the kernel $K(t, s)$ continuous on $D = \{(t, s), 0 \leqslant s \leqslant t \leqslant T\}$. Furthermore, let $R(t, s)$ be the resolvent kernel associated with K defined by

$$R(t, s) := \lim_{\nu \to \infty} \sum_{n=1}^{\nu} K_n(t, s),$$
$$K_n(t, s) := \int_s^t K_r(t, v)K_{n-r}(v, s)\mathrm{d}v, \quad (t, s) \in D,$$
$$K_1(t, s) := K(t, s).$$

Then for any $f \in C(I)$ the second kind Volterra integral equation

$$u(t) - (\mathcal{V}u)(t) = f(t),$$

posesses a unique solution $u \in C(I)$ which can be written in the form

$$u(t) = f(t) + \int_0^t R(t,s)f(s)\mathrm{d}s, \quad t \in I.$$

Proof. For a proof of this result see [21, Chapter 1.2.1]. □

Theorem 2.3. *Let $K \in C(D)$ with $D = \{(t,s), 0 \leqslant s \leqslant t \leqslant T\}$ and $\frac{\partial K}{\partial t} \in C(D)$ and let $K(t,t) \neq 0$ for all $t \in I := [0,T]$. Then for any $g \in C^1(I)$ with $g(0) = 0$, the Volterra integral equation of first kind*

$$\int_0^t K(t,s)u(s)\mathrm{d}s = g(t), \quad t \in I,$$

posesses a unique solution $u \in C(I)$ satisfying

$$u(0) = \frac{g'(0)}{K(0,0)}.$$

Proof. For a proof of this result we refer to [21, Chapter 1.4.1]; the original proof is due to Volterra himself [109]. □

Note that existence and uniqueness of solutions for Volterra integral equations has been studied in more general spaces such as $L^2(I)$ as well as for more general kernels for which we refer to [21, 88, 113] and the references therein.

For numerical convergence, our proof strategy is to find a representation of the to-be-inverted operators as compact perturbations of the identity, i.e.

$$(I + \mathcal{K})u = g, \tag{2.10}$$

where $\mathcal{K}$ is a compact operator. By the Fredholm alternative, see e.g. [13, 60], we then immediately know that the operators are either invertible or neither injective nor surjective. Standard convergence results from the theory of finite section methods then complete the convergence proofs. While the general strategy is thus similar for both first and second-kind equations, the way we derive a representation for them in terms of compact perturbations of the identity differ substantially and we thus address them separately – beginning with the easier to analyze second-kind equations.

Lemma 2.1. *The Volterra integral operator* $\mathrm{V}_K : \ell^2 \to \ell^2$ *with limits of integration from* 0 *to* x *acting on the coefficient Banach space of the Legendre polynomial basis* $\tilde{\mathbf{P}}(x)$ *can be represented as*

$$\mathrm{V}_K = \mathrm{RL}^{(0,0)}_{(1,0)}\mathrm{Q}_y K(I - \mathrm{X}, \mathrm{Y})\mathrm{E}_y\mathrm{S}^{(1,0)}_{(0,0)},$$

for a given kernel function $K(x, y) \in L^2[T^2]$ *and with the respective operators as defined in Section 2.3. Furthermore, this operator is* compact.

Proof. The form of the operator was derived in Section 2.3. The compactness of V_K follows from its relationship to the known to be compact Volterra integral operator on the space of square integrable functions which we write $\mathcal{V}_K$ for a $K(x, y) \in L^2[T^2]$:

$$\begin{array}{ccc} L^2(0,1) & \xrightarrow{\mathcal{V}_K} & L^2(0,1) \\ \mathcal{E}\downarrow & & \uparrow\mathcal{E}^{-1} \\ \ell^2 & \xrightarrow[\mathrm{V}_K]{} & \ell^2 \end{array}$$

The compactness of $\mathcal{V}_K$ (which is a Hilbert-Schmidt operator) is a classical result of functional analysis, cf. [68]. Since V_K is thus a finite composition of bounded and a compact operators from and to Banach spaces, it is itself also compact. □

Lemma 2.2. *The coefficient space Volterra integral operator* V_K *and truncation projection operator* $\mathcal{P}_n$*, defined as above, satisfy*

$$\lim_{n\to\infty} \|\mathrm{V}_K - \mathcal{P}_n \mathrm{V}_K \mathcal{P}_n^{\mathsf{T}}\| = 0.$$

Proof. This is a corollary of the compactness of V_K and ℓ^2 having the approximation property as it is a Hilbert space, cf. [60]. □

Corollary 2.1. *For well-posed Volterra integral equations of second-kind, Algorithm 2 converges in the sense that*

$$\|\mathbf{u} - \mathcal{P}_n \mathbf{u}\| \to 0 \quad as \quad n \to \infty.$$

Proof. By Lemma 2.1 the operator for which we intend to solve truncated problems can be written as a compact perturbation of the identity, i.e. $I + \mathcal{K}$ with $\mathcal{K} = -\mathrm{V}_K$ compact. The result is then a corollary of Lemmas 2.1 and 2.2 combined with the convergence results for problems involving compact perturbations of the identity in the theory of finite section methods, for which we refer to [18]. □

Remark 2.1. *For polynomial kernels* $K(x, y)$*, our method (for both equations of first and second kind) computes the expansion coefficients in the orthogonal polynomial basis in the sense discussed in Chapter 1. In particular, this means that the convergence rate with respect to the degree of the polynomial approximation* n *follows known convergence properties for these bases, with the precise convergence properties depending e.g. on the smoothness of the solution. We refer to [106] for a standard work discussing these convergence rates.*

The three above results provide the necessary justification to treat the solutions obtained by means of Algorithm 2 as approximations to the unique solution of a Volterra integral equation of second-kind. We will now prove a similar result for Algorithm 1. The proof of the analogous first-kind result should be expected to be substantially different, since as we saw in Lemma 2.1, both operators $\mathcal{V}_K$ and V_K are compact on the respective spaces. To obtain a sense in which we can still invert these operators and approximate them in a convergent way, we need to introduce some restrictions to our spaces. To that end, we introduce the following definition:

Definition 2.6. *We denote by* ℓ^2_λ, $\lambda \geqslant 0$ *the Banach sequence space with norm*

$$\|\mathbf{u}\|_{\ell^2_\lambda} = \sqrt{\sum_{n=0}^{\infty} \left((1+n)^\lambda |u_n|\right)^2} < \infty.$$

We may loosely think of these λ-spaces as a Sobolev space analogue for sequence spaces. In what follows we will use the fact that for any $\mathbf{u} \in \ell^2_\lambda$, we also have $\mathbf{u} \in \ell^2$, meaning that $\ell^2_\lambda \subset \ell^2$ (the converse of this does not hold for $\lambda > 0$). We will see that by restricting our Volterra operator to acting on such λ-spaces, we can obtain the desired convergence results as the operator turns out to no longer be compact.

We will present the proofs for the example of monomial expansions of the kernel as opposed to the orthogonal polynomial Clenshaw approach we described, as while it is less efficient computationally it is mathematically equivalent and much easier to work with.

Lemma 2.3. *For a given* polynomial *kernel of general form*

$$K(x,y) = \sum_{n=0}^{M} \sum_{j=0}^{n} k_{nj} x^{n-j} y^j,$$

the Volterra integral operator with limits of integration from 0 *to* x *acting on the coefficient*

space of the shifted Legendre polynomials $\tilde{\mathbf{P}}(x)$ *satisfies*

$$\mathrm{V}_K = \mathrm{RL}^{(0,0)}_{(1,0)}\mathrm{D}\left(\mathrm{D}^{-1}\sum_{n=0}^{M}\sum_{j=0}^{n} k_{nj}(I-\bar{\mathrm{X}})^{n-j}\mathrm{D}\bar{\mathrm{X}}^j\right)\mathrm{S}^{(1,0)}_{(0,0)},$$

where the diagonal operator D *satisfies* $\mathrm{D} = \mathrm{Q}_y\mathrm{E}_y$*, with* Q_y *and* E_y *as in Section 2.3.*

Proof. That the Volterra operator is of this form if D^{-1} exists and that $\mathrm{D} = \mathrm{Q}_y\mathrm{E}_y$ is diagonal with n-th diagonal entry $\frac{(-1)^{n+1}}{n}$ was shown in Section 2.3, compare also [73, 18.6.1 and 18.17.1]. Note that importantly, by definition of the λ sequence spaces one finds that D actually maps into ℓ^2_1, that is $\mathrm{D} : \ell^2 \to \ell^2_1$, making D an invertible bounded operator with inverse $\mathrm{D}^{-1} : \ell^2_1 \to \ell^2$. The result then follows immediately from $D^{-1}D = I$. □

Lemma 2.4. *The Volterra operator* V_K *has a representation in terms of a product of invertible operators with a compact perturbation of a Toeplitz operator, i.e.:*

$$\tilde{\mathrm{V}}_K = \mathrm{L}^{(0,0)}_{(1,0)}\mathrm{D}(\mathrm{T}[f] + \mathcal{K})\mathrm{S}^{(1,0)}_{(0,0)},$$

where $\mathrm{T}[f]$ *is a Toeplitz operator with symbol* f *and* $\mathcal{K}$ *is a compact operator. The symbol* f *of the Toeplitz operator* $\mathrm{T}[f]$ *has explicit form*

$$f(z) = \sum_{n=0}^{M}\sum_{j=0}^{n} k_{nj}\cos^{2n}\left(\frac{\theta}{2}\right) \quad \textit{with} \quad z = \mathrm{e}^{\mathrm{i}\theta},$$

where k_{nj} *are the unique coefficients of the polynomial kernel*

$$K(x,y) = \sum_{n=0}^{M}\sum_{j=0}^{n} k_{nj}x^{n-j}y^j$$

Proof. By Lemma 2.3 the Volterra operator V_K is known to be of the form

$$\mathrm{V}_K = \mathrm{L}^{(0,0)}_{(1,0)}\mathrm{D}\left(\sum_{n=0}^{M}\sum_{j=0}^{n} k_{nj}\mathrm{D}^{-1}(I-\bar{\mathrm{X}})^{n-j}\mathrm{D}\bar{\mathrm{X}}^j\right)\mathrm{S}^{(1,0)}_{(0,0)}.$$

We thus seek a representation of $\left(\sum_{n=0}^{M}\sum_{j=0}^{n} k_{nj}\mathrm{D}^{-1}(I-\bar{\mathrm{X}})^{n-j}\mathrm{D}\bar{\mathrm{X}}^{j}\right)$ as a compact perturbation of a Toeplitz operator. We will make use of the result that given sufficient continuity assumptions on the kernel (which are automatically satisfied in this case because it is a polynomial) the following relationship holds for a multiplication of two Toeplitz operators:

$$T[a]T[b] = T[ab] - H[a]H[\bar{b}], \tag{2.11}$$

with the operators $H[a]$, $H[\bar{a}]$ and $H[\bar{b}]$ being compact Hankel operator – we refer to [17] for discussion and proof of this result. In the case that $a = b$ the above result reduces to

$$T[a]T[a] = T[a^2] - H[a]H[\bar{a}].$$

An important corollary of the above statement is that any finite power of an asymptotically Toeplitz operator (satisfying the appropriate continuity assumptions on the symbol) again yields an asymptotically Toeplitz operator, since e.g.

$$(T+\mathcal{K})^2 = T^2 + T\mathcal{K} + \mathcal{K}T + \mathcal{K}^2.$$

This is asymptotically Toeplitz because T^2 is asymptotically Toeplitz by the above cited result, while the remaining terms are compositions of bounded operators and compact operators, making $T\mathcal{K} + \mathcal{K}T + \mathcal{K}^2$ compact. Induction may be used to prove this result for any finite power. Since $\bar{X}$ is known to be an asymptotically Toeplitz operator, the above discussion shows that all operators of the form $\bar{X}^j$ as well as $\mathrm{D}^{-1}(I-\bar{\mathrm{X}})^j\mathrm{D}$ are also asymptotically Toeplitz. Furthermore, we note that the operators $\bar{\mathrm{X}}$ and $\mathrm{D}^{-1}(I-\bar{\mathrm{X}})\mathrm{D}$ differ only in their compact part, with their Toeplitz component being the same. As sums of asymptotically Toeplitz operators are straightforwardly seen to be asymptotically Toeplitz as well,

this proves that the expression

$$\left(\sum_{n=0}^{M}\sum_{j=0}^{n} k_{nj}\mathrm{D}^{-1}(I-\bar{\mathrm{X}})^{n-j}\mathrm{D}\bar{\mathrm{X}}^{j}\right)$$

indeed does have a representation as $(\mathrm{T}[f]+\mathcal{K})$. What remains to be demonstrated is the claimed explicit form of the symbol f of $\mathrm{T}[f]$. Since the multiplication operator $\bar{\mathrm{X}}$ for the basis $\tilde{\mathbf{P}}^{(1,0)}(x)$ is banded with explicitly known entries it is straightforward to observe that its symbol is

$$\left(\frac{1}{2}+\frac{z}{4}+\frac{\bar{z}}{4}\right)=\cos^2\left(\frac{\theta}{2}\right).$$

As discussed above, this is thus also the symbol of the Toeplitz component of $\mathrm{D}^{-1}(I-\bar{\mathrm{X}})\mathrm{D}$. Furthermore, we have

$$\mathrm{D}^{-1}(I-\bar{\mathrm{X}})^{n-j}\mathrm{D}=(\mathrm{D}^{-1}(I-\bar{\mathrm{X}})\mathrm{D})^{n-j}.$$

Putting all of these observations together, we obtain the explicit form of the desired symbol of $\left(\sum_{n=0}^{M}\sum_{j=0}^{n} k_{nj}\mathrm{D}^{-1}(I-\bar{\mathrm{X}})^{n-j}\mathrm{D}\bar{\mathrm{X}}^{j}\right)$:

$$f(z)=\sum_{n=0}^{M}\sum_{j=0}^{n} k_{nj}\cos^{2n}\left(\frac{\theta}{2}\right).$$

□

Theorem 2.4. *The method described in Algorithm 1 converges for well-posed Volterra integral equations of the first-kind* $\mathrm{V}_K\mathbf{u}=\mathbf{g}$ *with limits of integration* 0 *to* x *and with a polynomial kernel* $K(x,y)\in L^2[T^2]$ *if both of the following conditions are true:*

- $\mathfrak{g}\in\ell_1^2$, *where* $\mathfrak{g}$ *is defined by* $(1-x)g(x)=\tilde{\mathbf{P}}^{(1,0)}(x)\mathfrak{g}$.
- *The symbol of the Toeplitz component of the asymptotically Toeplitz part of the Volterra*

operator in Lemma 2.4 does not vanish on the unit circle – an equivalent condition is that $\forall x \in [0,1] : K(x,x) \neq 0$.

Proof. The first condition is a consequence of the spaces the operator in Lemma 2.3 maps between. One way to see this is that, after expanding $g(1-x) = \tilde{\mathbf{P}}(x)\mathrm{R}\mathbf{g}$ in Legendre basis, inverting the partial operators sequentially from the left requires using $D^{-1}\left(\mathrm{L}^{(0,0)}_{(1,0)}\right)^{-1}\mathrm{R}^{-1}$. We then note that by definition of the respective operators

$$\left(\mathrm{L}^{(0,0)}_{(1,0)}\right)^{-1}\mathrm{R}^{-1}\mathrm{R}\mathbf{g} = (I - \bar{X})\mathrm{S}^{(1,0)}_{(0,0)}\mathbf{g} = \mathfrak{g}$$

where $\mathfrak{g}$ are the coefficients of $(1-x)g(x)$ in the basis $\tilde{\mathbf{P}}^{(1,0)}(x)$. Finally, since D maps into ℓ^2_1, that is $\mathrm{D} : \ell^2 \to \ell^2_1$, taking its inverse puts the stated condition on the Jacobi polynomial coefficients of $(1-x)g(x)$.

The proof of the second condition requires the introduction of some auxilliary results: An asymptotically Toeplitz operator of the form $(\mathrm{T} + \mathcal{K})$ is known to be invertible if it is a Fredholm operator, its index is 0 and its kernel is trivial, cf. [51, 18, 43] and the references therein. Additionally, a sufficient condition for an asymptotically Toeplitz operator to be Fredholm is for its symbol, i.e. the symbol of its Toeplitz component, to not be zero anywhere on the complex unit circle. The final auxilliary result we require is that the index of a Fredholm Toeplitz operator is the sign-inverted winding number of its symbol on the complex unit disk, cf. [18].

We saw in Lemma 2.4 that the symbol of the T appearing in the Volterra operator is real valued and continuous. As a result, its index is 0 if and only if it does not vanish on the complex unit circle which as noted above is equivalent to the operator being Fredholm. Next we investigate possible vanishing points of the symbol: Since $\cos^2\left(\frac{\theta}{2}\right) \in [0,1]$, requiring that

$$\sum_{n=0}^{M}\sum_{j=0}^{n} k_{nj}\cos^{2n}\left(\frac{\theta}{2}\right) = 0,$$

for some $\theta \in [0, 2\pi)$ is equivalent to requiring that for some $x \in [0, 1]$ we have

$$\sum_{n=0}^{M} \sum_{j=0}^{n} k_{nj} x^n = 0.$$

This is turn is equivalent to the condition that the polynomial kernel $K(x, y)$ evaluated at $y = x$ vanishes:

$$K(x, x) = \sum_{n=0}^{M} \sum_{j=0}^{n} k_{nj} x^{n-j} x^j = \sum_{n=0}^{M} \sum_{j=0}^{n} k_{nj} x^n.$$

Consequently, if we have $\forall x \in [0, 1] : K(x, x) \neq 0$, then the operator $(\mathrm{T} + \mathcal{K})$ appearing in the Volterra operator is a Fredholm operator because its symbol does not vanish anywhere on the complex unit circle. Furthermore, if this is the case, we also know that its index is 0 since the symbol is real-valued and thus has winding number 0. The final part is to show that $(\mathrm{T} + \mathcal{K})$ has a trivial kernel, which is a consequence of the Volterra integral operator having no non-zero eigenvalues. The convergence of the method then becomes a straightforward consequence of known results in finite section method theory for which we refer to [51]. □

The above results show convergence for well-posed linear Volterra integral equations of first-kind under appropriate conditions but only for *polynomial* kernels. To prove that we may extend theses results to general kernels we will require the following known auxilliary theorem, cf. [12, 107], which we restate here:

Theorem 2.5. *Let X and Y be normed linear spaces with at least one of them also being a Banach space. Furthermore, let $\mathcal{T} : X \to Y$ be a bounded and invertible operator. If the operator $\mathcal{M} : X \to Y$ is bounded and satisfies*

$$\|\mathcal{M} - \mathcal{T}\| < \frac{1}{\|\mathcal{T}^{-1}\|},$$

then $\mathcal{M}$ is invertible with bounded inverse $\mathcal{M}^{-1} : Y \to X$ satisfying

$$\|\mathcal{M}^{-1}\| \leqslant \frac{\|\mathcal{T}^{-1}\|}{1 - \|\mathcal{T}^{-1}\|\|\mathcal{T} - \mathcal{M}\|}$$

and

$$\|\mathcal{M}^{-1} - \mathcal{T}^{-1}\| \leqslant \frac{\|\mathcal{T}^{-1}\|^2\|\mathcal{T} - \mathcal{M}\|}{1 - \|\mathcal{T}^{-1}\|\|\mathcal{T} - \mathcal{M}\|}.$$

Proof. We refer to [12, 107] for discussions of this result. □

Next, we show how to use Theorem 2.5 to extend our convergence result for linear Volterra integral equations to more general kernels.

Lemma 2.5. *If a sequence of reduced Volterra integral operators for polynomial kernels $K_M(x, y)$ of degree M converges as $M \to \infty$ in the sense that*

$$\|\tilde{\mathrm{V}}_{K_M} - \tilde{\mathrm{V}}_K\| \xrightarrow[M\to\infty]{} 0,$$

then the solutions to their respective first-kind equations also satisfy

$$\|\mathbf{u}_M - \mathbf{u}\| \xrightarrow[M\to\infty]{} 0,$$

where $\mathbf{u}_M$ is the solution to the M-th degree approximate equation $\tilde{\mathrm{V}}_{K_M}\mathbf{u}_M = \mathbf{q}$.

Proof. Setting $\mathcal{M} = \tilde{\mathrm{V}}_{K_M}$ and $\mathcal{T} = \tilde{\mathrm{V}}_K$, the result follows via Theorem 2.5: If we have

$$\|\tilde{\mathrm{V}}_{K_M} - \tilde{\mathrm{V}}_K\| \xrightarrow[M\to\infty]{} 0,$$

then it follows from Theorem 2.5 that

$$\|\tilde{\mathrm{V}}_{K_M} - \tilde{\mathrm{V}}_K\| < \frac{1}{\|\tilde{\mathrm{V}}_K^{-1}\|}.$$

This implies, again via Theorem 2.5, that if $\tilde{\mathrm{V}}_K$ is invertible then so is $\tilde{\mathrm{V}}_{K_M}$ but more importantly it shows that the solutions to the sequence of equations with increasing polynomial degree converge in the sense that

$$\|\tilde{\mathrm{V}}_{K_M}^{-1} - \tilde{\mathrm{V}}_K^{-1}\| < \frac{\|\tilde{\mathrm{V}}^{-1}\|^2\|\tilde{\mathrm{V}}_{K_M} - \tilde{\mathrm{V}}_K\|}{1 - \|\tilde{\mathrm{V}}^{-1}\|\|\tilde{\mathrm{V}}_{K_M} - \tilde{\mathrm{V}}_K\|} \xrightarrow[M\to\infty]{} 0$$

□

2.8 Numerical experiments and validation

The numerical experiments in this section were performed using an open source proof-of-concept implementation of the methods introduced in this chapter. The code is freely available at [44] and makes use of the ApproxFun [1] Julia package ecosystem for approximating functions in orthogonal polynomial bases.

2.8.1 Linear Volterra integral equations

Simple examples with known solutions

We seek numerical solutions to the following linear Volterra integral equations for $x \in [0, 1]$:

$$u_1(x) = x + \int_0^{1-x} (y - x) \sinh(x^2) u_1(y) \mathrm{d}y \tag{2.12}$$

$$\int_0^{1-x} y u_2(y) \mathrm{d}y = \frac{x-1}{2\pi} \cos(-2\pi x) + \frac{4\pi^2 + 1}{4\pi^2} \sin(2\pi(1-x)), \tag{2.13}$$

$$\int_0^{x} e^{y-x} u_3(y) \mathrm{d}y = \frac{e^{-x}}{2} + \frac{e^x(2x-1)}{2}. \tag{2.14}$$

Note that Equation (2.12) is a Volterra integral equation of second-kind, while Equation (2.13) and Equation (2.14) are Volterra integral equations of first-kind. The analytic solutions to the above integral equations are known to be:

$$u_1 = \frac{(x-1)^2(2-5x)\sinh(x^2)}{6}, \tag{2.15}$$

$$u_2 = \sin(-2\pi x), \tag{2.16}$$

$$u_3 = 2xe^x. \tag{2.17}$$

In Figure 2.1 we plot the absolute error between numerically obtained and analytic solutions for suitably converged fixed order of approximation. In Figure 2.2 we plot the convergence behavior with increasing degree of the polynomial approximation. In agreement with expectation we observe exponential convergence in the form of a linear plot on semi-logarithmic

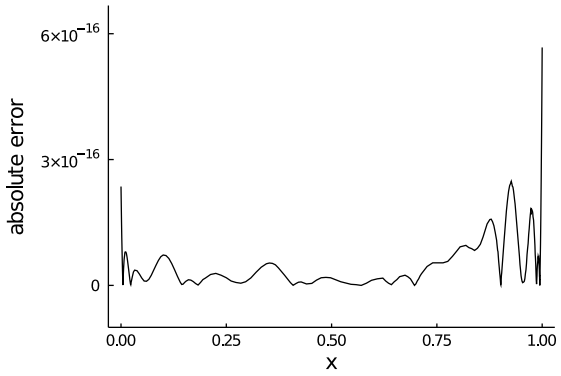

(a) $u_1, n = 25$

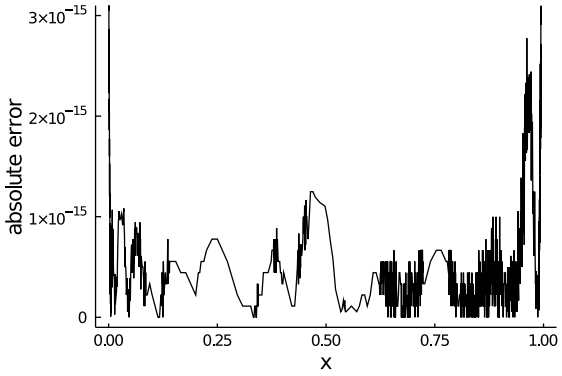

(b) $u_2, n = 20$

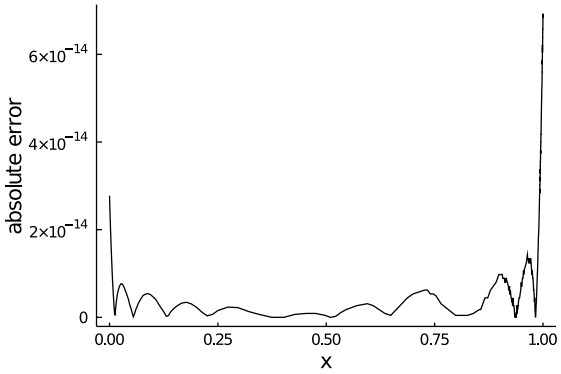

(c) $u_3, n = 20$

Figure 2.1: Absolute error between numerically obtained solutions for the linear Volterra integral equations in (2.12-2.14) and their analytic solutions in (2.15-2.17) for indicated fixed degree of the polynomial approximation.

axes.

Direct comparisons with other available methods

In this section we present a comparison with state-of-the-art collocation method Matlab software package Chebfun [33]. Solving Volterra integral equations with Chebfun was addressed in a recent paper by Driscoll, see [32]. We use the following problem for our comparison which is same problem compared in [49]:

$$u_k(x) = g_k(x) + \int_0^x (x + y)u_k(y)\mathrm{d}y, \tag{2.18}$$

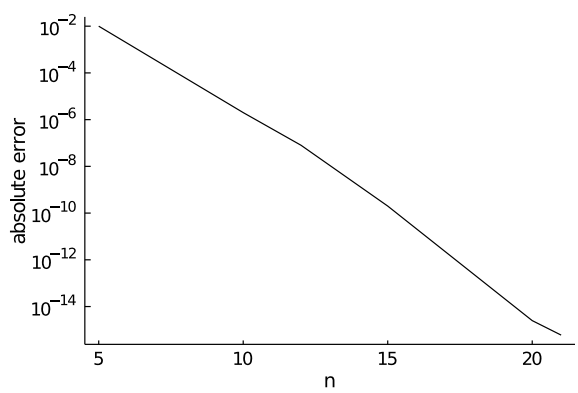

(a) u_1

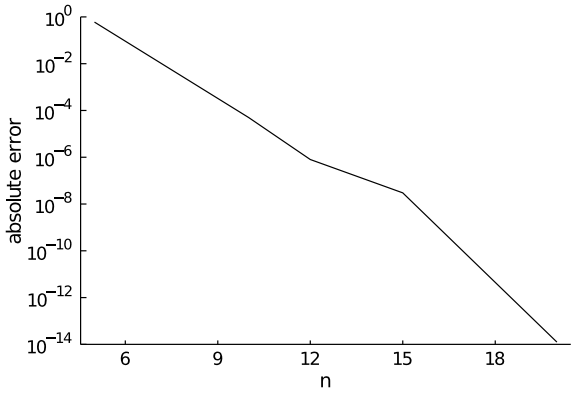

(b) u_2

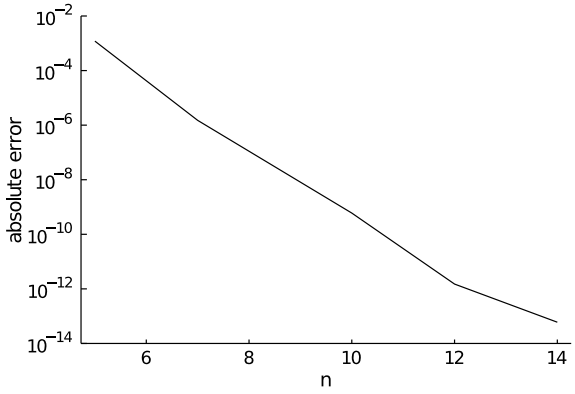

(c) u_3

Figure 2.2: Semi-logarithmic convergence plots of numerically obtained solutions for the linear Volterra integral equations in (2.12-2.14) to their analytic solutions in (2.15-2.17).

Method	k	CPU time	approximation degree	absolute error
Sparse method	1	0.001s	19	7.8e-16
	10	0.002s	128	4.0e-14
	50	0.08s	2200	9.0e-13
	75	0.29s	3850	3.1e-12
Chebfun	1	0.18s	17	1.0e-15
	10	0.48s	119	2.9e-14
	50	27.0s	1768	7.9e-13
	75	163.5s	4096	2.0e-12

Table 2.1: Accuracy and performance comparison of sparse method and Chebfun for Equation (2.18) first published in [49]. The CPU time was measured on an Intel Core i7-6700T CPU @ 2.80GHz.

where $g_k(x)$ contains a type-S Fresnel integral [73, 7.2(iii)]:

$$g_k(x) = \frac{\cos\left(k^2x^2\right) + 2k^2\sin\left(k^2x^2\right) - 1}{2k^2} - \frac{x}{k}\sqrt{\frac{\pi}{2}}\int_0^{\sqrt{\frac{2}{\pi}}kx} \sin\left(\frac{\pi y^2}{2}\right) \mathrm{d}y.$$

The above equation has analytically known solutions $\forall k \in \mathbb{N}$:

$$u_k(x) = \sin(k^2x^2). \tag{2.19}$$

A comprehensive comparison for errors and processing time with increasing k using our sparse method and Chebfun is presented in Table 2.1 which was first published in [49] (note that Chebfun automatically chooses its approximation order based on convergence criteria). To keep the comparison fair, we do not include the approximation of $g_k(x)$ in the benchmark for either our sparse method or Chebfun, as language inherent differences for the computation of Fresnel integrals otherwise obscure the difference between the Volterra integral aspects of the methods. The sparse method compares favorably both in accuracy and performance, the latter being a consequence of the bandedness of the involved operators. We present similar successes for integro-differential equations as part of the next section.

Linear Volterra integral equations of third-kind

As mentioned in Section 2.1 the methods introduced in this chapter can also be extended to certain kinds of third-kind equations, here understood to mean equations of the form

$$x^{\mu}u(x) = g(x) + \int_0^x K(x,y)u(y)\mathrm{d}y,$$

although currently no guarantees for convergence are known. We present the following third-kind equation

$$x^{\mu}u_{\mu}(x) = x^{\mu} + x^{\mu+1} + x^{\mu+2} + \int_0^x y^{\mu-1}u_{\mu}(y)\mathrm{d}y \tag{2.20}$$

as an example for which our sparse method successfully converges to the analytically known solution (see [114] for a derivation):

$$u_{\mu}(x) = \frac{\mu}{\mu-1} + \frac{\mu+1}{\mu}x + \frac{\mu+2}{\mu+1}x^2. \tag{2.21}$$

In Figure 2.3 we plot the absolute errors between the numerically obtained polynomial approximation and analytic solutions for three different values of μ. As is to be expected, the error is orders of magnitude worse near the boundary singularity of the third-kind equation (in this case $x = 0$). An additional third-kind example where similar behavior is observed is discussed in [49] but as mentioned above, unlike the first and second-kind case for now no numerical guarantees, e.g. via regularization or constraints on functions, are known for this class of equations.

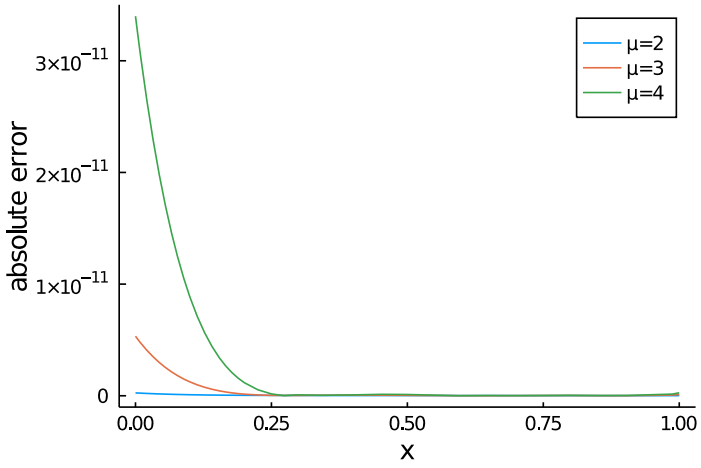

Figure 2.3: Absolute error between numerically obtained solutions for the linear Volterra integral equation of third-kind in (2.20) and analytic solution in (2.21) for fixed approximation degree $n = 7$ and three different values of μ.

2.8.2 Linear Volterra integro-differential equations

Simple examples with known solutions

We seek numerical solutions to the following integro-differential equations:

$$\frac{\mathrm{d}^2 u_1}{\mathrm{d}x^2} = 1 + \int_0^x (x-y)u_1(y)\mathrm{d}y, \tag{2.22}$$

$$\frac{\mathrm{d}^3 u_2}{\mathrm{d}x^3} = 1 + x + \frac{x^2}{2} - \frac{x^4}{4!} + \int_0^x \frac{(x-y)^2}{2}u_2(y)\mathrm{d}y, \tag{2.23}$$

Given the initial conditions

$$u_1(0) = 1, \quad u_1'(0) = 0, \tag{2.24}$$

$$u_2(0) = 1, \quad u_2'(0) = 2, \quad u_2''(0) = 1 \tag{2.25}$$

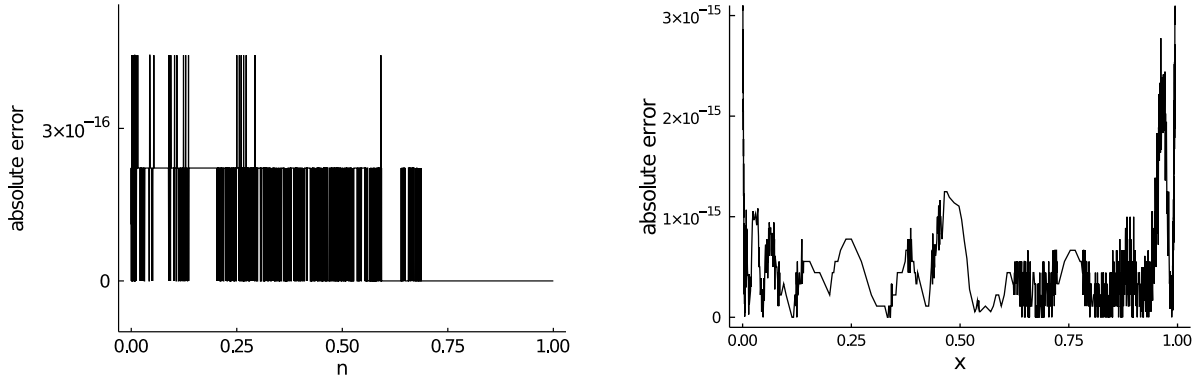

(a) $u_1, n = 15$ (b) $u_2, n = 20$

Figure 2.4: Absolute error between numerically obtained solutions for the linear Volterra integro-differential equations in (2.22-2.23) with initial conditions in (2.24-2.25) and their analytic solutions in (2.26-2.27) for indicated fixed degree of the polynomial approximation.

the analytic solutions to the above integro-differential equations are known to be:

$$u_1(x) = \cosh(x), \tag{2.26}$$

$$u_2(x) = x + e^x. \tag{2.27}$$

The two above equations were also discussed as numerical examples in [45]. In Figure 2.4 and 2.5 we plot the absolute error between numerically obtained and analytic solutions for a suitably converged fixed order of approximation, as well as the convergence behavior with increasing degree of the polynomial approximation.

A high order example involving approximations of a step function

Most of the above examples require only a very small number of polynomial degrees to successfully approximate solutions to machine precision due to the simplicity required to obtain analytic solutions for comparison. In this section we compute numerical solutions for a Volterra integro-differential equation involving approximations of the step-function in the sense of

$$u(x, k) = \arctan(kx).$$

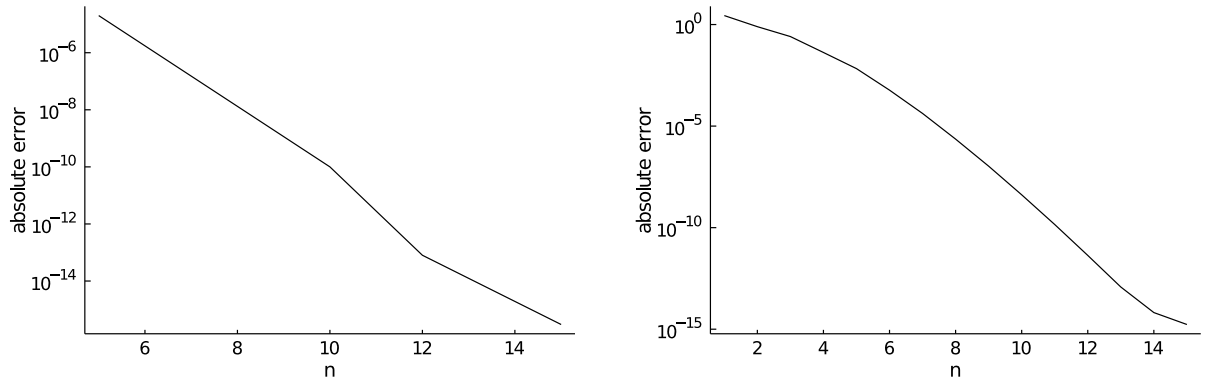

(a) u_1 (b) u_2

Figure 2.5: Semi-logarithmic convergence plots of numerically obtained solutions for the linear Volterra integro-differential equations in (2.22-2.23) with initial conditions in (2.24-2.25) to their analytic solutions in (2.26-2.27).

We plot examples of this function in Figure 2.6(a) to showcase its rapid convergence to a step function as $k \to \infty$. A Volterra integro-differential equation which is solved by the above function $u(x, k)$ is:

$$u'(x,k) = g(x,k) + \int_0^x y e^{x^2} u(y,k) \mathrm{d}y, \tag{2.28}$$

with

$$g(x,k) = \frac{k}{k^2x^2+1} - \frac{e^{x^2}\arctan(kx)}{2k^2} + \frac{e^{x^2}x}{2k} - \frac{1}{2}e^{x^2}x^2\arctan(kx).$$

In Table 2.2, which was first published in [45], we present a comprehensive comparison for errors and processing time using our sparse method and state-of-the-art collocation method Matlab software package Chebfun [33] for increasing orders. To aid with the interpretation of Table 2.2, we again note that Chebfun automatically chooses its approximation degree based on convergence heuristics. While in the case of linear Volterra integral equations our method obtained similar accuracy with substantially less computing time, linear Volterra integro-differential equations are not only sped up but also simultaneously more accurate. To provide a practical example of operator quasi-bandedness for integro-differential equations,

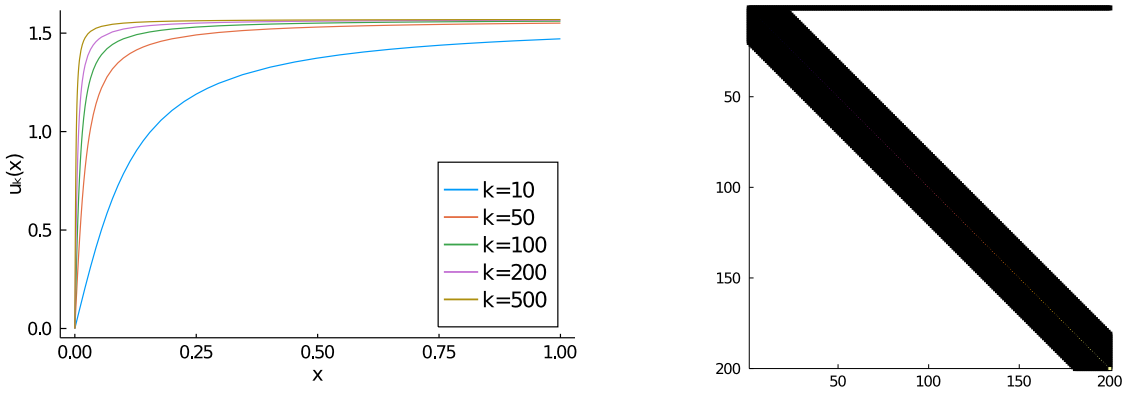

(a) (b)

Figure 2.6: (a) shows convergence of $u(x,k) = \arctan(kx)$ to step function as k increases. (b) shows spy plot of computed quasi-banded Volterra integro-differential operator for equation (2.28) with $n = 200$.

we also provide a spy plot of the obtained operator in Figure 2.6(b).

A high order example involving oscillatory Bessel kernels

This example was first presented in [52] as an example for evaluating the adequacy of a convolution-kernel only spectral method and then again in [45] for the method discussed in this chapter. The previous section showcased an example where high polynomial orders were required as a result of approximations to a step function. In this section we discuss an example of a more common scenario requiring high polynomial orders: highly oscillatory functions. We seek numerical solution to the following equation:

$$10^{-3}u''(x) + \omega^2 u(x) = g(x,\mu,\nu) - \omega \int_0^x J_\mu(\omega(x-y))u_2(y)\mathrm{d}y, \tag{2.29}$$

with

$$g(x,\mu,\nu) = J_{\mu+\nu}(\omega x) + \frac{1}{2x^2}((\nu-1)(\nu-2)J_{\nu-1}(\omega x) + (\nu+1)(\nu+2)J_{\nu+1}(\omega x)).$$

Method	k	CPU time	approx. order	abs. error
Sparse method	100	0.3s	300	6.0e-15
	1000	0.4s	800	2.9e-14
	10000	0.8s	2000	9.3e-14
	50000	3.5s	5000	2.8e-13
	100000	8.8s	8000	8.1e-12
Chebfun	100	1.4s	196	4.8e-14
	1000	2.1s	540	6.6e-12
	10000	10.7s	1477	1.2e-09
	50000	10.4s	2863	4.1e-08

Table 2.2: Accuracy and performance comparison of sparse method and Chebfun for Equation (2.28) first published in [45]. For $k = 100,000$ Chebfun fails to converge, so it is not included. CPU time measured on Intel Core i7-6700T CPU @ 2.80GHz.

In the above, the functions J_μ are first-kind Bessel functions and we further have $\mu > 0$ and $\omega \in \mathbb{R}$. The equation is solved with the following initial conditions:

$$u(0) = u'(0) = 0.$$

The method introduced in this chapter can be used for general kernels; this naturally also includes convolution kernels. In Figure 2.7 we plot the numerical solution for a high polynomial order of approximation ($n = 3000$) for the case ($\nu = 3, \mu = 2, \omega = 20$) to give an idea of the highly oscillatory nature of the solution as well as an error convergence plot comparing obtained solutions to the high degree approximation (as no analytic solution is available for this equation). We observe exponential convergence once the degree of the polynomial approximation overcomes an initial threshold required to resolve the oscillations, compatible and comparable with what was observed in [52] (as they also discuss the example case ($\nu = 3, \mu = 2, \omega = 20$)).

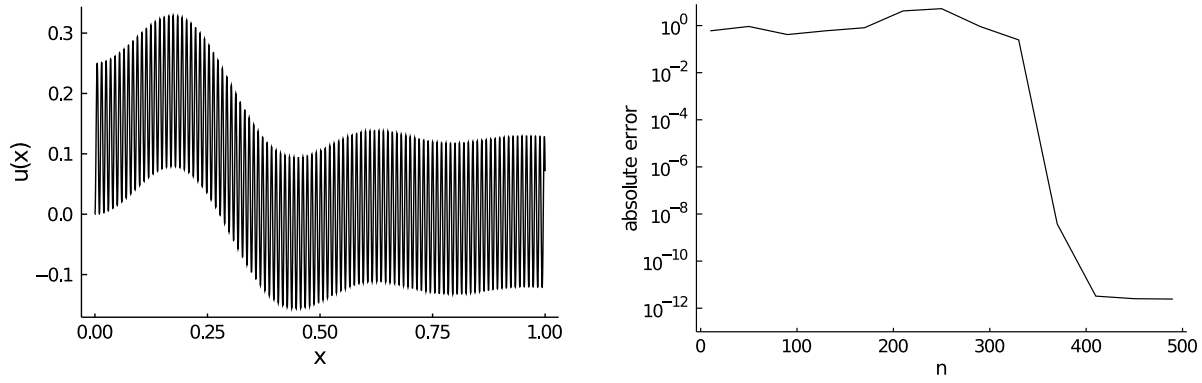

(a) (b)

Figure 2.7: (a) shows numerical solution to Equation (2.29) for degree of approximation $n = 3000$. (b) shows semi-logarithmic convergence plot of numerical solutions to the $n = 3000$ solution with increasing degree of approximation n.

2.8.3 Nonlinear Volterra integro-differential equations

In this section we provide some numerical examples for nonlinear Volterra integral and integro-differential equations. First, we seek numerical solutions to the following nonlinear Volterra integral equations

$$u_1(x) = e^x + \frac{x(1 - e^{3x})}{3} + \int_0^x x u_1^3(y)\mathrm{d}y, \tag{2.30}$$

$$u_2(x) = \sin(x) + \frac{\sin^2(x)}{4} - \frac{x^2}{4} + \int_0^x (x - y) u_2^2(y)\mathrm{d}y, \tag{2.31}$$

with known solutions

$$u_1(x) = e^x, \tag{2.32}$$

$$u_2(x) = \sin(x). \tag{2.33}$$

These problems were also discussed in [45]. We plot error convergence with increasing polynomial degree in Figure 2.9 and the absolute error at a fixed polynomial approximation degree in Figure 2.8.

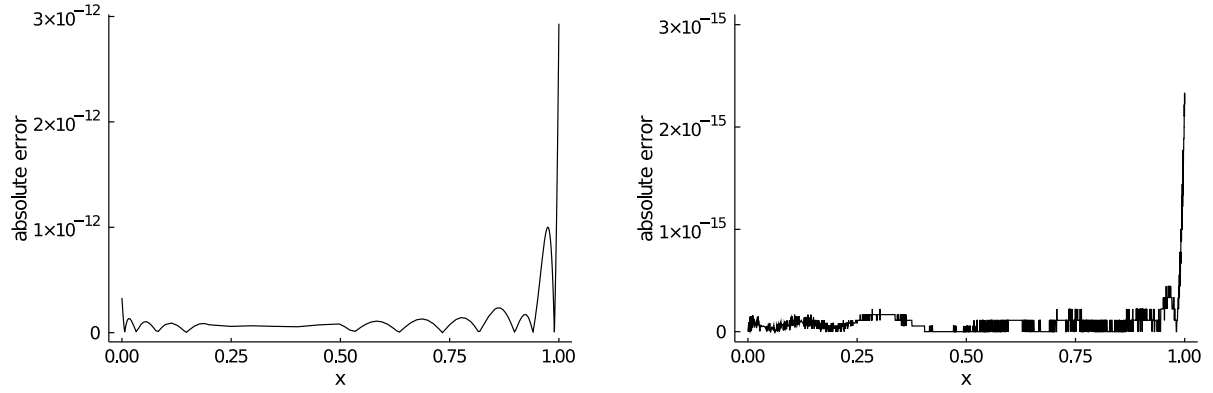

(a) $u_1, n = 15$ (b) $u_2, n = 14$

Figure 2.8: Absolute error between numerically obtained solutions for the linear Volterra integro-differential equations in (2.30-2.31) and their analytic solutions in (2.32-2.33) for indicated fixed degree of the polynomial approximation.

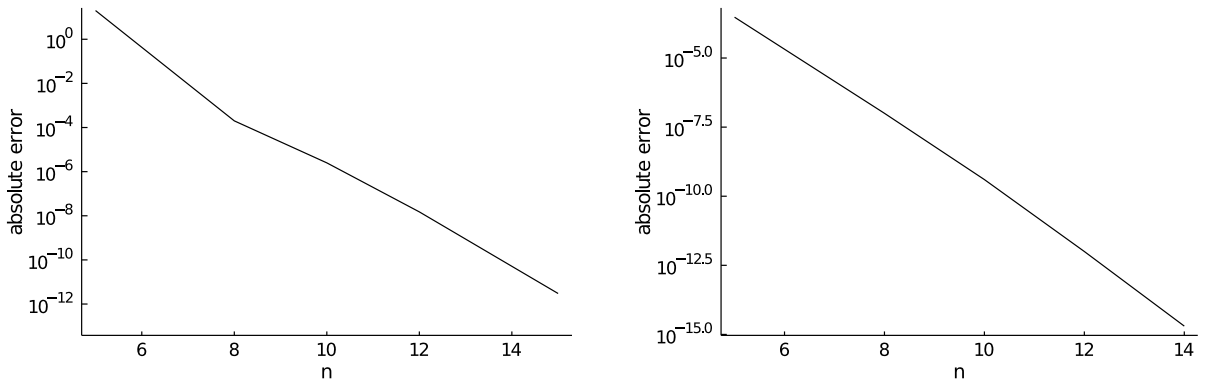

(a) u_1 (b) u_2

Figure 2.9: Semi-logarithmic convergence plots of numerically obtained solutions for the linear Volterra integro-differential equations in (2.30-2.31) to their analytic solutions in (2.32-2.33).

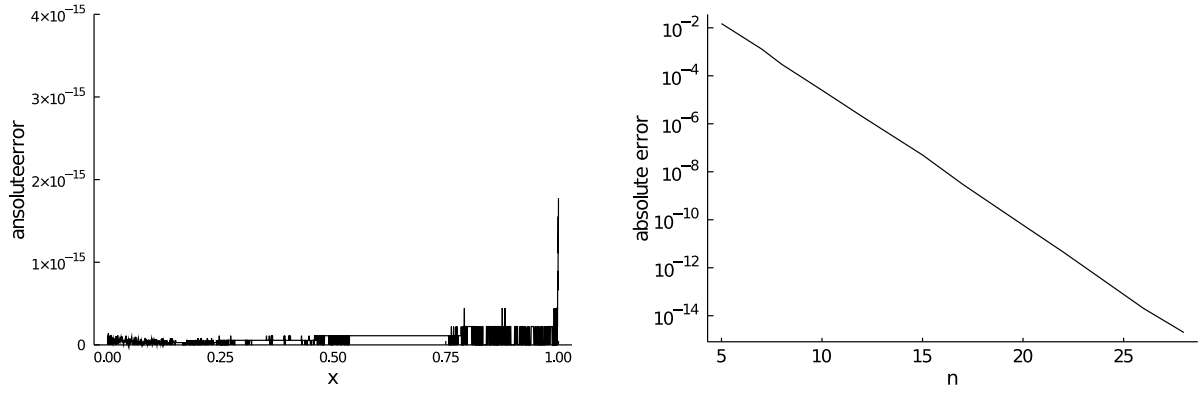

(a) (b)

Figure 2.10: (a) shows absolute error between numerically obtained solution for the nonlinear Volterra integro-differential equation in (2.34) and its analytic solution $\tan(x)$ for approximation degree $n = 28$. (b) shows a semi-logarithmic convergence plot of the numerically obtained solutions for (2.34).

Finally, we seek a numerical solution to the following nonlinear integro-differential equation:

$$\frac{\mathrm{d}}{\mathrm{d}x}u(x) = x + \cos(x) - \tan(x) + \tan^2(x) + \int_0^x u^2(y)\mathrm{d}y, \tag{2.34}$$

with initial conditions

$$u(0) = 0. \tag{2.35}$$

and known solution

$$u_2(x) = \tan(x). \tag{2.36}$$

This equation was previously discussed in [45]. We plot the absolute error at a fixed polynomial approximation degree in Figure 2.10(a) and error convergence with increasing polynomial degree in Figure 2.10(b).

2.9 Discussion

In this chapter we introduced a banded spectral method for linear and nonlinear Volterra integral and integro-differential equations using appropriately chosen orthogonal (Jacobi and Proriol) polynomial bases, in particular making use of multivariate orthogonal polynomials on triangle domains. The methods outperform state-of-the-art collocation methods in computational cost and as we saw in some examples in the numerical experiments section also match or outperform them in accuracy. The methods are furthermore not restricted to convolution kernels which is a common constraint of currently available competitive methods, cf. [52, 62]. For the linear first and second-kind equations, we provided proofs of convergence based on finite section theory and a connection to the theory of Toeplitz operators.
In the next chapter, we introduce a sparse spectral method using ultraspherical and Jacobi polynomials for equilibrium measures for power law kernels, which involve integral equations with convolution kernels of the form $K(x,y) = \frac{|x-y|^\alpha}{\alpha} - \frac{|x-y|^\beta}{\beta}$. We will see that the equilibrium measure problem essentially splits into one part linear Fredholm integral equation of first-kind solver and one part optimization.

Chapter 3

Computing power law equilibrium measures

The content of this chapter is based on research published in [48] and [47]. For the purposes of this thesis, the content of the papers has been rewritten and merged into one coherent chapter. Furthermore, all appearing figures for the numerical experiments included in this chapter are original and were generated exclusively for this thesis.

3.1 Introduction to equilibrium measure problems

In this section we introduce the problem of equilibrium measures starting with the application-oriented motivation from particle swarm dynamics. The following is a system of equations of motion describing a generic classical Newtonian one-species particle swarm consisting of N particles described by their positions $x_i \in \mathbb{R}^d$:

$$\frac{\mathrm{d}^2 x_i}{\mathrm{d}t^2} = f\left(\left|\frac{\mathrm{d}x_i}{\mathrm{d}t}\right|\right)\frac{\mathrm{d}x_i}{\mathrm{d}t} - \frac{1}{N}\sum_{j\neq i}\nabla K(|x_i - x_j|).$$

The function $K(\cdot)$ in this context describes the particle's interaction potential which depends only on the pairwise distance of two distinct particles. The function $f(\cdot)$ is related to self-propulsion and friction [25]. Systems which may successfully be modelled by the above, particularly the case of two and three dimensions, arise in a multitude of applications. In classical physics one may encounter such systems when modelling classical (in the sense of 'non-quantum') particles and particulates such as (charged) dust or aerosols, while biological swarms such as cellular motion, e.g. in a petri dish, or animal (e.g. bird or fish) flocking

behavior [82, 104, 110, 15, 23, 50] are life sciences applications.

In the absence of friction, that is when $f\left(\left|\frac{\mathrm{d}x_i}{\mathrm{d}t}\right|\right) = 0$, taking the continuous limit $N \to \infty$ (partially motivated by the study of very large N particle systems) leads to the well-studied aggregation equation:

$$\rho_t = \nabla \cdot (\rho \nabla K * \rho) \tag{3.1}$$

Depending on problem-inherent quantities, in particular the interaction kernel and the dimension of the problem, some such aggregation equations may have steady equilibrium states characterized by

$$\nabla K * \rho = 0 \quad \text{on} \quad \text{supp}(\rho).$$

We note at this point that due in part to the natural science applications in the background of this problem, only non-negative measures ρ qualify as admissible solutions to the equilibrium measure problem. Stable stationary states, i.e. equilibrium states, are by their definition (local) minimizers of the energy expression

$$\tilde{E} = \int \rho (K * \rho) \mathrm{d}x.$$

We also have to impose a mass condition for the problem to become well-posed, i.e. $\int \rho \mathrm{d}x = M$. Stated as above, the equilibrium measure problem appears numerically intractable in two different ways. First, the naive approach of performing classical particle simulations to approximate solutions to the continuous problems is doomed by the rapidly growing computational cost as N and d increase, and we will see in the numerical experiments sections that even simple problems in low dimensions (even 1D and 2D) often show very poor convergence. Meanwhile, the continuous problem itself is a constrained energy optimization problem over a measure space with measures of unknown support – it is unclear how one could iterate over such a general space numerically in a structured, let alone fast, way. To

alleviate this problem we employ a strategy also used in analytic discussions of equilibrium measures, cf. [25]: Using an Euler-Lagrange type approach one can show that the minimizers of the above energy expression in fact must be among the non-negative densities satisfying

$$K * \rho = E \quad \text{on} \quad \text{supp}(\rho),$$

where E is a constant expression different from the above-defined energy $\tilde{E}$ by a factor given by the mass of the measure, cf. the discussion in [25]. For the purposes of our numerical method, E and $\tilde{E}$ will play effectively equivalent roles and we thus refer to both as energies. We can equivalently write the above problem as

$$\int_{\text{supp}(\rho)} K(|x-y|)\rho(y)\mathrm{d}y = E,$$

to instead highlight the integral equation nature of the now slightly more tractable problem. By restricting our search to compactly supported measures for general attractive-repulsive power law kernels, i.e.

$$K(|x-y|) = \frac{|x-y|^\alpha}{\alpha} - \frac{|x-y|^\beta}{\beta}, \tag{3.2}$$

we show in what follows that a sparse spectral method for the integral equation part combined with a straightforward constrained optimization can not only solve equilibrium measure problems but do so in a highly efficient way with rapid convergence.

The existence of global minimizers for attractive-repulsive power law equilibrium measures was recently discussed by Canizo, Carrillo and Patacchini in [22]. Some uniqueness results also exist for $\alpha \in (2, 4)$ and $\beta \in (-1, 0)$ [61, 28]. Further candidate solutions for the case where either α or β are an even integer were derived in [25] and later proved to be the minimizers in [27] (see also [40]). Numerical approaches to equilibrium measure problems have mostly been limited to discrete particle simulations [14, 111, 39], which have hinted at many interesting phenomena about which little is known in the continuous limit. We will

investigate one such phenomenon – the void formation behavior for high repulsive powers – using our method in the numerical experiments section of this chapter. More recently, Olver [74] introduced a spectral method for the closely related one-dimensional equilibrium measure problem with logarithmic interaction kernel using Chebyshev polynomials.

The structure of the remaining sections is as follows: In Section 3.2 we briefly discuss the above-mentioned method due to Olver [74] for computing equilibrium measures for logarithmic kernels to highlight similarities as well as substantial differences to the power law kernel approach introduced in this chapter. In Section 3.3 we formally introduce the fractional Laplacian and Riesz potential as well as the Riemann-Liouville fractional integral and describe their relationship with the power law equilibrium measure problem. In Section 3.4 we derive recurrence relationships leading to banded and approximately banded power law integral operators in specialized ultraspherical polynomial bases. Section 3.5 explains how to construct a numerical algorithm for power law equilibrium measures based on the aforementioned recurrence relationships. In Section 3.6 we discuss how the one interval method of the previous sections may be extended to two interval methods in one dimension, while Section 3.7 covers a different generalization based on radial Jacobi polynomial recurrence relationships on arbitrary dimensional balls. The higher-dimensional spectral method algorithm on arbitrary dimensional balls is further detailed in Section 3.8. Section 3.9 introduces Tikhonov regularization as a way to improve the stability of the introduced algorithms both in one and higher dimensions. Finally, Section 3.5 and 3.8 show numerical experiments, including verifications with known results, comparison with other methods as well as exploration of novel phenomena for the one-dimensional and higher-dimensional method respectively. The results of this chapter are then summarized and reviewed in a discussion section.

3.2 Olver's method for computing equilibrium mesures with logarithmic kernels

Methods to approximate continuous equilibrium measures for logarithmic kernels, that is

$$K(|x-y|) = \log\left(\frac{1}{|x-y|}\right),$$

based on Leja points have been available for almost a century [58, 42], but their convergence properties are relatively poor [74]. More recently, Olver [74] introduced a spectral method using Chebyshev polynomials for computing equilibrium measures based on reformulating them in terms of a Riemann-Hilbert problem.

Olver's method only applies to equilibrium measure problems with logarithmic kernels in one dimension, specifically with non-vanishing potentials. As it applies only to one type of kernel as opposed to a class of kernels, it cannot be used for attractive-repulsive problems with non-vanishing potentials, which are the primary focus of this chapter. We nevertheless include a brief overview of this method for logarithmic kernels in this section since (1) the logarithmic kernel case is understood to formally arise from the power law kernel case as the kernel power approaches 0, cf. [25], (2) the methodological similarities and differences to our power law kernel method are noteworthy for general continuous numerics of equilibrium measures and (3) because the problem of equilibrium measures for logarithmic kernels are known to have interesting connections with random matrix theory, cf. [31], which raises interesting questions about whether such connections also exist for other kernels.

As mentioned above, Olver's method is based on reformulating the logarithmic kernel equilibrium measure problem, i.e. finding a non-negative measure which minimizes

$$\tilde{E} = \int\int \log\left(\frac{1}{|x-y|}\right) \mathrm{d}\rho(x)\mathrm{d}\rho(y) + \int V(y)\mathrm{d}\rho(y),$$

as a Riemann-Hilbert problem. This is accomplished via the following theorem:

Theorem 3.1. *Let* $\mathrm{supp}(\rho)$ *consist of a finite number of intervals and let* ϕ *be a function which is analytic and bounded on* $\mathbb{C}\backslash\mathrm{supp}(\rho)$ *satisfying*

$$\phi^+(x) + \phi^-(x) = V'(x), \quad \textit{for } x \in \mathrm{supp}(\rho),$$

where $\phi^\pm(x)$ *denotes the following limits:*

$$\phi^\pm(x) = \lim_{\epsilon \to 0^+} \phi(x \pm i\epsilon).$$

Let ϕ *furthermore satisfy*

$$\phi(z) = \frac{1}{z} + \mathcal{O}\left(\frac{1}{z^2}\right), \quad \textit{as } z \to \infty.$$

Then we have

$$\phi(z) = \int \frac{\mathrm{d}\rho}{z - y}$$

and

$$\mathrm{d}\rho(y) = \frac{i}{2\pi}\left(\phi^+(y) - \phi^-(y)\right)\mathrm{d}y.$$

Proof. A proof of this result may be found in [95], see also the discussion in [74]. □

By using fast cosine transforms and Chebyshev polynomials [74, 75] Olver's method proceeds to solve

$$\phi^+(x) + \phi^-(x) = V'(x),$$

for $x \in (a, b)$ with $\lim_{z\to\infty} \phi(z) = 0$. This approach only determines the solution up to a

parameter ξ, which can be fixed by using the additional constraint that for the logarithmic kernel equilibrium measures it is known that the measure vanishes at the support boundary (a fact which generally does not hold for power law equilibrium measures). This then allows the definition of a function $F(a, b)$ which satisfies $F(\text{supp}(\rho)) = 0$, meaning that a Newton method may be used to find the support interval if the equilibrium measure is unique.

While Olver's method differs substantially from the method we introduce in this chapter, in particular as we primarily treat attractive-repulsive power law equilibrium measure problems and approach them from the point of view of fractional integral equations as opposed to Riemann-Hilbert problems, we will see that the two methods end up relying on similar ideas: The most important similarity is that the equilibrium measure problems are both initially reduced from an optimization problem over a measure space to an optimization problem over the support boundary. This step is what prevents the computation of continuous equilibrium measures from being an intractable problem. Additionally, both equilibrium measure problems are initially underdetermined and thus require the use of additional constraints - we will discuss the nature of these constraints for the power law kernel case in the coming sections. Finally, both methods make use of the excellent convergence properties of expansions in orthogonal polynomials as well as the specific action of the respective convolution kernel operators on the Chebyshev, ultraspherical and radial Jacobi polynomials respectively. Finally, we note that Olver also presents a generalization of his method to multiple interval support [74], motivating some of the ideas for two interval methods for power law equilibrium measures which we discuss in Section 3.6.

3.3 Riesz potential theory and fractional Laplacians

The integrals found in power law equilibrium measure problems are essentially Riesz potentials, except with slightly different normalization constants:

Definition 3.1 (Riesz kernel)**.** *The Riesz kernel $k_\gamma(|x-y|)$, with $x, y \in \mathbb{R}^d$ is defines as*

$$k_\gamma(|x-y|) = \frac{\Gamma(\frac{d-\gamma}{2})}{\pi^{\frac{d}{2}} 2^\gamma \Gamma(\frac{\gamma}{2})} \frac{1}{|x-y|^{d-\gamma}}.$$

Definition 3.2 (Riesz potential)**.** *The Riesz potential of $u(y)$ with $y \in \operatorname{supp}(\rho) \subseteq \mathbb{R}^d$ and $\gamma \in (0, d)$ is*

$$(-\Delta)^{-\frac{\gamma}{2}} u(x) = \frac{\Gamma(\frac{d-\gamma}{2})}{\pi^{\frac{d}{2}} 2^\gamma \Gamma(\frac{\gamma}{2})} \int_{\operatorname{supp}(\rho)} \frac{1}{|x-y|^{d-\gamma}} u(y) \mathrm{d}y.$$

The constants in the above definitions are chosen to ensure that it is the inverse of the so-called fractional Laplace operator:

Definition 3.3 (Fractional Laplace operator)**.** *The fractional Laplace operator $(-\Delta)^{\frac{\gamma}{2}}$ for $\gamma \in (0, 2)$ is defined via singular integral*

$$(-\Delta)^{\frac{\gamma}{2}} f(x) = \frac{2^\gamma |\Gamma(\frac{d+\gamma}{2})|}{\pi^{\frac{d}{2}} \Gamma(-\frac{\gamma}{2})} \lim_{\epsilon \to 0^+} \int\limits_{\mathbb{R}^d \setminus B_\epsilon} \frac{f(x) - f(y)}{|x-y|^{d+\gamma}} \, dy,$$

where $B_\epsilon = B(0, \epsilon)$ denotes the origin-centered ball of radius ϵ. If $\gamma \in (0, d)$ this is equivalent to the inverse of the Riesz potential, see [57], which is thus sometimes denoted $(-\Delta)^{-\frac{\gamma}{2}}$.

The above definitions are valid for arbitrary dimension d. In the special case $d = 1$ the Riesz potential may be further split up into two distinct but closely related fractional integral operators which are known as left and right-handed Riemann-Liouville integrals:

Definition 3.4 (Riemann-Liouville integrals)**.** *For $\gamma > 0$ the left and right-handed Riemann-*

Liouville fractional integrals are defined by

$$I_{L,a}^{\gamma}[u](x) := \frac{1}{\Gamma(\gamma)} \int_a^x (x-y)^{\gamma-1} u(y) \mathrm{d}y,$$
$$I_{R,b}^{\gamma}[u](x) := \frac{1}{\Gamma(\gamma)} \int_x^b (y-x)^{\gamma-1} u(y) \mathrm{d}y.$$

Up to a multiplicative constant, a sum of appropriate left and right-handed Riemann-Liouville fractional integrals precisely yields the Riesz potential on a one-dimensional interval:

$$\begin{aligned} I_{L,a}^{\gamma}[u](x) + I_{R,b}^{\gamma}[u](x) &= \frac{1}{\Gamma(\gamma)} \int_a^b |x-y|^{\gamma-1} u(y) \mathrm{d}y \\ &= \frac{1}{\Gamma(\gamma)} \int_a^b \frac{1}{|x-y|^{1-\gamma}} u(y) \mathrm{d}y. \end{aligned} \tag{3.3}$$

While there are conceptually related methods for splitting up a higher-dimensional Riesz potential into different fractional integrals in higher dimensions, mostly due to Rubin [94, 93, 92, 91], we will not list them here as they do not lead to any directly useful simplifications for the numerical methods we introduce below.

The Riemann-Liouville integrals are fractional integrals in the sense that they satisfy the following relationships with the conventional integration and differentiation operators:

$$\frac{\mathrm{d}}{\mathrm{d}x} I_{L,a}^{s+1}[f](x) = I_{L,a}^{s}[f](x), \quad \frac{\mathrm{d}}{\mathrm{d}x} I_{R,b}^{s+1}[f](x) = -I_{R,b}^{s}[f](x), \tag{3.4}$$

$$I_{L,a}^{s}\left[I_{L,a}^{t}[f]\right] = I_{L,a}^{s+t}[f], \quad I_{R,b}^{s}\left[I_{R,b}^{t}[f]\right] = I_{R,b}^{s+t}[f], \tag{3.5}$$

for $t > 0$. We refer to [64, Section 2] and [65, Section 2] for a more in-depth review of fractional integrals and their properties.

3.4 Recurrence results for ultraspherical polynomials in one dimension

In one dimension, the most natural basis to search for a banded representation of power law integrals is found in the ultraspherical polynomials as introduced in 1.1.4. In higher dimensions, which we discuss in Section 3.7, we will be using the radial Jacobi polynomial bases on balls as introduced in Section 1.3.3 instead. As the one-dimensional results do not require radial symmetry (or mirror symmetry in one dimension), the ultraspherical polynomial results are in a sense more general than the radial Jacobi polynomial alternative in the special case of one dimension.

The initial motivation for using the ultraspherical polynomials is the following result for power law integrals, valid for low powers $\alpha \in (-1, 1)$, which has been known since at least Popov's 1960s publication [83]:

Lemma 3.1. *Let $\alpha \in (-1, 1)$ and $x \in (-1, 1)$. Then the action of the power law integral operator $Q^\alpha[u](x) = \int_{-1}^{1} |x - y|^\alpha u(y)\mathrm{d}y$ on the ultraspherical polynomials $C_n^{\left(-\frac{\alpha}{2}\right)}(y)$, i.e. $C_n^{(\lambda)}$ with choice $\lambda = -\frac{\alpha}{2}$, is:*

$$Q^\alpha\left[w^{(-\frac{\alpha}{2})}C_n^{\left(-\frac{\alpha}{2}\right)}\right](x) = \frac{(-1)^n\pi}{nB(-n+\alpha+1,n)\cos\left(\frac{\pi\alpha}{2}\right)}C_n^{\left(-\frac{\alpha}{2}\right)}(x).$$

where B is the Beta function $B(x, y) = \frac{\Gamma(x)\Gamma(y)}{\Gamma(x+y)}$ and $w^{(\lambda)}(y) = (1 - y^2)^{\lambda-\frac{1}{2}}$.

Proof. We refer to [83] for a proof of this result. □

The restriction on the power, i.e. $\alpha \in (-1, 1)$, is important and means that we cannot use this to study the primary range of interest where analytic methods are unavailable and the measures show interesting gap formation behavior (we discuss this in more detail in the numerical experiments at the end of this chapter). The goal is thus to find a similarly powerful expression but generalized to work for arbitrary powers. The first step towards

this goal is to prove the following recurrence relationship result for the Riemann-Liouville integrals which as we saw in Section 3.3 sum to the Riesz potential in one dimension:

Theorem 3.2. *The left and right-handed Riemann–Liouville fractional integral operators in Definition 3.4 satisfy the following two-term recurrence relationship on weighted ultraspherical polynomials $C_n^{(\lambda)}(y)$ with $n \geqslant 2$:*

$$xI_{L,-1}^{1+\alpha}\left[w^{(\lambda)}C_n^{(\lambda)}\right](x) = \kappa_1 I_{L,-1}^{1+\alpha}\left[w^{(\lambda)}C_{n-1}^{(\lambda)}\right](x) + \kappa_2 I_{L,-1}^{1+\alpha}\left[w^{(\lambda)}C_{n+1}^{(\lambda)}\right](x),$$
$$xI_{R,1}^{1+\alpha}\left[w^{(\lambda)}C_n^{(\lambda)}\right](x) = \kappa_1 I_{R,1}^{1+\alpha}\left[w^{(\lambda)}C_{n-1}^{(\lambda)}\right](x) + \kappa_2 I_{R,1}^{1+\alpha}\left[w^{(\lambda)}C_{n+1}^{(\lambda)}\right](x),$$

where $w^{(\lambda)}(y) = (1-y^2)^{\lambda-\frac{1}{2}}$ is the ultraspherical weight and κ_1 and κ_2 have explicit form:

$$\kappa_1 = \frac{(n-\alpha-1)(2\lambda+n-1)}{2n(\lambda+n)},$$
$$\kappa_2 = \frac{(n+1)(2\lambda+n+\alpha+1)}{2(\lambda+n)(2\lambda+n)}.$$

Proof. We begin with the left-handed case:

$$xI_{L,-1}^{1+\alpha}\left[w^{(\lambda)}C_n^{(\lambda)}\right](x) = \tfrac{1}{\Gamma(1+\alpha)}\int_{-1}^{x} x(x-y)^{\alpha}w^{(\lambda)}(y)C_n^{(\lambda)}(y)dy$$
$$= \tfrac{1}{\Gamma(1+\alpha)}\int_{-1}^{x}(x-y)(x-y)^{\alpha}w^{(\lambda)}(y)C_n^{(\lambda)}(y)dy + \tfrac{1}{\Gamma(1+\alpha)}\int_{-1}^{x} y(x-y)^{\alpha}w^{(\lambda)}(y)C_n^{(\lambda)}(y)dy.$$

The two resulting terms are addressed differently: for the second term, we can use the classical two term recurrence relationship of ultraspherical polynomials (in Eq. (1.15)) to expand $yC_n^{(\lambda)}(y)$. The first term makes use of the Riemann-Liouville fractional integrals properties in Eq. (3.5):

$$\tfrac{1}{\Gamma(1+\alpha)}\int_{-1}^{x}(x-y)^{\alpha+1}w^{(\lambda)}(y)C_n^{(\lambda)}(y)dy = (1+\alpha)I_{L,-1}^{2+\alpha}\left[w^{(\lambda)}C_n^{(\lambda)}\right](x)$$
$$= (1+\alpha)I_{L,-1}^{1+\alpha}\left[I_{L,-1}^{1}\left[w^{(\lambda)}C_n^{(\lambda)}\right]\right](x). \tag{3.6}$$

Using the ultraspherical polynomial property for integration in Eq. (1.17) we then obtain:

$$(1+\alpha)I^1_{L,-1}\left[w^{(\lambda)}C^{(\lambda)}_n\right](y) = -\tfrac{(1+\alpha)2\lambda}{n^2+2\lambda n}\left(1-y^2\right)^{\lambda+\frac{1}{2}}C^{(\lambda+1)}_{n-1}(y),$$

Which after a final application of the classical two term recurrence of the ultraspherical polynomials in Eq. (1.15) results in:

$$\begin{aligned}&-\tfrac{(1+\alpha)2\lambda}{n^2+2\lambda n}\left(1-y^2\right)^{\lambda+\frac{1}{2}}C^{(\lambda+1)}_{n-1}(y)\\&=\tfrac{(1+\alpha)(n+1)}{2(n+\lambda)(n+2\lambda)}\left(1-y^2\right)^{\lambda-\frac{1}{2}}C^{(\lambda)}_{n+1}(y)-\tfrac{(1+\alpha)(n+2\lambda-1)}{2n(n+\lambda)}\left(1-y^2\right)^{\lambda-\frac{1}{2}}C^{(\lambda)}_{n-1}(y),\end{aligned}$$

Thus we have reduced both terms on the RHS of Eq. (3.6) to lower degree terms. Putting the components together yields

$$xI^{1+\alpha}_{L,-1}\left[w^{(\lambda)}C^{(\lambda)}_n\right](x) = \tfrac{(n+1)(2\lambda+n+\alpha+1)}{2(\lambda+n)(2\lambda+n)}I^{1+\alpha}_{L,-1}\left[w^{(\lambda)}C^{(\lambda)}_{n+1}\right](x)+\tfrac{(n-\alpha-1)(2\lambda+n-1)}{2n(\lambda+n)}I^{1+\alpha}_{L,-1}\left[w^{(\lambda)}C^{(\lambda)}_{n-1}\right](x),$$

if $n \geqslant 2$ as desired.

To prove the right-handed case, we proceed similarly but with a slightly different starting point:

$$\begin{aligned}&xI^{1+\alpha}_{R,1}\left[w^{(\lambda)}C^{(\lambda)}_n\right](x) = \tfrac{1}{\Gamma(1+\alpha)}\int_x^1 x(y-x)^\alpha w^{(\lambda)}(y)C^{(\lambda)}_n(y)\mathrm{d}y\\&=\tfrac{1}{\Gamma(1+\alpha)}\int_x^1 (x-y)(y-x)^\alpha w^{(\lambda)}(y)C^{(\lambda)}_n(y)\mathrm{d}y+\tfrac{1}{\Gamma(1+\alpha)}\int_x^1 y(y-x)^\alpha w^{(\lambda)}(y)C^{(\lambda)}_n(y)\mathrm{d}y,\\&=\tfrac{-1}{\Gamma(1+\alpha)}\int_x^1 (y-x)^{\alpha+1} w^{(\lambda)}(y)C^{(\lambda)}_n(y)\mathrm{d}y+\tfrac{1}{\Gamma(1+\alpha)}\int_x^1 y(y-x)^\alpha w^{(\lambda)}(y)C^{(\lambda)}_n(y)\mathrm{d}y.\end{aligned}$$

As before, the second term in the resulting equation is expanded using the classical two term recurrence relationship of ultraspherical polynomials in Eq. (1.15). For the first term

we proceed as before:

$$\begin{aligned}\frac{-1}{\Gamma(1+\alpha)}\int_x^1 (y-x)^{\alpha+1} w^{(\lambda)}(y) C_n^{(\lambda)}(y)\mathrm{d}y &= (-1-\alpha) I_{R,1}^{2+\alpha}\left[w^{(\lambda)} C_n^{(\lambda)}\right](x) \\ &= (-1-\alpha) I_{R,1}^{1+\alpha}\left[I_{R,1}^{1}\left[w^{(\lambda)} C_n^{(\lambda)}\right]\right](x).\end{aligned}$$

By the property in (1.17) we then obtain

$$(-1-\alpha) I_{R,1}^{1}\left[w^{(\lambda)} C_n^{(\lambda)}\right](y) = -\tfrac{(1+\alpha)2\lambda}{n^2+2\lambda n}\left(1-y^2\right)^{\lambda+\frac{1}{2}} C_{n-1}^{\lambda+1}(y).$$

A favorable cancellation of signs then results in a recurrence relationship with the same recurrence coefficients as the left-handed case:

$$\begin{aligned}&x I_{R,1}^{1+\alpha}\left[w^{(\lambda)} C_n^{(\lambda)}\right] \\ &= \tfrac{(n+1)(2\lambda+n+\alpha+1)}{2(\lambda+n)(2\lambda+n)} I_{R,1}^{1+\alpha}\left[w^{(\lambda)} C_{n+1}^{(\lambda)}\right] + \tfrac{(n-\alpha-1)(2\lambda+n-1)}{2n(\lambda+n)} I_{R,1}^{1+\alpha}\left[w^{(\lambda)} C_{n-1}^{(\lambda)}\right],\end{aligned}$$

concluding the proof. □

Together with the observation in Equation 3.3 this leads to the following recurrence relationship for the one-dimensional Riesz potential / power law integral:

Corollary 3.1. *The power law integral operator* $Q^{\alpha}[u](x) := \int_{-1}^{1} |x-y|^{\alpha} u(y)\mathrm{d}y$ *satisfies the following two-term recurrence relationship on the weighted ultraspherical polynomials* $C_n^{(\lambda)}(y)$ *with* $n \geqslant 2$*:*

$$x Q^{\alpha}\left[w^{(\lambda)} C_n^{(\lambda)}\right](x) = \kappa_1 Q^{\alpha}\left[w^{(\lambda)} C_{n-1}^{(\lambda)}\right](x) + \kappa_2 Q^{\alpha}\left[w^{(\lambda)} C_{n+1}^{(\lambda)}\right](x),$$

where $w^{(\lambda)}(y) = (1-y^2)^{\lambda-\frac{1}{2}}$ *is the ultraspherical weight and* κ_1 *and* κ_2 *have explicit form:*

$$\begin{aligned}\kappa_1 &= \frac{(n-\alpha-1)(2\lambda+n-1)}{2n(\lambda+n)}, \\ \kappa_2 &= \frac{(n+1)(2\lambda+n+\alpha+1)}{2(\lambda+n)(2\lambda+n)}.\end{aligned}$$

Proof. This is an immediate corollary of Theorem 3.2 combined with the observation that a sum of left and right-handed Riemann-Liouville integral operators results in the Riesz potential, see Eq. (3.3). □

Since the recurrences above only hold for $n \geqslant 2$, we will require some auxiliary initial results for $n = 0$ and $n = 1$ to generate the full operators which we collect below. Since the $n = 0$ case is simply the power law integral of $C_0^\lambda(x) = 1$ multiplied by the ultraspherical weight, we begin with the following lemma which was previously proved in the context of fractional Laplacians:

Lemma 3.2. *The power law integral of power α of the ultraspherical weight $w^{(\lambda)} = (1 - x^2)^{\lambda - \frac{1}{2}}$ evaluates to the following explicit expression for the choice $\lambda = \frac{2k-\alpha-1}{2}$:*

$$\int_{-1}^{1} |x - y|^\alpha (1 - y^2)^{\frac{2k-\alpha-1}{2}} \mathrm{d}y = B\left(\tfrac{\alpha+1}{2}, \tfrac{2k+1-\alpha}{2}\right) {}_2F_1\left(-\tfrac{\alpha}{2}, -k; \tfrac{1}{2}; x^2\right). \tag{3.7}$$

Proof. A proof of this result can be found in [55]. □

Note that Lemma 3.2 is a generalization of Lemma 3.1. Similar results to the above will come up again when we discuss the higher-dimensional case in Section 3.7. The next result shows how to evaluate the $n = 1$ case for the two Riemann-Liouville integrals:

Lemma 3.3. *The left and right-handed Riemann–Liouville fractional integral operators in Definition 3.4 evaluate as follows when acting on the $n = 1$ ultraspherical polynomial $C_1^{(\lambda)}(y) = 2\lambda y$ with weight $w^{(\lambda)}(y) = (1 - y^2)^{\lambda - \frac{1}{2}}$:*

$$I^{1+\alpha}_{L,-1}\left[w^{(\lambda)} C_1^{(\lambda)}\right](x) = -\tfrac{2\lambda}{\Gamma(1+\alpha)} \int_{-1}^{x} (x - y)^{\alpha+1} w^{(\lambda)}(y) \mathrm{d}y + \tfrac{2\lambda x}{\Gamma(1+\alpha)} \int_{-1}^{x} (x - y)^{\alpha} w^{(\lambda)}(y) \mathrm{d}y,$$
$$I^{1+\alpha}_{R,1}\left[w^{(\lambda)} C_1^{(\lambda)}\right](x) = \tfrac{2\lambda}{\Gamma(1+\alpha)} \int_{x}^{1} (y - x)^{\alpha+1} w^{(\lambda)}(y) \mathrm{d}y + \tfrac{2\lambda x}{\Gamma(1+\alpha)} \int_{x}^{1} (y - x)^{\alpha} w^{(\lambda)}(y) \mathrm{d}y.$$

Proof. We begin by proving the left-handed case:

$$\begin{aligned} I_{L,-1}^{1+\alpha}\left[w^{(\lambda)}C_1^{(\lambda)}\right](x) &= \tfrac{2\lambda}{\Gamma(1+\alpha)}\int_{-1}^{x} y(x-y)^{\alpha}w^{(\lambda)}(y)\mathrm{d}y \\ &= \tfrac{2\lambda}{\Gamma(1+\alpha)}\int_{-1}^{x}(y-x)(x-y)^{\alpha}w^{(\lambda)}(y)\mathrm{d}y + \tfrac{2\lambda}{\Gamma(1+\alpha)}\int_{-1}^{x} x(x-y)^{\alpha}w^{(\lambda)}(y)\mathrm{d}y \\ &= \tfrac{-2\lambda}{\Gamma(1+\alpha)}\int_{-1}^{x}(x-y)^{\alpha+1}w^{(\lambda)}(y)\mathrm{d}y + \tfrac{2\lambda x}{\Gamma(1+\alpha)}\int_{-1}^{x}(x-y)^{\alpha}w^{(\lambda)}(y)\mathrm{d}y. \end{aligned}$$

The right-handed case is proved similarly:

$$\begin{aligned} I_{R,1}^{1+\alpha}\left[w^{(\lambda)}C_1^{(\lambda)}\right](x) &= \tfrac{2\lambda}{\Gamma(1+\alpha)}\int_{-1}^{x} y(y-x)^{\alpha}w^{(\lambda)}(y)\mathrm{d}y \\ &= \tfrac{2\lambda}{\Gamma(1+\alpha)}\int_{-1}^{x}(y-x)(y-x)^{\alpha}w^{(\lambda)}(y)\mathrm{d}y + \tfrac{2\lambda}{\Gamma(1+\alpha)}\int_{-1}^{x} x(y-x)^{\alpha}w^{(\lambda)}(y)\mathrm{d}y \\ &= \tfrac{2\lambda}{\Gamma(1+\alpha)}\int_{-1}^{x}(y-x)^{\alpha+1}w^{(\lambda)}(y)\mathrm{d}y + \tfrac{2\lambda x}{\Gamma(1+\alpha)}\int_{-1}^{x}(y-x)^{\alpha}w^{(\lambda)}(y)\mathrm{d}y. \end{aligned}$$

□

As with the recurrence relationship in Corollary 3.1, the above evaluation lemma for the Riemann-Liouville integrals of a weighted $n = 1$ ultraspherical polynomial leads directly to a power law integral corollary:

Corollary 3.2. *The power law integral operator* $Q^{\alpha}[u](x) := \int_{-1}^{1}|x-y|^{\alpha}u(y)\mathrm{d}y$ *evaluates as follows when acting on the* $n = 1$ *ultraspherical polynomial* $C_1^{(\lambda)}(y) = 2\lambda y$ *with weight* $w^{(\lambda)}(y) = (1-y^2)^{\lambda-\frac{1}{2}}$*:*

$$Q^{\alpha}\left[w^{(\lambda)}C_1^{(\lambda)}\right](x) = 2\lambda\left(\int_{x}^{1}(y-x)^{\alpha+1}w^{(\lambda)}(y)\mathrm{d}y - \int_{-1}^{x}(x-y)^{\alpha+1}w^{(\lambda)}(y)\mathrm{d}y\right) + 2\lambda x Q^{\alpha}\left[w^{(\lambda)}\right](x).$$

Proof. The result is an immediate consequence of combining Lemma 3.3 with the observation that a sum of left and right-handed Riemann-Liouville integral operators results in the Riesz potential, see Eq. (3.3). □

3.5 Numerical method on intervals in one dimension

In this section we describe how to use the recurrence results derived in the previous section to construct banded and approximately banded operators acting on a well-chosen ultraspherical polynomial basis in one dimension as well as how to use them to solve power law equilibrium measure problems.

First, we show that a single power law integral acting on the ultraspherical polynomial basis on an interval can be made diagonal or at least banded for particular basis parameter choices:

Lemma 3.4. *Let $\alpha > -1$ and $\lambda > -\frac{1}{2}$. With λ chosen such that $0 < \lambda + \frac{\alpha}{2} \in \mathbb{N}$ is a non-negative integer the power law integrals*

$$\int_{-1}^{1} |x-y|^{\alpha}(1-y^2)^{\lambda-\frac{1}{2}}\mathrm{d}y$$

and

$$\int_{-1}^{1} |x-y|^{\alpha}(1-y^2)^{\lambda-\frac{1}{2}}C_1^{(\lambda)}(y)\mathrm{d}y$$

evaluate to finite degree polynomials.

Proof. From Lemma 3.2 we know that for the choice $\lambda = \frac{2k-\alpha}{2}$ the analytic solution of the $n = 0$ case expression is:

$$\int_{-1}^{1} |x-y|^{\alpha}(1-y^2)^{\frac{2k-\alpha-1}{2}}\mathrm{d}y = B\left(\tfrac{\alpha+1}{2}, \tfrac{2k+1-\alpha}{2}\right) {}_2F_1\left(-\tfrac{\alpha}{2}, -k; \tfrac{1}{2}; x^2\right).$$

Gaussian hypergeometric functions ${}_2F_1$ are polynomials if one of their first two arguments is a negative integer and the third parameter is not a positive integer [73, 15.2.4]. Thus, choosing $k \in \mathbb{N}$ or equivalently $0 < k = \lambda + \frac{\alpha}{2} \in \mathbb{N}$ results in a polynomial right-hand side.

It remains to be shown that the $n = 1$ case with this basis choice also results in a finite

polynomial. We can evaluate the $n = 1$ case using Corollary 3.2:

$$Q^\alpha\left[w^{(\lambda)}C_1^{(\lambda)}\right](x) = 2\lambda\left(\int_x^1 (y-x)^{\alpha+1}w^{(\lambda)}(y)\mathrm{d}y - \int_{-1}^x (x-y)^{\alpha+1}w^{(\lambda)}(y)\mathrm{d}y\right) + 2\lambda x Q^\alpha\left[w^{(\lambda)}\right](x).$$

The last term in the above equation is a finite polynomial by the argument for the $n = 0$ case above. What remains to be shown is that the term in parentheses also evaluates to a finite degree polynomial. The expression in parenthesis can be shown to evaluate to the following expression for $\alpha > -1$ and $\lambda > -\frac{1}{2}$:

$$\begin{aligned}&\int_x^1 (y-x)^{\alpha+1}(1-y^2)^{\lambda-\frac{1}{2}}\mathrm{d}y - \int_{-1}^x (x-y)^{\alpha+1}(1-y^2)^{\lambda-\frac{1}{2}}\mathrm{d}y\\ &= -2^{1-\alpha}\sqrt{\pi}\frac{\Gamma(\alpha+2)\Gamma\left(\lambda+\frac{1}{2}\right)}{\Gamma\left(\frac{\alpha}{2}\right)\Gamma\left(\frac{\alpha}{2}+\lambda+1\right)}\frac{\left(2x^2(\alpha+\lambda+1)\right){}_2F_1\left(-\frac{\alpha}{2},-\lambda-\frac{\alpha}{2};\frac{1}{2};x^2\right)+\left(x^2-1\right){}_2F_1\left(-\frac{\alpha}{2},-\lambda-\frac{\alpha}{2};-\frac{1}{2};x^2\right)}{\alpha(\alpha+1)(\alpha+2\lambda+1)x}\end{aligned}$$

A simple change of variables in the $n = 0$ condition shows that the appearing hypergeometric functions in the numerator of the $n = 1$ case are simultaneously polynomial if $0 < \lambda + \frac{\alpha}{2} \in \mathbb{N}$:

$$\int_{-1}^1 |x-y|^\alpha(1-y^2)^{\lambda-\frac{1}{2}}\mathrm{d}y = \frac{\Gamma\left(\frac{\alpha+1}{2}\right)\Gamma\left(\lambda+\frac{1}{2}\right)}{\Gamma\left(\lambda+\frac{\alpha}{2}+1\right)}\,{}_2F_1\left(-\tfrac{\alpha}{2},-\lambda-\tfrac{\alpha}{2};\tfrac{1}{2};x^2\right).$$

What remains to be shown is that the division by x in the $n = 1$ case does not destroy the finite polynomial form. Most of the hypergeometric terms in the numerator are multiplied by x^2, so we do not need to discuss them further. We are thus left to investigate the action of the division by x on the $j = 0$ case of the remaining standalone term:

$$\begin{aligned}&{}_2F_1\left(-\tfrac{\alpha}{2},-\lambda-\tfrac{\alpha}{2};\tfrac{1}{2};x^2\right) - {}_2F_1\left(-\tfrac{\alpha}{2},-\lambda-\tfrac{\alpha}{2};-\tfrac{1}{2};x^2\right)\\ &= \sum_{j=0}^{\lambda+\frac{\alpha}{2}}(-1)^j\binom{\lambda+\frac{\alpha}{2}}{j}\frac{\left(-\frac{\alpha}{2}\right)_j}{\left(\frac{1}{2}\right)_j}x^{2j} - \sum_{j=0}^{\lambda+\frac{\alpha}{2}}(-1)^j\binom{\lambda+\frac{\alpha}{2}}{j}\frac{\left(-\frac{\alpha}{2}\right)_j}{\left(-\frac{1}{2}\right)_j}x^{2j}\\ &= \sum_{j=1}^{\lambda+\frac{\alpha}{2}}(-1)^j\binom{\lambda+\frac{\alpha}{2}}{j}\left(-\frac{\alpha}{2}\right)_j\left(\frac{1}{\left(\frac{1}{2}\right)_j}-\frac{1}{\left(-\frac{1}{2}\right)_j}\right)x^{2j}.\end{aligned}$$

As for $j = 0$ both terms appearing in the cental subtraction are equal to 1 the resulting sum only involving terms where $j = 1$ or higher. Division by x thus yields a finite degree polynomial. □

In light of Corollary 3.1, the above result shows that the operators acting on the ultraspherical polynomial coefficient space are banded with compatible λ parameter choice $0 < \lambda + \frac{\alpha}{2} \in \mathbb{N}$.

As the equilibrium measure problems we wish to solve have an attractive-repulsive kernel and thus consist of a sum of two power law integrals of different powers it is straightforward to see that unfortunately, except for rare special cases, no basis choice can be made in which both operators are banded. However, the recurrence result we proved was not restricted to a particular basis choice, so we may still compute the operators for an unmatched basis and as a result we can obtain approximately banded operators in the sense of operators that decay off-band. In Figure 3.1 we show spy plots of operators corresponding to the α and β terms for a representative example case using densely stored operators to show the emergent banded structure. In practice, e.g. for the numerical experiments in Section 3.10.1 and 3.10.2, the recurrence results are implemented in a banded way such that no dense operator is ever computed or stored.

Remark 3.1 (Basis parameter choice strategy)**.** *For $\alpha > -1$ the following basis choice strategy always results in a banded operator for a single power law integral since the $n = 0$ and $n = 1$ cases evaluate to polynomials:*

$$\lambda = \begin{cases} \left\lfloor \frac{\alpha}{2} \right\rfloor - \frac{\alpha}{2}, & \text{if } \left\lfloor \frac{\alpha}{2} \right\rfloor - \frac{\alpha}{2} > -\frac{1}{2} \\ \left\lceil \frac{\alpha}{2} \right\rceil - \frac{\alpha}{2}, & \text{otherwise.} \end{cases} \tag{3.8}$$

While this choice is not unique, it is the smallest parameter choice with this property which satisfies the integrability condition $\lambda > -\frac{1}{2}$.

With the structure of the operators known and their entries being efficiently computable

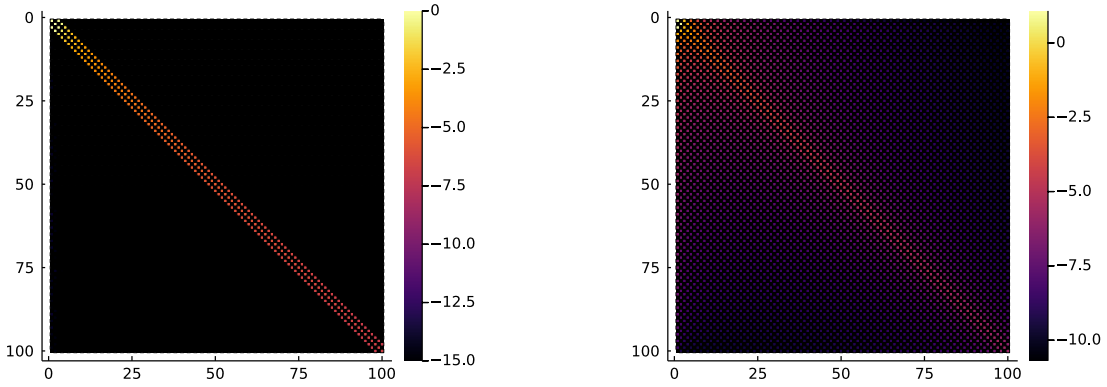

(a) α operator (b) β operator

Figure 3.1: (a) shows a spy plot of the α operator corresponding to the attractive term of the kernel for the parameter combination $\alpha = 2.6, \beta = 1.8$ in one dimension, while (b) shows the β operator corresponding to the repulsive term. The basis was chosen to make α operator banded, resulting in an banded-dominant β operator. The number of bands required in the α operator is determined by the value of α. The scale of the legend is logarithmic, indicating order of magnitude of the absolute values.

via a recurrence, we now address how to use these operators to solve equilibrium measure problems. We describe two different methods for one-dimensional problems, one valid for the primary case of interest with vanishing external potentials, i.e. the purely attractive-repulsive case, and one which also works in the presence of external potentials, captured in Algorithm 6 and 7 respectively. Note that we have to perform a regularization step in these algorithms due to the appearing first-kind problem – we explain this procedure known as Tikhonov regularization in Section 3.9.

3.6 Two interval methods in one dimension

We have previously hinted that the single interval support assumption we have made above is known to break down from numerical experiments with particle simulations as well as limited analytic results [25]. Studying this gap formation behavior is one of the primary motivations behind this work. In one dimension, we may not only compute the point at which a single interval method breaks down (which we discuss in Section 3.10.1) but also compute the resulting two interval support equilibrium measures. Due to the translation

Algorithm 6 1D single interval attractive-repulsive power law equilibrium measures

Find polynomial approximation of non-negative equilibrium measure $\mathrm{d}\rho = \rho(x)\mathrm{d}x$ and single interval support $\mathrm{supp}(\rho) = (a, b)$ such that the value of

$$E = \frac{1}{\alpha}\int_a^b |x-y|^\alpha \rho(y)\mathrm{d}y - \frac{1}{\beta}\int_a^b |x-y|^\beta \rho(y)\mathrm{d}y$$

is minimized with mass condition $\int_{\mathrm{supp}(\rho)} \rho(y)\mathrm{d}y = M$ for given M.

1. The algorithm takes an initial guess for the support as input but due to translation symmetry of the problem a single guess is sufficient by e.g. setting $a = -b$. This input is varied during the optimization part in the last step.

2. Perform a variable transformation to the unit interval, thus instead minimizing the expression

$$E = \tfrac{1}{\alpha}\left(\tfrac{b-a}{2}\right)^{\alpha+1}\int_{-1}^{1} |s-t|^\alpha \tilde{\rho}(t)\mathrm{d}t - \tfrac{1}{\beta}\left(\tfrac{b-a}{2}\right)^{\beta+1}\int_{-1}^{1} |s-t|^\beta \tilde{\rho}(t)\mathrm{d}t,$$

   where $\tilde{\rho}(t) = \rho\left(\frac{b+a}{2} + \frac{b-a}{2}t\right)$ and $\tilde{V}(s) = V\left(\frac{b+a}{2} + \frac{b-a}{2}s\right)$.

3. Assume the density $\tilde{\rho}$ is expanded in the weighted ultraspherical polynomial basis with parameter λ_α chosen according to Remark 3.1 (choosing the α operator to be banded), i.e.:

$$\tilde{\rho}(t) = (1-t^2)^{\lambda_\alpha - \frac{1}{2}}\mathbf{C}^{(\lambda_\alpha)}(t)\tilde{\boldsymbol{\rho}},$$

   resulting in approximately banded operator form for the linear problem which is solved for $\frac{\tilde{\boldsymbol{\rho}}}{E}$ after Tikhonov regularization as discussed in Section 3.9:

$$\mathbf{e}_1 = \left(\tfrac{1}{\alpha}\left(\tfrac{b-a}{2}\right)^{\alpha+1} Q^\alpha - \tfrac{1}{\beta}\left(\tfrac{b-a}{2}\right)^{\beta+1} Q^\beta\right)\tfrac{\tilde{\boldsymbol{\rho}}}{E}.$$

4. Use the property of the ultraspherical polynomials in Eq. (1.18) and the mass condition on the measure density $\left(\frac{b-a}{2}\right)\int_{-1}^{1}\tilde{\rho}(y)\mathrm{d}y = M$ to obtain the correctly scaled value of $\tilde{\boldsymbol{\rho}}$ from $\frac{\tilde{\boldsymbol{\rho}}}{E}$.

5. Compute the value of E in the sense of

$$E = \tfrac{1}{\alpha}\left(\tfrac{b-a}{2}\right)^{\alpha+1}\int_{-1}^{1} |s-t|^\alpha \tilde{\rho}(t)\mathrm{d}t - \tfrac{1}{\beta}\left(\tfrac{b-a}{2}\right)^{\beta+1}\int_{-1}^{1} |s-t|^\beta \tilde{\rho}(t)\mathrm{d}t,$$

   by using the already stored operators and loop over these steps using any constrained optimization algorithm to minimize E with non-negative ρ, e.g. by penalizing negative minima of ρ on (a, b).

Algorithm 7 1D single interval power law equilibrium measures with $V(x) \neq 0 \neq V'(x)$

Find polynomial approximation of equilibrium measure $\mathrm{d}\rho = \rho(x)\mathrm{d}x$ and single interval support $\mathrm{supp}(\rho) = (a, b)$ such that the value of

$$E = \frac{1}{\alpha}\int_a^b |x-y|^\alpha \rho(y)\mathrm{d}y + V(x)$$

is minimized with mass condition $\int_{\mathrm{supp}(\rho)} \rho(y)\mathrm{d}y = M$ for given M.

1. The algorithm takes an initial guess of the support boundary points a and b as input which are varied during the optimization part in the last step.

2. Perform a variable transformation to the unit interval, thus instead minimizing the expression

$$E = \tfrac{1}{\alpha}\left(\tfrac{b-a}{2}\right)^{\alpha+1}\int_{-1}^{1} |s-t|^\alpha \tilde{\rho}(t)\mathrm{d}t + \tilde{V}(s),$$

   where $\tilde{\rho}(t) = \rho\left(\frac{b+a}{2} + \frac{b-a}{2}t\right)$ and $\tilde{V}(s) = V\left(\frac{b+a}{2} + \frac{b-a}{2}s\right)$.

3. Assume the density $\tilde{\rho}$ is expanded in the weighted ultraspherical polynomial basis with parameter λ_α chosen according to Remark 3.1, i.e.:

$$\tilde{\rho}(t) = (1-t^2)^{\lambda_\alpha - \frac{1}{2}}\mathbf{C}^{(\lambda_\alpha)}(t)\tilde{\boldsymbol{\rho}},$$

   resulting in a banded operator form for the linear problem

$$E - \tilde{V} = \frac{1}{\alpha}\left(\tfrac{b-a}{2}\right)^{\alpha+1} Q^\alpha \tilde{\boldsymbol{\rho}}.$$

4. Differentiate once and solve the resulting linear problem for $\tilde{\boldsymbol{\rho}}$ after Tikhonov regularization as discussed in Section 3.9:

$$-D\tilde{V} = \frac{1}{\alpha}\left(\tfrac{b-a}{2}\right)^{\alpha+1} DQ^\alpha \tilde{\boldsymbol{\rho}}.$$

5. Use the property of the ultraspherical polynomials in Eq. (1.18) and the mass condition on the measure density $\left(\frac{b-a}{2}\right)\int_{-1}^{1}\tilde{\rho}(y)\mathrm{d}y = M$ to determine the correct value of the $n = 0$ coefficient of $\tilde{\boldsymbol{\rho}}$.

6. Compute the value of E in the sense of

$$E = \tfrac{1}{\alpha}\left(\tfrac{b-a}{2}\right)^{\alpha+1}\int_{-1}^{1} |s-t|\tilde{\rho}(t)\mathrm{d}t + \tilde{V}(s),$$

   by using the already stored operators and loop over these steps using any constrained optimization algorithm to minimize E with non-negative ρ, e.g. by penalizing negative minima of ρ on (a, b).

invariance of the problem, we may freely choose the two intervals to be symmetrically placed around the origin, that is

$$\operatorname{supp}(\rho) = (-b, -a) \cup (a, b).$$

We will need to extend some of our recurrence and initial condition results from Section 3.4 to the two interval case:

Lemma 3.5. *The equilibrium measure $\rho(x)$ with two interval support* $\operatorname{supp}(\rho) = (-b, -a) \cup (a, b)$ *minimizing the governing equation*

$$\begin{aligned}\tfrac{1}{\alpha}\int_{-b}^{-a} |x-y|^{\alpha}\rho_l(y)\mathrm{d}y + \tfrac{1}{\alpha}\int_{a}^{b} |x-y|^{\alpha}\rho_r(y)\mathrm{d}y \\ - \tfrac{1}{\beta}\int_{-b}^{-a} |x-y|^{\beta}\rho_l(y)\mathrm{d}y - \tfrac{1}{\beta}\int_{a}^{b} |x-y|^{\beta}\rho_r(y)\mathrm{d}y = E(x),\end{aligned}$$

with

$$\rho(y) = \begin{cases} \rho_l(y), & \text{if} \quad y \in [-b, -a] \\ \rho_r(y), & \text{if} \quad y \in [a, b], \end{cases}$$

is equivalent to the equilibrium measure minimizing

$$\begin{aligned}&\tfrac{1}{\alpha}\left(\tfrac{b-a}{2}\right)^{\alpha+1}\int_{-1}^{1}\left|-\left(\tfrac{2(b+a)}{b-a}+s\right)-t\right|^{\alpha}\rho_r(t)\mathrm{d}t + \tfrac{1}{\alpha}\left(\tfrac{b-a}{2}\right)^{\alpha+1}\int_{-1}^{1}|s-t|^{\alpha}\rho_r(t)\mathrm{d}y \\ &- \tfrac{1}{\beta}\left(\tfrac{b-a}{2}\right)^{\beta+1}\int_{-1}^{1}\left|-\left(\tfrac{2(b+a)}{b-a}+s\right)-t\right|^{\beta}\rho_r(t)\mathrm{d}t + \tfrac{1}{\beta}\left(\tfrac{b-a}{2}\right)^{\beta+1}\int_{-1}^{1}|s-t|^{\beta}\rho_r(t)\mathrm{d}y = E(s),\end{aligned}$$

where $y = \left(\tfrac{b+a}{2}\right) + \left(\tfrac{b-a}{2}\right)t$ *and* $x = \left(\tfrac{b+a}{2}\right) + \left(\tfrac{b-a}{2}\right)s$ *with* $s, t \in [-1, 1]$.

Proof. We prove this equivalence for an operator with single power α, the rest follows immediately by linearity. First, note that by rotational symmetry of the equilibrium measure problem without external potentials we have $\rho_l(-y) = \rho_r(y)$. Performing the substitution

$y \to -y$ one thus obtains

$$\int_a^b |x+y|^\alpha \rho_r(y)\mathrm{d}y + \int_a^b |x-y|^\alpha \rho_r(y)\mathrm{d}y, \tag{3.9}$$

for a single power operator. The appearance of the $|x+y|^\alpha$ kernel is expected from the discrete physical interpretation of the problem, as it accounts for long-range interactions between particles in the two separate clusters of the support. Noting that we can write

$$|x+y|^\alpha = |y-(-x)|^\alpha$$

and performing the variable transformations $y = \left(\frac{b+a}{2}\right) + \left(\frac{b-a}{2}\right)t$ and $x = \left(\frac{b+a}{2}\right) + \left(\frac{b-a}{2}\right)s$ with $s, t \in [-1,1]$ completes the proof. □

Lemma 3.5 shows that we can use the recurrence in Corollary 3.1 to compute the power law integral operators, as long as we use the following $n = 0$ and $n = 1$ case starting points for the terms which require evaluation outside of a support component:

$$\int_{-1}^{1} |x-y|^\alpha w^{(\lambda)}(y)\mathrm{d}y = \frac{\sqrt{\pi}\Gamma(\lambda+\frac{1}{2})|x|^\alpha {}_2F_1\left(\frac{1-\alpha}{2}, -\frac{\alpha}{2}; 1+\lambda; \frac{1}{x^2}\right)}{\Gamma(1+\lambda)}, \text{ if } |x| > 1.$$

$$\int_{-1}^{1} |x-y|^\alpha w^{(\lambda)}(y) C_1^{(\lambda)}(x)\mathrm{d}y = \begin{cases} \frac{\sqrt{\pi}\alpha\lambda\Gamma(\lambda+\frac{1}{2})(-x)^{\alpha-1} {}_2F_1\left(\frac{1-\alpha}{2}, 1-\frac{\alpha}{2}; 2+\lambda; \frac{1}{x^2}\right)}{\Gamma(2+\lambda)}, & \text{if } x < -1, \\ \frac{-\sqrt{\pi}\alpha\lambda\Gamma(\lambda+\frac{1}{2})x^{\alpha-1} {}_2F_1\left(\frac{1-\alpha}{2}, 1-\frac{\alpha}{2}; 2+\lambda; \frac{1}{x^2}\right)}{\Gamma(2+\lambda)}, & \text{if } x > 1. \end{cases}$$

It is straightforward to see using similar arguments as in the previous sections that this does not result in banded operators. Instead we choose a fixed approximation degree for the initial conditions and recursively generate approximately banded operators. We can then use a straightforwardly modified version of Algorithm 6 to also compute two interval equilibrium measures.

3.7 Recurrence results for radial Jacobi polynomials in arbitrary dimensions

The previous section showed how the one-dimensional equilibrium measure algorithm may be extended from single interval support to two interval support. A different direction to generalize the method in is to support higher dimensions. In this section we show how recurrence results obtained by entirely different means in higher-dimensional ball domains (the natural radially symmetric generalization of single intervals to higher dimensions) in practice allow us to compute arbitrary dimensional equilibrium measures for attractive-repulsive power law kernels.

Instead of relying on the ultraspherical polynomials as in previous sections, we require an orthogonal polynomial basis on arbitrary dimensional balls. Higher dimensional analogues of the Zernike polynomials can be used in arbitrary dimensions but these bases are unnecessarily general for our purposes.

The assumption that the power law equilibrium measure problem without external potential is radially symmetric is what guarantees that our domain will be a ball in the first place. As a consequence, we can drop all angular dependence from our basis, meaning that the radial Jacobi polynomial basis in Section 1.3.3 is the natural choice. This is further substantiated by recent results from the theory of fractional Laplacians and Riesz potentials by Dyda, Kuznetsov and Kwaśnicki in [36]. The following result is a minor extension to include $\gamma \in (-2, 0)$ in the parameter range of Theorem 3 in [36] which holds for $\gamma > 0$.

Theorem 3.3. *Let $\gamma \in (-2, 0)$, $l, n \geqslant 0$ and $1 \leqslant m \leqslant M_{d,l}$. Then the Riesz potential of*

$$(1 - |x|^2)^{\frac{\gamma}{2}} V_{l,m}(x) P_n^{\left(\frac{\gamma}{2}, \frac{d-2}{2} + l\right)}(2|x|^2 - 1)$$

on the unit ball $B_1 \subset \mathbb{R}^d$ evaluates as follows:

$$(-\Delta)^{\frac{\gamma}{2}}(1-|x|^2)^{\frac{\gamma}{2}}V_{l,m}(x)P_n^{\left(\frac{\gamma}{2},\frac{d-2}{2}+l\right)}(2|x|^2-1) \\ = \frac{2^\gamma\Gamma\left(1+\frac{\gamma}{2}+n\right)\Gamma\left(\frac{\delta+\alpha}{2}+n\right)}{n!\Gamma\left(\frac{\delta}{2}+n\right)}V_{l,m}(x)P_n^{\left(\frac{\gamma}{2},\frac{d-2}{2}+l\right)}(2|x|^2-1),$$

for all $x \in \mathbb{R}^d$ such that $|x| < 1$ and where $\delta := d + 2l$. In the above $V_{l,m}(x)$ denotes a linear basis of the finite dimensional space with dimension

$$M_{d,l} = \frac{d+2l-2}{d+l-2}\begin{pmatrix} 2+l-2 \\ l \end{pmatrix}$$

spanned by solid harmonic polynomials, i.e. polynomial solutions to Laplace's equation, with degree $l \geqslant 0$.

Proof. A proof for an analogous result with $\gamma > 0$ is given in [36]. While the proof strategies are more or less identical, we nevertheless include the full modified proof for the stated parameter range for completion.

Throughout this proof we will be abbreviating our notation by setting $V_{l,m}(x) = V(x)$. Using the explicit hypergeometric function representation of the shifted radial Jacobi polynomials in Eq. (1.43) we obtain:

$$\frac{n!}{\Gamma(1+\frac{\gamma}{2}+n)}(1-|x|^2)^{\frac{\gamma}{2}}V(x)P_n^{\left(\frac{\gamma}{2},\frac{d-2}{2}+l\right)}(2|x|^2-1) \\ = V(x)(1-|x|^2)^{\frac{\gamma}{2}}{}_2F_1\left(\begin{matrix} -n, & \frac{\delta+\gamma}{2}+n \\ & 1+\frac{\gamma}{2} \end{matrix}; 1-|x|^2\right) \\ = V(x)G^{2,0}_{2,2}\left(\begin{matrix} 1+\frac{\gamma}{2}+n, & 1-\frac{\delta}{2}-n \\ 1-\frac{\delta}{2}, & 0 \end{matrix}; |x|^2\right), \\ = (-1)^n V(x)G^{1,1}_{2,2}\left(\begin{matrix} 1-\frac{\delta}{2}-n, & 1+\frac{\gamma}{2}+n \\ 0, & 1-\frac{\delta}{2} \end{matrix}; |x|^2\right),$$

where the second and third equalities make use of properties of the Meijer-G function cf. [87, 8.4.49.22] and [36, Eq. 51]. Dyda, Kuznetsov and Kwaśnicki's next step for their proof of the $\gamma > 0$ case is to use Theorem 2 in their paper [36]. To obtain the desired $\gamma \in (-2, 0)$ result we instead use their Theorem 1 in combination with the Meijer-G cancellation rules in Eq. (1.51), yielding:

$$
\begin{aligned}
&(-\Delta)^{\frac{\gamma}{2}} \frac{n!}{\Gamma(1+\frac{\gamma}{2}+n)} (1-|x|^2)^{\frac{\gamma}{2}} V(x) P_n^{\left(\frac{\gamma}{2}, \frac{d-2}{2}+l\right)}(2|x|^2-1) \\
&\quad = (-1)^n 2^\gamma V(x) G_{4,4}^{2,2}\left(\begin{matrix} 1-\frac{\delta+\gamma}{2}, & 1-\frac{\delta+\gamma}{2}-n, & 1+n, & -\frac{\gamma}{2} \\ 0, & -\frac{\gamma}{2}, & 1-\frac{\delta+\gamma}{2}, & 1-\frac{\delta}{2} \end{matrix} ; |x|^2 \right) \\
&\quad = (-1)^n 2^\gamma V(x) G_{2,2}^{1,1}\left(\begin{matrix} 1-\frac{\delta+\gamma}{2}-n, & 1+n \\ 0, & 1-\frac{\delta}{2} \end{matrix} ; |x|^2 \right) \\
&\quad = \frac{(-1)^n 2^\gamma V(x) \Gamma\left(\frac{\delta+\gamma}{2}+n\right)}{n!} {}_2F_1\left(\begin{matrix} \frac{\delta+\gamma}{2}+n, & -n \\ & \frac{\delta}{2} \end{matrix} ; |x|^2 \right),
\end{aligned}
$$

for $|x| < 1$. All that remains to obtain the desired statement are simplifications to reduce the hypergeometric function to Jacobi polynomial form as seen in the representation in Eq. (1.43). Note that $\gamma > -2$ follows from the requirement that the Jacobi polynomial basis parameters must be greater than -1. □

To generalize the above result to be sufficient for our equilibrium measure computations, we will require the following auxiliary Lemmas:

Lemma 3.6. *For $x \in B_R \subset \mathbb{R}^d$ the power law potential of $(R^2 - |y|^2)^{\ell - \frac{\alpha+d}{2}}$, with parameter $\alpha \in (-d, 2+2\ell-d)$, evaluates to:*

$$
\int_{B_R} |x-y|^\alpha \left(R^2-|y|^2\right)^{\ell-\frac{\alpha+d}{2}} \mathrm{d}y = \frac{\pi^{\frac{d}{2}} R^{2\ell}}{\Gamma\left(\frac{d}{2}\right)} B\left(\tfrac{\alpha+d}{2}, \tfrac{2\ell+2-\alpha-d}{2}\right) {}_2F_1\left(\begin{matrix} -\frac{\alpha}{2}, & -\ell, \\ & \frac{d}{2} \end{matrix} ; \tfrac{|x|^2}{R^2} \right).
$$

Proof. This is a slightly more general statement of the result in Lemma 3.2, the proof for

both is found in [55]. □

Corollary 3.3. *For $x \in B_R \subset \mathbb{R}^d$ the power law potential of $(R^2-|y|^2)^{m-\frac{\alpha+d}{2}}$ with parameters $\alpha \in (-d, 2+2m-d)$, $m \in \mathbb{N}_0$ and $\beta > -d$, evaluates to:*

$$\int_{B_R} |x-y|^\beta (R^2-|y|^2)^{m-\frac{\alpha+d}{2}} \mathrm{d}y = \frac{\pi^{\frac{d}{2}} R^{2m+\beta-\alpha}}{\Gamma\left(\frac{d}{2}\right)} B\left(\tfrac{\beta+d}{2}, \tfrac{2m+2-\alpha-d}{2}\right) {}_2F_1\left(\begin{matrix} -\frac{\beta}{2}, & -m-\frac{\beta-\alpha}{2} \\ & \frac{d}{2} \end{matrix}; \frac{|x|^2}{R^2}\right).$$

Proof. This result is an immediately corollary of Lemma 3.6 by making the substitutions $\ell = m + \frac{\beta-\alpha}{2}$ in $\int_{B_R} |x-y|^\beta (R^2-|y|^2)^{\ell-\frac{\beta+d}{2}} \mathrm{d}y$. □

The next result generalizes Theorem 3.3 to be suitable for our application:

Theorem 3.4. *The power law integral on the unit ball $B_1 \subset \mathbb{R}^d$ with $\alpha \in (-d, 2+2m-d)$, $m \in \mathbb{N}_0$ and $\beta > -d$ of a weighted radial Jacobi polynomial*

$$(1-|y|^2)^{m-\frac{\alpha+d}{2}} P_n^{(m-\frac{\alpha+d}{2}, \frac{d-2}{2})}(2|y|^2-1)$$

can be evaluated as a Gaussian hypergeometric function:

$$\begin{aligned} &\int_{B_1} |x-y|^\beta (1-|y|^2)^{m-\frac{\alpha+d}{2}} P_n^{(m-\frac{\alpha+d}{2}, \frac{d-2}{2})}(2|y|^2-1)\mathrm{d}y \\ &\quad = \frac{\pi^{d/2}\Gamma\left(1+\frac{\beta}{2}\right)\Gamma\left(\frac{\beta+d}{2}\right)\Gamma\left(m+n-\frac{\alpha+d}{2}+1\right)}{\Gamma\left(\frac{d}{2}\right)\Gamma(n+1)\Gamma\left(\frac{\beta}{2}-n+1\right)\Gamma\left(\frac{\beta-\alpha}{2}+m+n+1\right)} {}_2F_1\left(\begin{matrix} n-\frac{\beta}{2}, & -m-n+\frac{\alpha-\beta}{2} \\ & \frac{d}{2} \end{matrix}; |x|^2\right). \end{aligned}$$

Proof. We begin by expanding the Jacobi polynomial on the left-hand side using the series representation in Eq. (1.42):

$$\begin{aligned} &\int_{B_1} |x-y|^\beta (1-|y|^2)^{m-\frac{\alpha+d}{2}} P_n^{(m-\frac{\alpha+d}{2}, \frac{d-2}{2})}(2|y|^2-1)\mathrm{d}y \\ &\quad = \frac{\Gamma\left(m+n-\frac{\alpha+d}{2}+1\right)}{n!\Gamma\left(m+n-\frac{\alpha}{2}\right)} \sum_{k=0}^{n} (-1)^k \binom{n}{k} \frac{\Gamma\left(m+n+k-\frac{\alpha}{2}\right)}{\Gamma\left(m+k-\frac{\alpha+d}{2}+1\right)} \int_{B_1} |x-y|^\beta (1-|y|^2)^{k+m-\frac{\alpha+d}{2}} \mathrm{d}y. \end{aligned}$$

The integral on the right-hand side allows the use of Corollary 3.3 to obtain

$$\int_{B_1} |x-y|^\beta (1-|y|^2)^{m-\frac{\alpha+d}{2}} P_n^{(m-\frac{\alpha+d}{2},\frac{d-2}{2})}(2|y|^2-1)\mathrm{d}y$$
$$= \frac{\pi^{\frac{d}{2}}\Gamma\left(m+n-\frac{\alpha+d}{2}+1\right)}{n!\Gamma(\frac{d}{2})\Gamma\left(m+n-\frac{\alpha}{2}\right)} \sum_{k=0}^{n}(-1)^k\binom{n}{k}\frac{\Gamma\left(m+n+k-\frac{\alpha}{2}\right)\Gamma\left(\frac{d+\beta}{2}\right)}{\Gamma\left(k+m+\frac{\beta-\alpha}{2}+1\right)}{}_2F_1\left(\begin{matrix}-\frac{\beta}{2}, -m-k-\frac{\beta-\alpha}{2} \\ \frac{d}{2}\end{matrix}; |x|^2\right).$$

after expanding the Beta function into Gamma functions and performing the resulting cancellations. It is straightforward to see that this may be rewritten into the form

$$\int_{B_1} |x-y|^\beta (1-|y|^2)^{m-\frac{\alpha+d}{2}} P_n^{(m-\frac{\alpha+d}{2},\frac{d-2}{2})}(2|y|^2-1)\mathrm{d}y$$
$$= \kappa_{m,n}^{\alpha,\beta,d}\sum_{k=0}^{n}(-1)^k\binom{n}{k}\frac{\left(1-\left(-n-m+\frac{\alpha}{2}+1\right)\right)_k}{\left(1-\left(-m-\frac{\beta-\alpha}{2}\right)\right)_k}{}_2F_1\left(\begin{matrix}-\frac{\beta}{2}, & -m-k-\frac{\beta-\alpha}{2} \\ & \frac{d}{2}\end{matrix}; |x|^2\right),$$

with newly defined constant

$$\kappa_{m,n}^{\alpha,\beta,d} = \frac{\pi^{\frac{d}{2}}\Gamma\left(m+n-\frac{\alpha+d}{2}+1\right)\Gamma\left(\frac{d+\beta}{2}\right)\Gamma\left(-\frac{\alpha}{2}+m+n\right)}{n!\Gamma(\frac{d}{2})\Gamma\left(m+n-\frac{a}{2}\right)\Gamma\left(\frac{\beta-\alpha}{2}+m+1\right)}.$$

The finite sum appearing in this statement is of the form of Eq. (1.53), which means we may collapse the finite sum of ${}_2F_1$ functions to a ${}_3F_2$ function:

$$\kappa_{m,n}^{\alpha,\beta,d}\frac{(\mathfrak{b}-\mathfrak{a})_n}{(1-\mathfrak{a})_n}{}_3F_2\left(\begin{matrix}-\frac{\beta}{2}, & \mathfrak{a}-\mathfrak{b}+1, & \mathfrak{a}-n \\ \frac{d}{2}, & \mathfrak{a}-\mathfrak{b}-n+1 & \end{matrix}; |x|^2\right)$$
$$= \kappa_{m,n}^{\alpha,\beta,d}\frac{(1+\frac{\beta}{2}-n)_n}{(\frac{\beta-\alpha}{2}+m+1)_n}{}_3F_2\left(\begin{matrix}-\frac{\beta}{2}, & n-\frac{\beta}{2}, & -m-n+\frac{\alpha-\beta}{2} \\ & \frac{d}{2}, & -\frac{\beta}{2}\end{matrix}; |x|^2\right).$$

The cancellation property for the ${}_3F_2$ function we explicitly noted in Eq. (1.52) then allows a final simplification back to precisely the ${}_2F_1$ function version of the expression which we claimed in the theorem statement. □

Based on Theorem 3.4 we can also find the following recurrence relationship to efficiently compute the operators:

Corollary 3.4. *The power law integral on the unit ball $B_1 \subset \mathbb{R}^d$ with $\alpha \in (-d, 2+2m-d)$, $m \in \mathbb{N}_0$ and $\beta > -d$ of a weighted radial Jacobi polynomial*

$$(1-|y|^2)^{m-\frac{\alpha+d}{2}} P_n^{(m-\frac{\alpha+d}{2},\frac{d-2}{2})}(2|y|^2-1)$$

satisfies the three term recurrence relationship:

$$\begin{aligned}\int_{B_1} |x-y|^\beta (1-|y|^2)^{m-\frac{\alpha+d}{2}} P_{n+1}^{(m-\frac{\alpha+d}{2},\frac{d-2}{2})}(2|y|^2-1)\mathrm{d}y \\ = (\mathfrak{c}_a|x|^2+\mathfrak{c}_b)\int_{B_1} |x-y|^\beta (1-|y|^2)^{m-\frac{\alpha+d}{2}} P_n^{(m-\frac{\alpha+d}{2},\frac{d-2}{2})}(2|y|^2-1)\mathrm{d}y \\ + \mathfrak{c}_c \int_{B_1} |x-y|^\beta (1-|y|^2)^{m-\frac{\alpha+d}{2}} P_{n-1}^{(m-\frac{\alpha+d}{2},\frac{d-2}{2})}(2|y|^2-1)\mathrm{d}y,\end{aligned}$$

with constants

$$\begin{aligned}\mathfrak{c}_a &= -\tfrac{(-\alpha+2m+4n)(-\alpha+2m+4n+2)(\alpha+d-2(m+n+1))}{2(n+1)(-\alpha+\beta+2m+2n+2)(-\alpha+\beta+d+2m+2n)}, \\ \mathfrak{c}_b &= -\tfrac{(-\alpha+2m+4n)(\alpha+d-2(m+n+1))(d(-\alpha+2\beta+2m+2)-2(2n-\beta)(-\alpha+\beta+2m+2n))}{2(n+1)(-\alpha+2m+4n-2)(-\alpha+\beta+2m+2n+2)(-\alpha+\beta+d+2m+2n)}, \\ \mathfrak{c}_c &= \tfrac{(-\beta+2n-2)(\beta+d-2n)(-\alpha+2m+4n+2)(\alpha+d-2(m+n))(\alpha+d-2(m+n+1))}{4n(n+1)(-\alpha+2m+4n-2)(-\alpha+\beta+2m+2n+2)(-\alpha+\beta+d+2m+2n)}.\end{aligned}$$

Proof. The proof of this is an immediate consequence of Theorem 3.4 in combination with one of the recurrence relationships for Gaussian hypergeometric functions of general form

$${}_2F_1\left(\begin{matrix} a+\epsilon_1 n, & b+\epsilon_2 n \\ & c+\epsilon_3 n \end{matrix}; z\right)$$

with $\epsilon_i \in \{-1,0,1\}$ which we mentioned in Section 1.4 and which follow from the so-called contiguous relationships [73, 15.5.11–15.5.18]. The specific recurrence used to obtain this result from Theorem 3.4 is stated in Eq. (1.54). □

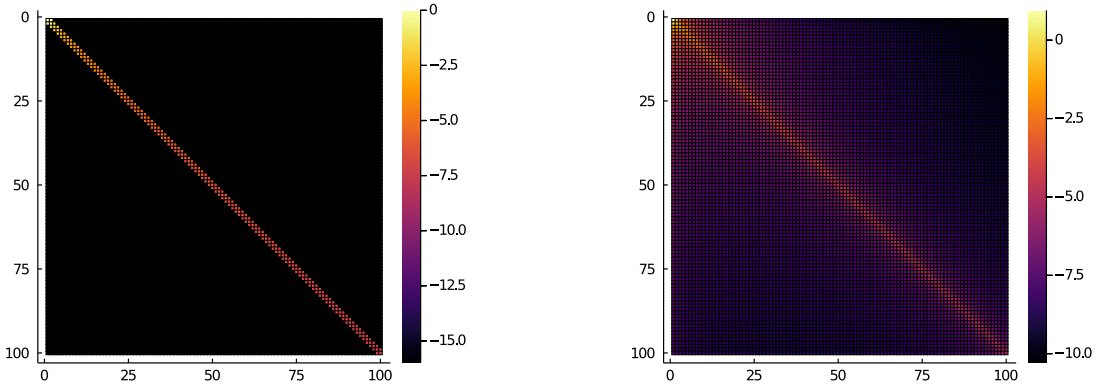

(a) α operator (b) β operator

Figure 3.2: (a) shows a spy plot of the α operator corresponding to the attractive term of the kernel for the parameter combination $d = 2, \alpha = 1.3, \beta = \frac{1}{\pi}$, while (b) shows the β operator corresponding to the repulsive term. The basis was chosen to make α operator banded (in this case tridiagonal), resulting in an approximately banded β operator. The number of bands required in the α operator is determined by the value of α and d. The scale of the legend is logarithmic, indicating order of magnitude of the absolute values.

Note that in the above results, in addition to the increased parameter range, the kernel and weight powers are now decoupled in contrast with Theorem 3.3, which makes it useful for the attractive-repulsive case. If $\alpha = \beta$ in Theorem 3.4 we once again obtain a banded operator, as is readily checked using the condition under which hypergeometric functions are finite polynomials. Likewise, the attractive-repulsive case once again yields approximately banded operators. We present some typical spy plots for different powers of these operators in Figure 3.2. In the original publication [47] that this chapter is based on, we showed how additional simpler forms of the recurrence relationships on arbitrary dimensional balls can also be obtained by different means which are nevertheless strictly special cases of the above recurrence. As they are all special cases of the above results which may be obtained by making appropriate choices of β and m, we only include the particularly interesting special cases of diagonal and tridiagonal operators.

Lemma 3.7. *The power law integral at $x = 0$ on the unit ball $B_1 \subset \mathbb{R}^d$ with $\alpha \in (-d, 2-d)$ of a weighted radial Jacobi polynomial*

$$(1-|y|^2)^{-\frac{\alpha+d}{2}} P_n^{(-\frac{\alpha+d}{2},\frac{d-2}{2})}(2|y|^2-1)$$

can be evaluated by means of a hypergeometric ${}_3F_2$ function:

$$\begin{aligned}
&\int_{B_1} |y|^p (1-|y|^2)^m P_n^{(a,b)}(2|y|^2-1)\mathrm{d}y \\
&\qquad = \sum_{k=0}^{n} (-1)^{n+k} \tfrac{(n+a+b+1)_k (b+k+1)_{n-k}}{k!\,(n-k)!} \frac{\pi^{\frac{d}{2}}}{\Gamma(\frac{d}{2})} B\left(\frac{2k+p+d}{2}, m+1\right) \\
&\qquad = \tfrac{(-1)^n \pi^{\frac{d}{2}+1} (\alpha+d)\Gamma\left(\frac{d}{2}+n\right)}{2\Gamma\left(\frac{d}{2}\right)^2 \Gamma(n+1)\sin\left(\frac{\pi(\alpha+d)}{2}\right)} {}_3F_2\left(\begin{matrix} -n, & n-\frac{\alpha}{2}, & 1+\frac{\alpha+d}{2} \\ & 2, & \frac{d}{2} \end{matrix}; 1\right).
\end{aligned}$$

Proof. This proof is obtained by expanding the Jacobi polynomial using the series representation in Eq. (1.41), then using the known result (c.f. [25, Appendix A])

$$\int_{B_R} (R^2-|y|^2)^m |y|^k \mathrm{d}y = R^{k+2m+d} \frac{\pi^{\frac{d}{2}}}{\Gamma(\frac{d}{2})} B\left(\frac{k+d}{2}, m+1\right)$$

to obtain

$$\begin{aligned}
&\int_{B_1} (1-|y|^2)^m |y|^p P_n^{(a,b)}(2|y|^2-1)\mathrm{d}y \\
&\qquad = \sum_{k=0}^{n} (-1)^{n+k} \tfrac{(n+a+b+1)_k (b+k+1)_{n-k}}{k!\,(n-k)!} \int_{B_1} (1-|y|^2)^m |y|^{2k+p} \mathrm{d}y \\
&\qquad = \sum_{k=0}^{n} (-1)^{n+k} \tfrac{(n+a+b+1)_k (b+k+1)_{n-k}}{k!\,(n-k)!} \frac{\pi^{\frac{d}{2}}}{\Gamma(\frac{d}{2})} B\left(\frac{2k+p+d}{2}, m+1\right).
\end{aligned}$$

The ${}_3F_2$ variant then follows via [73, 5.12, 16.2]. □

Lemma 3.8. *The power law integral on the unit ball $B_1 \subset \mathbb{R}^d$ with $\alpha \in (-d, 2-d)$ of a*

weighted radial Jacobi polynomial

$$(1-|y|^2)^{-\frac{\alpha+d}{2}} P_n^{(-\frac{\alpha+d}{2},\frac{d-2}{2})}(2|y|^2-1)$$

can be evaluated as a Jacobi polynomial:

$$\begin{aligned}\int_{B_1} |x-y|^\alpha (1-|y|^2)^{-\frac{\alpha+d}{2}} P_n^{(-\frac{\alpha+d}{2},\frac{d-2}{2})}(2|y|^2-1)\mathrm{d}y \\ = \frac{\pi^{\frac{d}{2}}\Gamma\left(\frac{\alpha+d}{2}\right)\Gamma\left(n-\frac{\alpha}{2}\right)\Gamma\left(1-\frac{\alpha+d}{2}+n\right)}{\Gamma\left(-\frac{\alpha}{2}\right)\Gamma\left(\frac{d}{2}+n\right)n!} P_n^{(-\frac{\alpha+d}{2},\frac{d-2}{2})}(2|x|^2-1) \\ = -\frac{\alpha\pi^{\frac{d}{2}+1}\left(1-\frac{\alpha}{2}\right)_{n-1}\left(1-\frac{\alpha+d}{2}\right)_n}{2\sin\left(\frac{\pi(\alpha+d)}{2}\right)\Gamma\left(\frac{d}{2}+n\right)n!} P_n^{(-\frac{\alpha+d}{2},\frac{d-2}{2})}(2|x|^2-1).\end{aligned}$$

Proof. The most direct way to this result is using our extension of the Dyda, Kuznetsov and Kwaśnicki in Theorem 3.3. The case $l = 0$ corresponds to the special case where $V(x) = 1$, hence we obtain

$$\begin{aligned}(-\Delta)^{-\frac{\alpha+d}{2}}(1-|x|^2)^{-\frac{\alpha+d}{2}} P_n^{(-\frac{\alpha+d}{2},\frac{d-2}{2})}(2|x|^2-1) \\ = \frac{\Gamma\left(1-\frac{\alpha+d}{2}+n\right)\Gamma\left(n-\frac{\alpha}{2}\right)}{2^{\alpha+d}\Gamma\left(\frac{d}{2}+n\right)n!} P_n^{(-\frac{\alpha+d}{2},\frac{d-2}{2})}(2|x|^2-1).\end{aligned}$$

where we have set $\gamma = -(\alpha+d)$. Following the domains of validity for individual steps via Theorem 3.3 we end up with range of validity $\alpha \in (-d, 2-d)$. Note from Definition 3.2 that there is a multiplicative constant distinguishing Riesz potentials and power law integrals, which results in the different constants in the statement of the Lemma. The second stated equality is a consequence of the known special case of the beta function [73, 5.5.3]:

$$B\left(\tfrac{\alpha+d}{2}, 1-\tfrac{\alpha+d}{2}\right) = \frac{\pi}{\sin\left(\frac{\pi(\alpha+d)}{2}\right)}.$$

□

Lemma 3.9. *The power law integral on the unit ball $B_1 \subset \mathbb{R}^d$ with $\alpha \in (2-d, 4-d)$ of a weighted radial Jacobi polynomial*

$$(1-|y|^2)^{1-\frac{\alpha+d}{2}} P_n^{(1-\frac{\alpha+d}{2},\frac{d-2}{2})}(2|y|^2-1)$$

satisfies the three term recurrence relationship:

$$\begin{aligned}\int_{B_1} |x-y|^\alpha (1-|y|^2)^{1-\frac{\alpha+d}{2}} P_n^{(1-\frac{\alpha+d}{2},\frac{d-2}{2})}(2|y|^2-1)\mathrm{d}y = \kappa_a P_{n-1}^{\left(1-\frac{\alpha+d}{2},\frac{d-2}{2}\right)}\left(2|x|^2-1\right) \\ + \kappa_b P_n^{\left(1-\frac{\alpha+d}{2},\frac{d-2}{2}\right)}\left(2|x|^2-1\right) \\ + \kappa_c P_{n+1}^{\left(1-\frac{\alpha+d}{2},\frac{d-2}{2}\right)}\left(2|x|^2-1\right),\end{aligned}$$

with constants

$$\begin{aligned}\kappa_a &= -\frac{4\pi^{d/2}\Gamma\left(\frac{\alpha+d}{2}\right)\Gamma\left(n-\frac{\alpha}{2}\right)\Gamma\left(n-\frac{\alpha+d}{2}+2\right)}{(\alpha-4n-2)(\alpha-4n)\Gamma\left(-\frac{\alpha}{2}\right)\Gamma(n+1)\Gamma\left(\frac{d}{2}+n-1\right)}, \\ \kappa_b &= \frac{8\pi^{d/2}\Gamma\left(\frac{\alpha+d}{2}\right)\Gamma\left(n-\frac{\alpha}{2}+1\right)\Gamma\left(n-\frac{\alpha+d}{2}+2\right)}{(\alpha-4n)(\alpha-4(n+1))\Gamma\left(-\frac{\alpha}{2}\right)\Gamma(n+1)\Gamma\left(\frac{d}{2}+n\right)}, \\ \kappa_c &= -\frac{4\pi^{d/2}\Gamma\left(\frac{\alpha+d}{2}\right)\Gamma\left(n-\frac{\alpha}{2}+2\right)\Gamma\left(n-\frac{\alpha+d}{2}+2\right)}{(\alpha-4n-2)(\alpha-4(n+1))\Gamma\left(-\frac{\alpha}{2}\right)\Gamma(n+1)\Gamma\left(\frac{d}{2}+n+1\right)}.\end{aligned}$$

Proof. The crucial observation for this result is that the ordinary Laplace operator acts as follows on power law integrals with $\alpha \in (-d, 2-d)$:

$$\begin{aligned}\Delta_x \int_{B_1} |x-y|^{\alpha+2}(1-|y|^2)^{-\frac{\alpha+d}{2}} P_n^{(-\frac{\alpha+d}{2},\frac{d-2}{2})}(2|y|^2-1)\mathrm{d}y = \\ (\alpha+d)(\alpha+2)\int_{B_1} |x-y|^\alpha (1-|y|^2)^{-\frac{\alpha+d}{2}} P_n^{(-\frac{\alpha+d}{2},\frac{d-2}{2})}(2|y|^2-1)\mathrm{d}y = \\ -\frac{(\alpha+d)(\alpha+2)\alpha\pi^{\frac{d}{2}} B\left(\frac{\alpha+d}{2},1-\frac{\alpha+d}{2}\right)\left(1-\frac{\alpha}{2}\right)_{n-1}\left(1-\frac{\alpha+d}{2}\right)_n}{2\Gamma\left(\frac{d}{2}+n\right)n!} P_n^{(-\frac{\alpha+d}{2},\frac{d-2}{2})}(2|x|^2-1).\end{aligned}$$

Note that we have used Lemma 3.8 to evaluate the power law integral in the final step. Before proceeding, we use basis conversion operators to raise the first parameter of the Jacobi polynomial basis by 2 in the above result because otherwise the chain of arguments

which follows fails to guarantee that the Jacobi polynomial parameters remain greater than -1. We thus use

$$\begin{aligned}P_n^{\left(-\frac{\alpha+d}{2},\frac{d-2}{2}\right)}(2|x|^2-1) =& \tfrac{(d+2n-4)(d+2n-2)}{(4n-\alpha)(-\alpha+4n-2)} P_{n-2}^{\left(2-\frac{\alpha+d}{2},\frac{d-2}{2}\right)}\left(2|x|^2-1\right)\\ &+\tfrac{2(d+2n-2)(\alpha-2n)}{(\alpha-4n)^2-4} P_{n-1}^{\left(2-\frac{\alpha+d}{2},\frac{d-2}{2}\right)}\left(2|x|^2-1\right)\\ &+\tfrac{(\alpha-2n)(\alpha-2n-2)}{(4n-\alpha)(-\alpha+4n+2)} P_n^{\left(2-\frac{\alpha+d}{2},\frac{d-2}{2}\right)}\left(2|x|^2-1\right).\end{aligned}$$

Due to the radial symmetry of the integrals we then obtain

$$\begin{aligned}&\int_{B_1}|x-y|^{\alpha+2}(1-|y|^2)^{-\frac{\alpha+d}{2}}P_n^{\left(-\frac{\alpha+d}{2},\frac{d-2}{2}\right)}(2|y|^2-1)\mathrm{d}y =\\ &c_{\mathrm{a}}P_{n-1}^{\left(-\frac{\alpha+d}{2},\frac{d-2}{2}\right)}\left(2|x|^2-1\right)+c_{\mathrm{b}}P_n^{\left(-\frac{\alpha+d}{2},\frac{d-2}{2}\right)}\left(2|x|^2-1\right)+c_{\mathrm{c}}P_{n+1}^{\left(-\frac{\alpha+d}{2},\frac{d-2}{2}\right)}\left(2|x|^2-1\right)+c_{\mathrm{d}},\end{aligned}$$

with the fixed constants

$$\begin{aligned}c_{\mathrm{a}} &= -\tfrac{4\pi^{d/2}\Gamma\left(\frac{1}{2}(d+\alpha+2)\right)\Gamma\left(n-\frac{\alpha}{2}-1\right)\Gamma\left(n-\frac{\alpha+d}{2}+1\right)}{\Gamma\left(-\frac{\alpha}{2}-1\right)(-\alpha+4n-2)(4n-\alpha)\Gamma(n+1)\Gamma\left(\frac{d}{2}+n-1\right)},\\ c_{\mathrm{b}} &= \tfrac{8\pi^{d/2}\Gamma\left(\frac{1}{2}(d+\alpha+2)\right)\Gamma\left(n-\frac{\alpha}{2}\right)\Gamma\left(n-\frac{\alpha+d}{2}+1\right)}{\Gamma\left(-\frac{\alpha}{2}-1\right)((\alpha-4n)^2-4)\Gamma(n+1)\Gamma\left(\frac{d}{2}+n\right)},\\ c_{\mathrm{c}} &= -\tfrac{4\pi^{d/2}\Gamma\left(\frac{1}{2}(d+\alpha+2)\right)\Gamma\left(n-\frac{\alpha}{2}+1\right)\Gamma\left(n-\frac{\alpha+d}{2}+1\right)}{\Gamma\left(-\frac{\alpha}{2}-1\right)(-\alpha+4n+2)(4n-\alpha)\Gamma(n+1)\Gamma\left(\frac{d}{2}+n+1\right)}.\end{aligned}$$

What remains to be proved is that the constant $c_{\mathrm{d}} = 0$. This is done using Lemma 3.7, which results in

$$\begin{aligned}&(-1)^n\left(-\frac{\left(\frac{d}{2}\right)_{n-1}}{(n-1)!}c_{\mathrm{a}}+\frac{\left(\frac{d}{2}\right)_n}{n!}c_{\mathrm{b}}-\frac{\left(\frac{d}{2}\right)_{n+1}}{(n+1)!}c_{\mathrm{c}}\right)+c_{\mathrm{d}} =\\ &\sum_{k=0}^{n}(-1)^{n+k}\tfrac{\left(n-\frac{\alpha+d}{2}+\frac{d-2}{2}+1\right)_k\left(\frac{d-2}{2}+k+1\right)_{n-k}}{k!\,(n-k)!}\frac{\pi^{\frac{d}{2}}}{\Gamma\left(\frac{d}{2}\right)}B\left(\tfrac{2k+\alpha+2+d}{2},1-\tfrac{\alpha+d}{2}\right),\end{aligned}$$

which may be solved to obtain $c_{\mathrm{d}} = 0$. The Lemma statement follows after performing the power shift $\alpha+2 \to \alpha$ to maintain consistent kernel power notation. □

These two results respectively show in which special cases one obtains diagonal or tridiagonal

operators from the more general results in 3.4. By using the methodology in the proof of Lemma 3.9 one can obtain further polynomial recurrences for appropriately matched basis and kernel powers with increasing bandwidth in the resulting operator as the parameters increase. All of the resulting recurrences valid for higher parameter ranges remain special cases of the fully general result in Corollary 3.4, so we do not pursue this different proof approach further than we did above.

3.8 Numerical method on arbitrary dimensional balls

The primary two results of the previous section, Theorem 3.4 and Corollary 3.4, can be used to construct an algorithm similar to Algorithm 6 but for arbitrary dimensions. We summarize this method in Algorithm 8. As before, we choose to delay the discussion of the Tikhonov regularization step to Section 3.9. In step 4 of Algorithm 8 we make use of the following result to correctly normalize the obtained measure:

Lemma 3.10. *Let $\rho(y) = \rho(|y|^2)$, $y \in B_1 \subset \mathbb{R}^d$ be a function of constant mass M in the sense that*

$$\int_{B_1} \rho(y)\mathrm{d}y = M.$$

If an expansion of $\rho(y)$ in weighted radial Jacobi polynomials

$$\rho(y) = \sum_{n=0}^{\infty} \rho_n (1-|y|^2)^a P_n^{(a,\frac{d-2}{2})}(2|y|^2-1)$$

exists and satisfies the condition

$$\int_{B_1} \sum_{n=0}^{\infty} \left| \rho_n (1-|y|^2)^a P_n^{(a,\frac{d-2}{2})}(2|y|^2-1) \right| \mathrm{d}y < \infty, \tag{3.10}$$

then

$$M = \int_{B_1} \rho(y)\mathrm{d}y = \frac{\pi^{\frac{d}{2}}\Gamma(a+1)}{\Gamma\left(a+\frac{d}{2}+1\right)}\rho_0.$$

Proof. Using hyperspherical coordinates, with $\sigma(S^{d-1}) = \frac{2\pi^{\frac{d}{2}}}{\Gamma(\frac{d}{2})}$ denoting the surface area of the $d-1$ dimensional sphere, we obtain

$$\begin{aligned} M_1 = \int_{B_1} \rho(y)dy &= \sum_{n=0}^{\infty} \rho_n \int_{B_1} (1-|y|^2)^a P_n^{(a,\frac{d-2}{2})}(2|y|^2-1)dy \\ &= \sum_{n=0}^{\infty} \rho_n \int_{S^{d-1}} \int_{r=0}^{1} (1-r^2)^a P_n^{(a,\frac{d-2}{2})}(2r^2-1) r^{d-1} dr d\sigma(\omega) \\ &= \sigma(S^{d-1}) \sum_{n=0}^{\infty} \rho_n \int_{r=0}^{1} (1-r^2)^a P_n^{(a,\frac{d-2}{2})}(2r^2-1) r^{d-1} dr. \end{aligned}$$

Note that the sum and integral order change in the first step uses the Fubini-Tonelli theorem, which is why the condition in (3.10) is part of the Lemma statement. The stated result then follows via

$$\begin{aligned} &\sum_{n=0}^{\infty} \rho_n \int_0^1 (1-r^2)^a P_n^{(a,\frac{d-2}{2})}(2r^2-1) r^{d-1} dr \\ &\qquad = \frac{1}{4} \sum_{n=0}^{\infty} \rho_n \int_{-1}^{1} \frac{(1-t)^a}{2^a} \frac{(1+t)^{\frac{d-2}{2}}}{2^{\frac{d-2}{2}}} P_n^{(a,\frac{d-2}{2})}(t) dt \\ &\qquad = 2^{\frac{-2-2a-d}{2}} \sum_{n=0}^{\infty} \rho_n \int_{-1}^{1} (1-t)^a (1+t)^{\frac{d-2}{2}} P_n^{(a,\frac{d-2}{2})}(t) dt \\ &\qquad = \frac{\Gamma(a+1)\Gamma\left(\frac{d}{2}\right)}{2\Gamma\left(a+\frac{d}{2}+1\right)} \rho_0. \end{aligned}$$

□

Remark 3.2. *Note that the operators Q^α and Q^β in the Algorithms (6-8) are independent of R or in the one-dimensional cases independent of a and b. The computational consequence of this is that one does not need to re-generate operators in each optimization step.*

Algorithm 8 Arbitrary dimensional ball power law equilibrium measures with $V(x) = 0$

Find polynomial approximation of non-negative equilibrium measure $\mathrm{d}\rho = \rho(x)\mathrm{d}x$ and radius of ball support centered on the origin

$$\mathrm{supp}(\rho) = B_R$$

such that the value of

$$\frac{1}{\alpha}\int_{B_R} |x-y|^\alpha \rho(y)dy - \frac{1}{\beta}\int_{B_R} |x-y|^\beta \rho(y)dy = E,$$

is minimized with mass condition $\int_{\mathrm{supp}(\rho)} \rho(y)\mathrm{d}y = M$ for given M.

1. The algorithm takes an initial guess for the support radius as input which is varied in the optimization part in the last step.

2. Perform a variable transformation to the unit ball, thus instead minimizing the expression
$$\frac{R^{\alpha+d}}{\alpha}\int_{B_1} |x-y|^\alpha \rho(Ry)dy - \frac{R^{\beta+d}}{\beta}\int_{B_1} |x-y|^\beta \rho(Ry)dy = E,$$
where now $|y|, |x| \leqslant 1$.

3. Assume the density $\tilde{\rho}(y) = \rho(Ry)$ is expanded in the weighted radial Jacobi polynomial basis
$$\tilde{\rho}(y) = \sum_{n=0}^{\infty} \tilde{\rho}_n (1-|y|^2)^{\ell-\frac{\alpha+d}{2}} P_n^{(\ell-\frac{\alpha+d}{2},\frac{d-2}{2})}(2|y|^2-1) = (1-|y|^2)^{\ell-\frac{\alpha+d}{2}} \mathbf{P}^{(\ell-\frac{\alpha+d}{2},\frac{d-2}{2})}(2|y|^2-1)\tilde{\boldsymbol{\rho}},$$
with ℓ chosen in accordance with Theorem 3.4 and Corollary 3.4, resulting in the following approximately banded operator form which is solved for $\frac{\tilde{\boldsymbol{\rho}}}{E}$ after Tikhonov regularization:
$$\left(\frac{R^{\alpha+d}}{\alpha}Q^\alpha - \frac{R^{\beta+d}}{\beta}Q^\beta\right)\frac{\tilde{\boldsymbol{\rho}}}{E} = \mathbf{e}_1.$$

4. Use Lemma 3.10 to normalize the obtained measure and obtain $\tilde{\boldsymbol{\rho}}$ from $\frac{\tilde{\boldsymbol{\rho}}}{E}$.

5. Compute the value of E in the sense of
$$\frac{R^{\alpha+d}}{\alpha}\int_{B_1} |x-y|^\alpha \rho(Ry)dy - \frac{R^{\beta+d}}{\beta}\int_{B_1} |x-y|^\beta \rho(Ry)dy = E,$$
by using the already stored operators and loop over these steps using any constrained optimization algorithm to minimize E with non-negative ρ, e.g. by penalizing negative minima on B_R.

3.9 Tikhonov regularization for power law equilibrium measure problems

The discussion of convergence and stability for the one-dimensional and higher-dimensional method is largely identical and respectively splits into two sub-questions regarding the convergence of the spectral method step and the convergence of the optimization step. As the optimization step simply inherits its convergence properties from the optimization method of choice, the value of E is well-behaved in the neighborhood of the equilibrium measures and we do not specify a concrete optimization method to use, we will focus on the spectral method step in this section.

As we saw in sections 3.5 and 3.8, the spectral method part of our solution algorithms may be reduced to solving the following system:

$$E = \frac{1}{\alpha}\int_{B_R} |x-y|^{\alpha}\rho(y)\mathrm{d}y - \frac{1}{\beta}\int_{B_R} |x-y|^{\beta}\rho(y)\mathrm{d}y, \tag{3.11}$$

where the ball B_R may be of arbitrary dimension, including the case $d = 1$. In Chapter 2 we noted how Volterra integral equations of first-kind, that is equations of the form $\mathrm{V}_K\mathbf{u} = \mathbf{g}$ were in a sense ill-posed without further specification as the Volterra integral operator is known to be compact on $L^2[0,1]$. While the integral operator in (3.11) is not a Volterra integral operator it is nevertheless a Fredholm integral operator for which similar results hold and finite section methods should not be expected to sensibly converge without additional constraints. Note that even in the case where the external potential V is non-vanishing as in Algorithm 7, the linear problem we end up solving in the algorithm is nevertheless a first-kind problem.

Unlike in the case of our convergence proof for Volterra integral equations of first-kind in Chapter 2, restricting the function space is not an option here. While such an approach *may* yield a convergence result, in an actual application we have little to no control over the function space of the equilibrium measure solutions we wish to compute for a given pair

of powers and thus require a method that regularizes these problems more generically. The method of choice in the literature to turn first-kind Fredholm integral equations into well-posed problems is known as Tikhonov regularization, named after Andrey Tikhonov who first discussed these ideas in the 1960s [103, 102]. The general idea of Tikhonov regularization is to solve an, in a suitably defined sense, *adjacent* second-kind problem of the first-kind problem we wish to solve. If the first-kind problem has a solution, which we assume is the case, then the error incurred from solving the second-kind problem instead may be bounded by how far away it is from the first-kind problem. To make this more explicit, instead of the above equation we solve

$$(sI + \mathcal{F}^*\mathcal{F})\rho_s = \mathcal{F}^*E, \tag{3.12}$$

where I is the identity matrix, and we have introduced a shorthand notation for the power law integral operators $\mathcal{F} = Q^\alpha - Q^\beta$. Note that in this notation the original equation in 3.11 is simply $\mathcal{F}\rho = E$. Solving the Tikhonov regularized equation 3.12 for small parameters s allows us to substantially improve the stability of our method – we explore this numerically in sections 3.10.1 and 3.10.2. Lastly, we note that the error incurred by using the n-th order polynomial approximation of ρ_s (with small s) denoted $\rho_{s,n}$ may be split into an error due to the Tikhonov regularization $\|\rho_s - \rho\|$ and one due to the spectral method $\|\rho_{s,n} - \rho_s\|$ by means of the triangle inequality:

$$\|\rho_{s,n} - \rho\| = \|\rho_{s,n} - \rho_s + \rho_s - \rho\| \leqslant \|\rho_{s,n} - \rho_s\| + \|\rho_s - \rho\|.$$

The literature on choice strategies for s and properties of Tikhonov regularizations is too extensive to include a detailed discussion here, so for additional details on the available options and trade-offs we refer to [71, 70] and the references therein.

3.10 Numerical experiments and validation

In this section we present numerical experiments with the aim of verifying the above-introduced algorithms against special case known solutions and particle-based simulations as well as explore presently poorly understood properties such as uniqueness and the void formation boundary of power law equilibrium measures in one and higher dimensions. Section 3.10.1 discusses the one-dimensional case, while Section 3.10.2 addresses the case of arbitrary dimensional ball support.

3.10.1 In one dimension

Special cases with known solutions

As mentioned in the introduction of this chapter, some uniqueness and existence results exist for special parameter cases. One such example is problems of the form

$$E = \frac{1}{2}\int_a^b |x-y|^2 \rho(y)\mathrm{d}y - \frac{1}{\beta}\int_a^b |x-y|^\beta \rho(y)\mathrm{d}y, \tag{3.13}$$

with $1 < \beta < 2$, for which the analytically obtained solution and support radius are:

$$b = -a = \left[\frac{\cos\left(\frac{(2-\beta)\pi}{2}\right)}{\pi(\beta-1)} B\left(\tfrac{1}{2}, \tfrac{3-\beta}{2}\right)\right]^{\frac{1}{\beta-2}}, \tag{3.14}$$

$$\rho(x) = \tfrac{M}{\beta-1}\frac{\cos\left(\frac{\pi(2-\beta)}{2}\right)}{\pi}\left(b^2 - x^2\right)^{\frac{1-\beta}{2}}. \tag{3.15}$$

In this section we compare numerically obtained solutions with these analytic special case solutions. In Figure 3.3 we plot the value of E obtained from different support radius assumptions for two examples with analytic solutions, showing how the analytic solution is located in a unique local minimum of E. When taking into account the constraint that the measure must be non-negative, the measure appears to in fact be globally unique. In Figure 3.4 and 3.5 we plot the obtained measures corresponding with the parameter choices

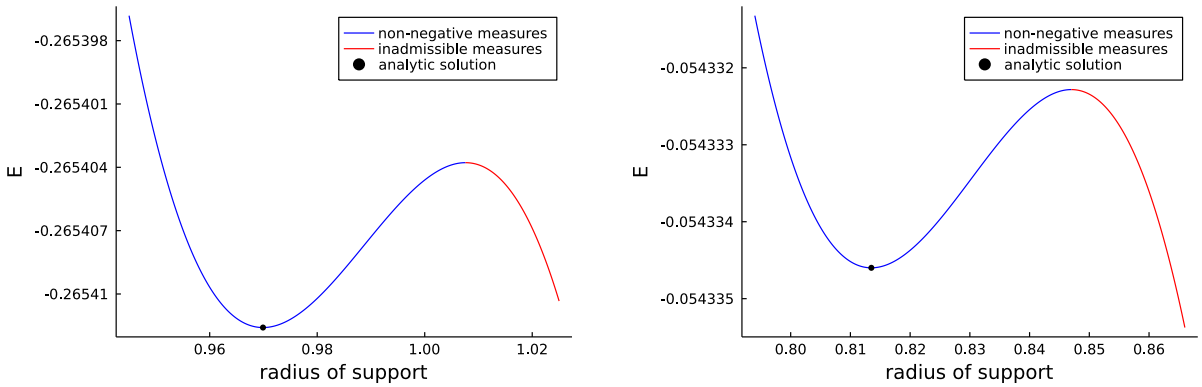

(a) $\beta = 1.1$ (b) $\beta = 1.68$

Figure 3.3: E computed from equilibrium measure candidates for the problem in (3.13) in the neighborhood of the analytic solution (with support radius on the x-axis). The indicated analytic radius of support seen in (3.14) agrees with the numerically found unique local minimum and any measures with lower E are found to not be admissible due to the non-negativity condition.

of Figure 3.3 on their support as well as the error compared to the analytic solution for a fixed approximation degree.

Exploring uniqueness and existence of solutions

Figure 3.3 in the previous section showed how uniqueness and existence of the numerically obtained solution is observed for the special cases where these properties are already analytically known. In this section we show that even when α and β are not of the even integer form for which solutions are known, uniqueness and existence still hold.

In Figure 3.6, we plot E as a function of the support radius as we did in Figure 3.3 but now for problems where no analytic solutions are known and observe the same qualitative behavior: A unique local minimum with admissible non-negative measures. This is observed as long as the value of the repulsive power β is lower than a certain void formation threshold which depends on α as well as the dimension of the problem. We discuss this void formation threshold in more detail in the final numerical experiments section of this chapter.

In Figure 3.7 we plot the equilibrium measure solutions corresponding to the problem parameters in Figure 3.6 including histograms generated from a particle simulation with 1000

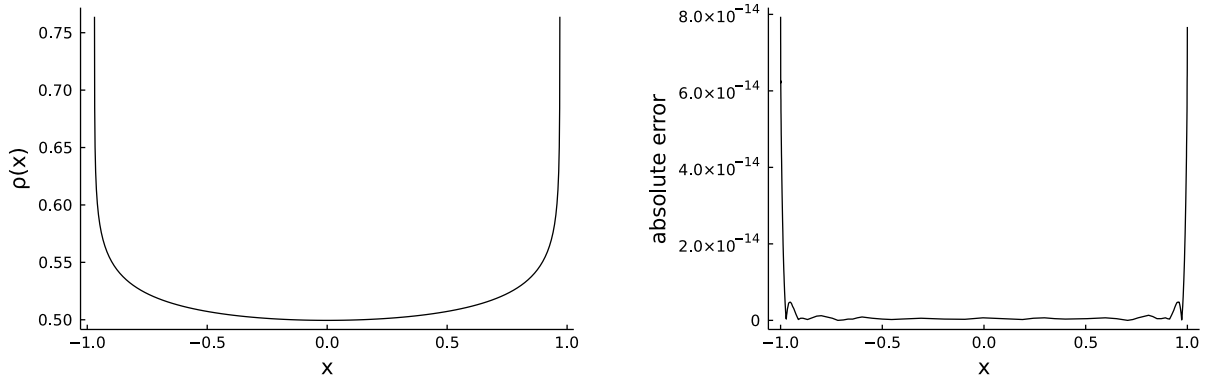

(a) (b)

Figure 3.4: (a) shows computed equilibrium measure for (3.13) with $\beta = 1.1$ on its radius of support. (b) shows the error compared to the analytic solution in (3.15) after both measures have been normalized to the unit interval $(-1, 1)$.

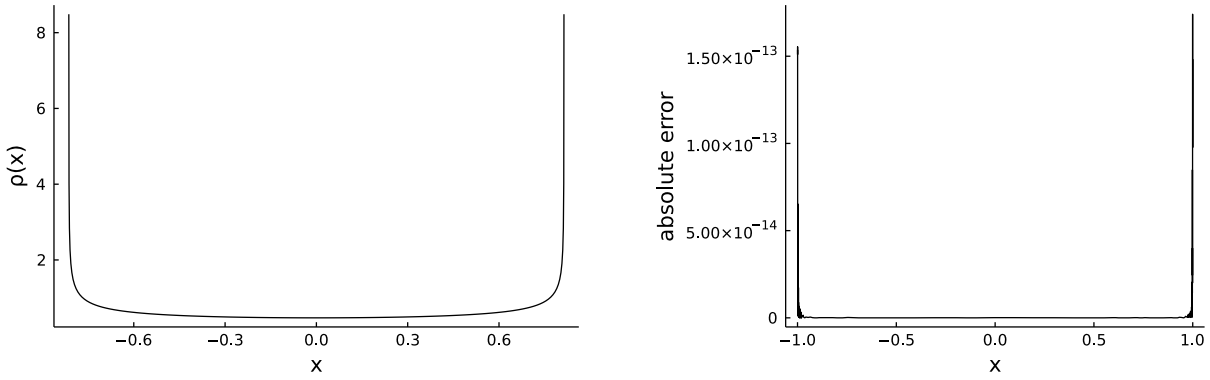

(a) (b)

Figure 3.5: (a) shows computed equilibrium measure for (3.13) with $\beta = 1.68$ on its radius of support. (b) shows the error compared to the analytic solution in (3.15) after both measures have been normalized to the unit interval $(-1, 1)$.

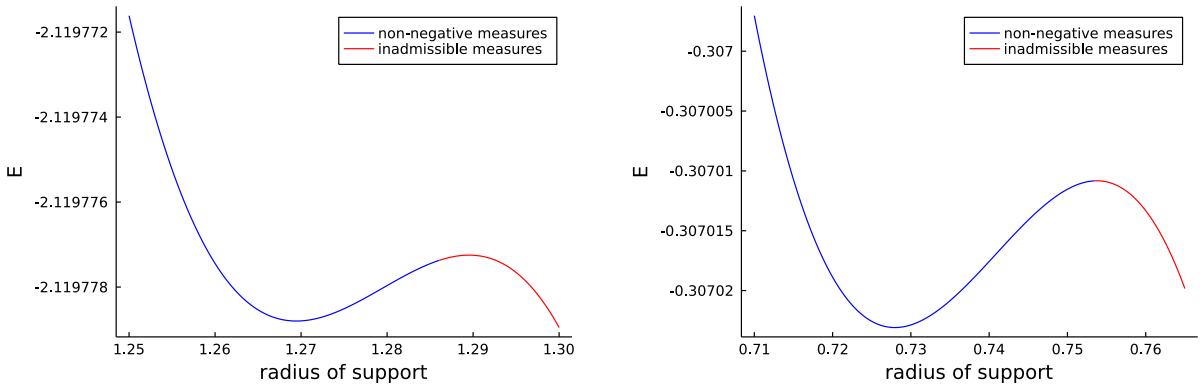

(a) $\alpha = 1.87, \beta = 0.33$ (b) $\alpha = 3.6, \beta = 1.2$

Figure 3.6: E computed from equilibrium measure candidates for the attractive-repulsive equilibrium measure problem with indicated parameters in the neighborhood of the only observed local minimum with non-negative measure. As no analytic solutions are available, we instead compare the computed measures with what is obtained from particle simulations in Figure 3.7.

particles showing that our continuous solutions agree with the only other currently available approach.

Two interval examples

We described how two interval attractive-repulsive problems may be solved using a variation of our method in section 3.6. These measures occur in practice when the repulsive power overcomes a void formation threshold which causes all single interval measures to have negative values around the origin. Thus, an implementation of the methods discussed in this chapter may automatically detect the need to use a two interval method based on the non-existence of non-negative measures of single interval support – we show an example of how this could work in Figure 3.8 where we show the single interval measures obtained from the unique local minimum (with the non-negativity condition turned off). Similar ideas were previously discussed for the case of log kernel equilibrium measures in [74].

In Figure 3.9 we plot a measure obtained using the two interval method for a parameter combination where single interval support yields no non-negative measures. Since no analytic solutions exist in these cases, we instead include a comparison with discrete particle

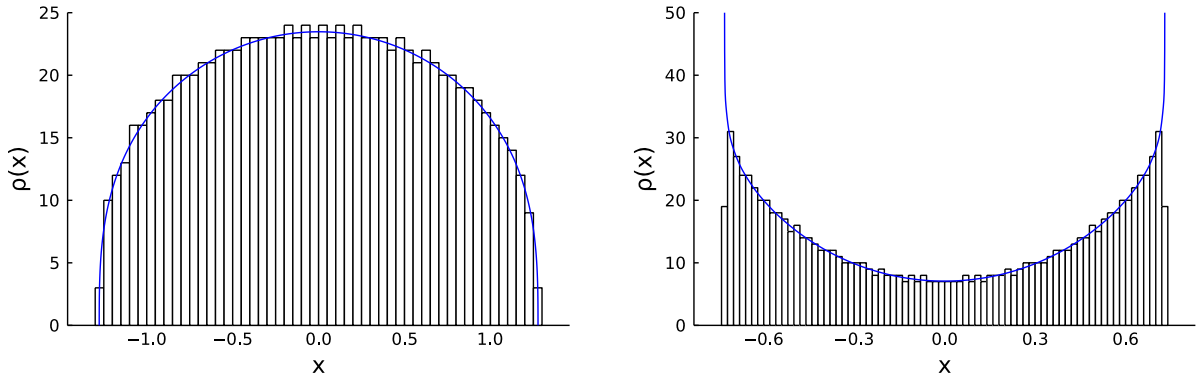

(a) $\alpha = 1.87, \beta = 0.33$ (b) $\alpha = 3.6, \beta = 1.2$

Figure 3.7: Plot of the numerically obtained measures for the attractive-repulsive power law equilibrium measure problems with indicated parameters (in blue). As no analytic solutions are available for comparison, we instead include histograms of a particle simulation using 1000 particles. The measure mass M was scaled to the histogram mass to allow comparison.

simulations. An animation generated using our method which shows the transition from single to two interval measures was previously made available as part of the publication [48] in [46]. While the two interval method works and agrees with particle simulations, the numerical experiments we performed suggest that the two interval approach is substantially more prone to instability and thus a more specialized regularization scheme or using different recurrences and bases than the ones discussed may be worth exploring in future research.

Examples with external potentials

While the bulk of the discussion in this chapter concerned attractive-repulsive equilibrium measures, we also discussed a method for a single power in combination with an external potential in Algorithm 7. In this section we show proof of concept of this algorithm in action for the following equilibrium measure problem:

$$E = -\frac{4}{3}\int_a^b |x-y|^{-\frac{3}{4}}\rho(y)\mathrm{d}y + V(x), \tag{3.16}$$

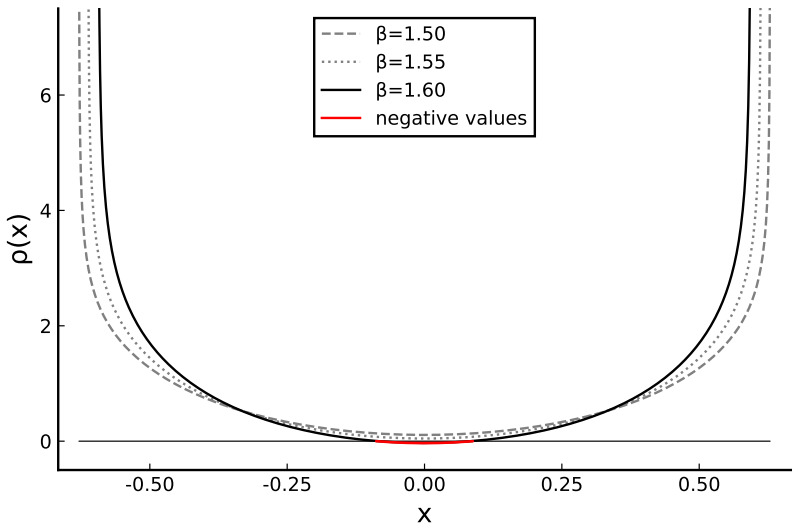

Figure 3.8: Plot of the numerically obtained measures for attractive-repulsive power law equilibrium measure problem with parameters $\alpha = 3.75$ and the indicated values of β. Above a void formation threshold of the repulsive power β (which depends on α) no non-negative measures on single interval support can be found. Choosing the local minimum in E disregarding the non-negativity condition results in a single interval measure with negative values around the origin, which can be used in code to automate splitting the support interval.

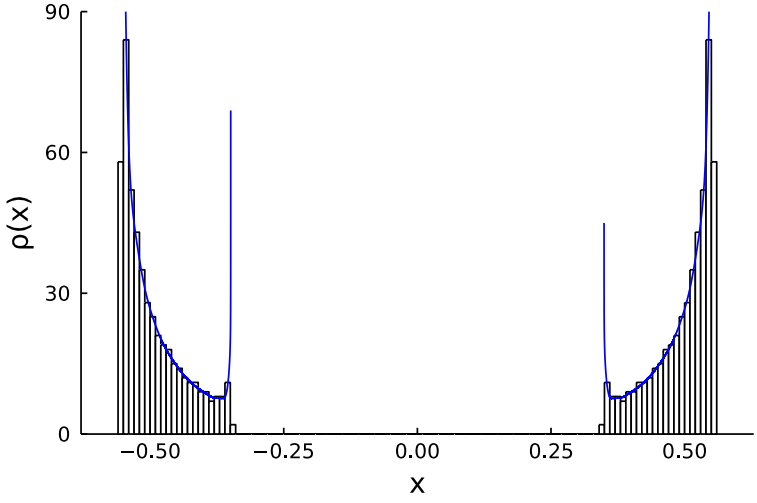

Figure 3.9: Plot of the numerically obtained measure for an attractive-repulsive power law equilibrium measure problem with parameters $\alpha = 3.37$ and $\beta = 1.81$ (in blue). As no analytic solutions are available for comparison, we instead include a histogram of a particle simulation using 1000 particles. The measure mass M was scaled to the histogram mass to allow comparison.

with asymmetric external potential

$$V(x) = -x^6 - \sin(2x). \tag{3.17}$$

We use an asymmetric external potential to showcase that Algorithm 7 does not require or assume radial symmetry. We plot the numerically obtained measure solving the equilibrium measure problem in Eq. (3.16) in Figure 3.10. An interesting consequence of problems involving external potentials is that the problem loses the translation invariance inherent in purely attractive-repulsive problems.

Since once again no analytic solutions are available, we instead compare with a differently obtained numerical solution in Figure 3.10. The alternative method we use as a comparison is an immediate consequence of the operator form derived for (3.16) as part of Algorithm 7 and is based on an idea found in [74]: For the special case in which the equilibrium measure is the unique solution which vanishes on its support boundary we can instead obtain a numerical solution by using a Newton iteration acting on each component of the approximation's polynomial coefficients to force the resulting approximation to vanish on the boundary. As we have seen in previous numerical experiments, most measures are not of this form and instead have non-trivial singularities on the boundary. Limited information for which parameter ranges allow for such an alternative approach can be inferred from results in [25] but to best of the knowledge of the authors no general results are known. Nevertheless, this alternative method provides a further check that the candidate measures our algorithms pick out are indeed the equilibrium measures. Note that this alternative method is not discussed in more detail because it is always less efficient than the method where we optimize over the support boundary points (since any reasonable approximation of ρ will have more than two coefficients) and for reasons outlined above is severely restricted in applicable range.

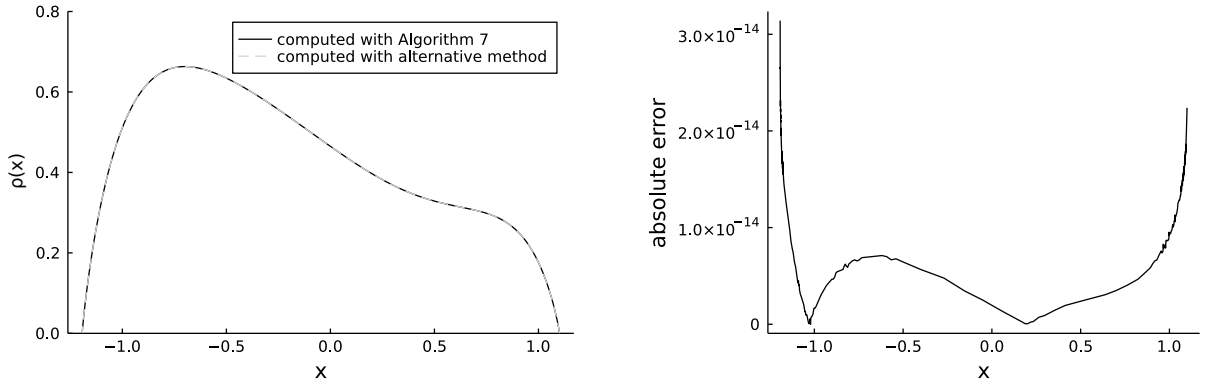

(a) (b)

Figure 3.10: (a) shows a plot of the numerically obtained measure (in black) for the asymmetric single power equilibrium measure problem in (3.16) with external potential in (3.17) and parameters $\alpha = 3.6$, $\beta = 1.2$. Note that unlike the purely attractive-repulsive equilibrium measure problems this measure is not translation invariant. No analytic solutions are available for comparison but as this is a special case where the candidate measure vanishes at the boundary, we instead overlay (in dashed gray) a measure obtained with an alternative coefficient space Newton iteration approach. (b) shows the absolute error between the two methods.

3.10.2 In higher dimensions

Special cases with known solutions

As in the one-dimensional case, analytic solutions with arbitrary ball support are known for the special case where either α or β are an even integer [25]. Here we consider the following special case solutions for $\alpha = 4$ and $\beta < \frac{(2+2d-d^2)}{(d+1)}$:

$$R = \left[\frac{d(d+2)\Gamma(\frac{d}{2})}{2\Gamma(\frac{\beta+d}{2})\Gamma(2-\frac{\beta}{2}))} \left(\frac{1}{4-\beta} + \frac{1}{\sqrt{(2-\beta)(6-\beta)}} \right) \right]^{-\frac{1}{4-\beta}}, \tag{3.18}$$

$$\rho(x) = (R^2 - |x|^2)^{1-\frac{\beta+d}{2}} \left(A_1 R^2 + A_2 (R^2 - |x|^2) \right), \tag{3.19}$$

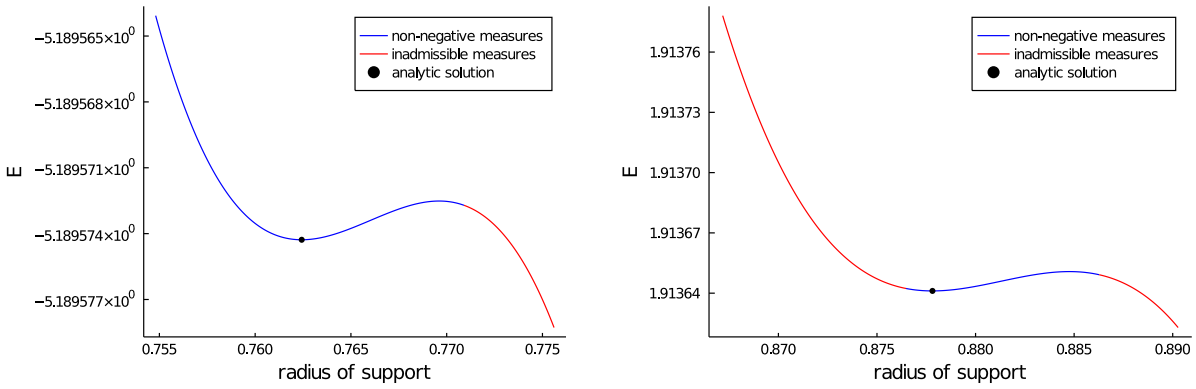

(a) $d = 2, \beta = \frac{1}{\pi}$ (b) $d = 6, \beta = 3.7$

Figure 3.11: E computed from equilibrium measure candidates for the attractive-repulsive problem with $\alpha = 4$ in indicated dimension d in the neighborhood of the analytic solution (with support radius on the x-axis). The indicated analytic radius of support seen in (3.18) agrees with the numerically found unique local minimum and any measures with lower E are found to not be admissible due to the non-negativity condition.

with functions

$$A_1(\beta, d) = \frac{\Gamma(\frac{d}{2})}{\pi^{\frac{d}{2}}} \frac{d(d+2)M}{2B\left(\frac{\beta+d}{2}, 2 - \frac{\beta+d}{2}\right)} \left[\frac{1}{\sqrt{(2-\beta)(6-\beta)}} + \frac{1}{2-\beta} \right],$$
$$A_2(\beta, d) = \frac{\Gamma(\frac{d}{2})}{\pi^{\frac{d}{2}}} \frac{d(d+2)M}{B\left(\frac{\beta+d}{2}, 3 - \frac{\beta+d}{2}\right) 4(\beta-2)M}.$$

In Figure 3.11 we plot the value of E obtained from different support radius assumptions for two examples in different dimensions with analytic solutions, showing how the analytic solution is located in the unique local minimum of E where non-negative measures exist. In Figure 3.12 we plot the measure corresponding with the $d = 2$ parameter choice found in Figure 3.11 as well as the absolute error compared with the analytic solution.

Exploring uniqueness and existence of solutions

In Figure 3.13 we plot E as a function of the support radius for generic cases in various dimensions d, showing that the behavior observed in the analytic case above also persists away from even integer powers. As in the one-dimensional case, the qualitative behavior of E does not change until a certain void formation threshold is reached, at which point no

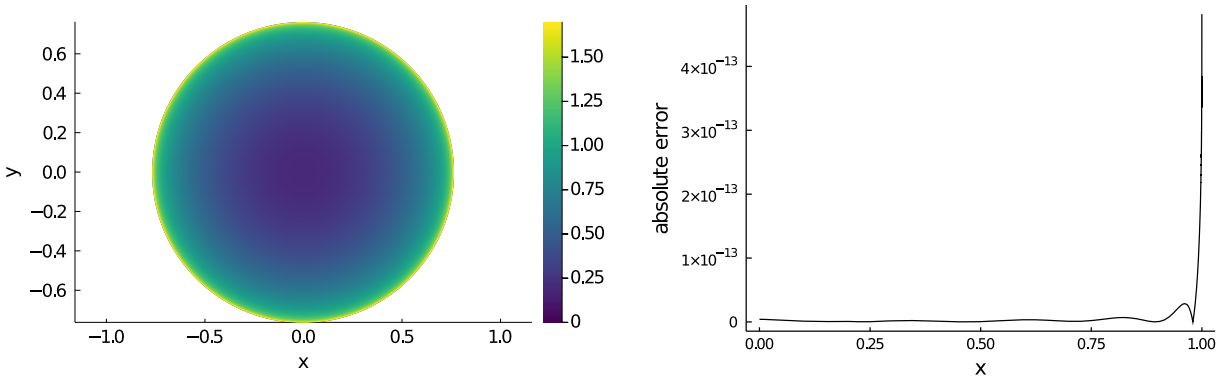

(a) (b)

Figure 3.12: (a) shows the numerically obtained solution for the attractive-repulsive equilibrium measure problem with $\alpha = 4$ and $\beta = \frac{1}{\pi}$ on its disk support (cf. Figure 3.11(a)). (b) shows the error compared to the analytic solution in (3.19) after both measures have been normalized to the unit ball.

non-negative measures on single ball support can be found. This void formation threshold is explored in more detail in a later numerical experiment.

As in the one-dimensional case we may in principle use particle simulations to verify the results of our higher-dimensional methods outside the special cases where analytic solutions exist. In practice this is a difficult task, however, as the number of particles required scaled poorly with dimension and soon exceeds reasonable computing times. In Figure 3.14 we plot the result of a simulation using 1000 particles and compare a rough two-dimensional histogram to the continuous measure obtained by our method for two examples with $d = 2$. While no sensible quantitative comparison can be made without using orders of magnitude more particles (exceeding available computing resources), we nevertheless observe qualitatively compatible measures as one would expect.

Errors, convergence and impact of regularization

As discussed in Section 3.9, two primary errors are to be considered for our method: The error incurred from the approximately banded spectral method and the error incurred from the optimization. In addition to these two sources of error, we also investigate the positive impact on stability due to the Tikhonov regularization.

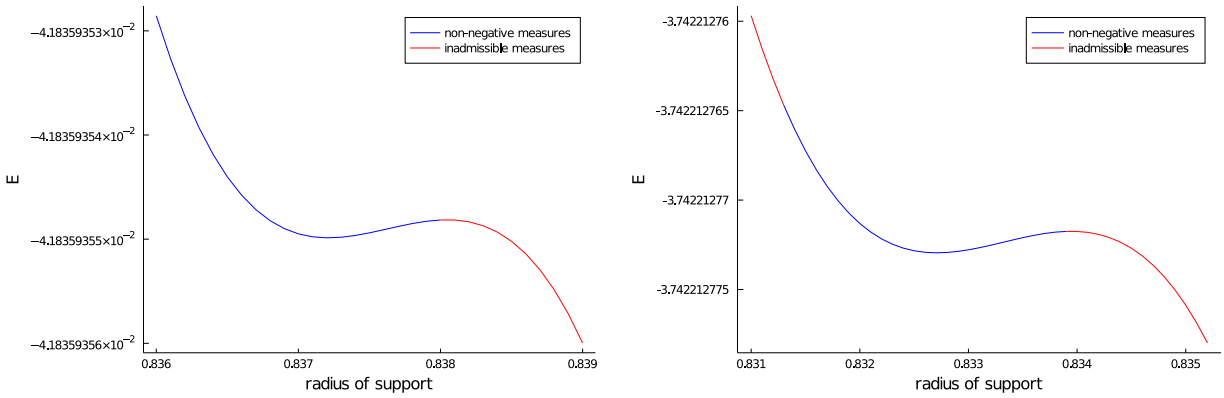

(a) $d = 2$, $\alpha = 1.31$, $\beta = 1.23$ (b) $d = 3$, $\alpha = 1.4$, $\beta = 0.22$

Figure 3.13: E computed from equilibrium measure candidates for the attractive-repulsive equilibrium measure problem with indicated parameters and dimension d in the neighborhood of the only observed local minimum with non-negative measure. No analytic solutions are available for these parameters. Instead, we qualitatively compare the $d = 2$ case to a particle simulation in Figure 3.14.

The output of our optimization step is the radius of support of the equilibrium measure. To explore the impact of errors due to the optimization method we thus explore how using slightly perturbed radii affect the resulting measures. We use the special cases discussed in Equation (3.13) for which analytic solutions are known to plot the error with radius perturbations in Figure 3.15 for the one-dimensional method. Similar plots can be generated for the higher-dimensional method showing the same linear relationship. We observe that perturbations in the radius propagate linearly to errors in the measures after normalization to unit ball support. In a given application this knowledge can be used to fine-tune the convergence criteria of the optimization step which has a support radius candidate as its output. In Figure 3.16(a) we show the convergence behavior of the approximation coefficients for the equilibrium measures obtained with and without using Tikhonov regularization for the $d = 3$ example without known analytic solutions discussed in Figure 3.13(b). In general, we find that while the methods obtained with the Tikhonov regularized method qualitatively agree with the non-regularized method, the non-regularized method is prone to (incorrect) oscillations near the boundary as a result of the numerical instability. We show an example of this behavior in Figure 3.16(b).

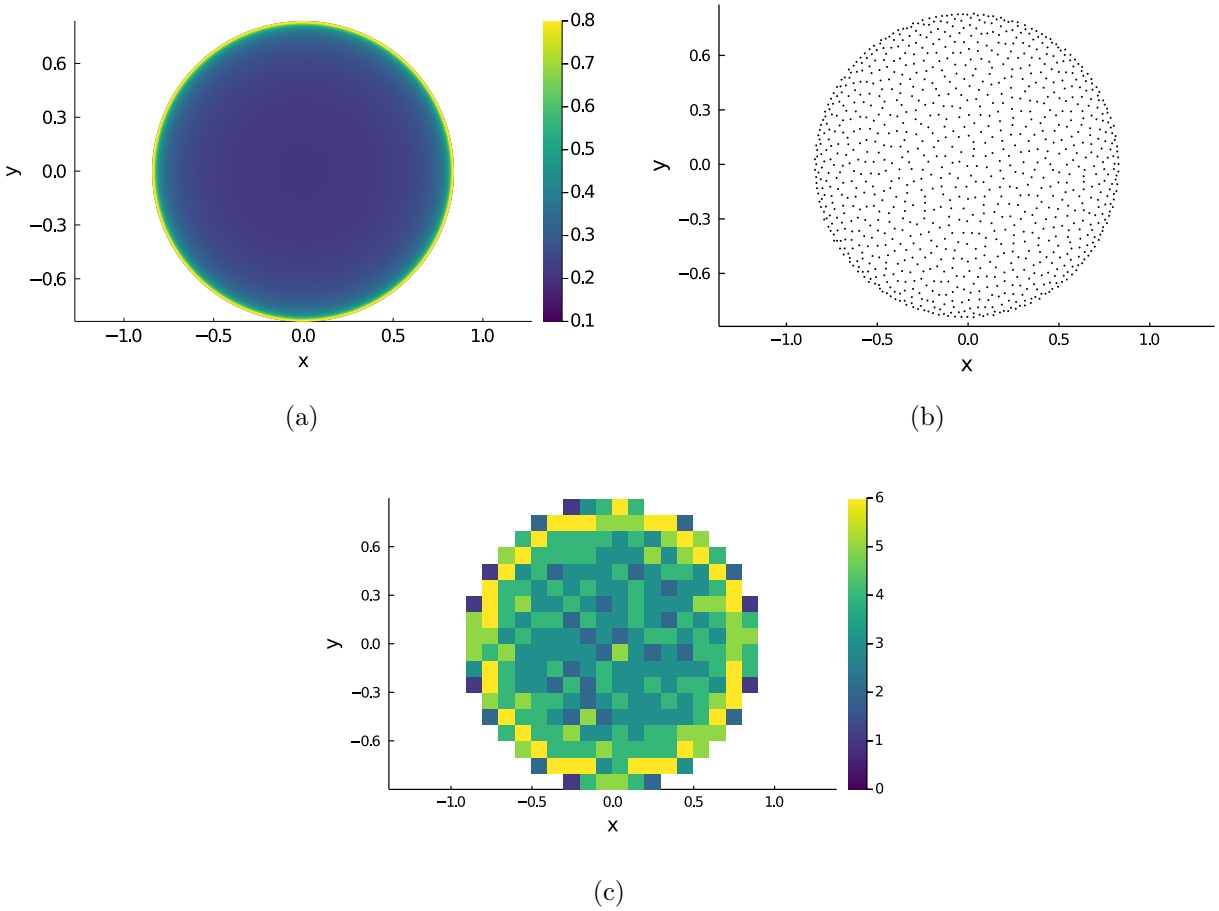

Figure 3.14: (a) shows a the numerically obtained equilibrium measure for the problem in Figure 3.13(a) with $d = 2$, $\alpha = 1.31$, $\beta = 1.23$ on its disk support. (b) shows a particle simulation with 1000 particles for the same problem. (c) shows a two-dimensional histogram generated based on the particle configuration in (b).

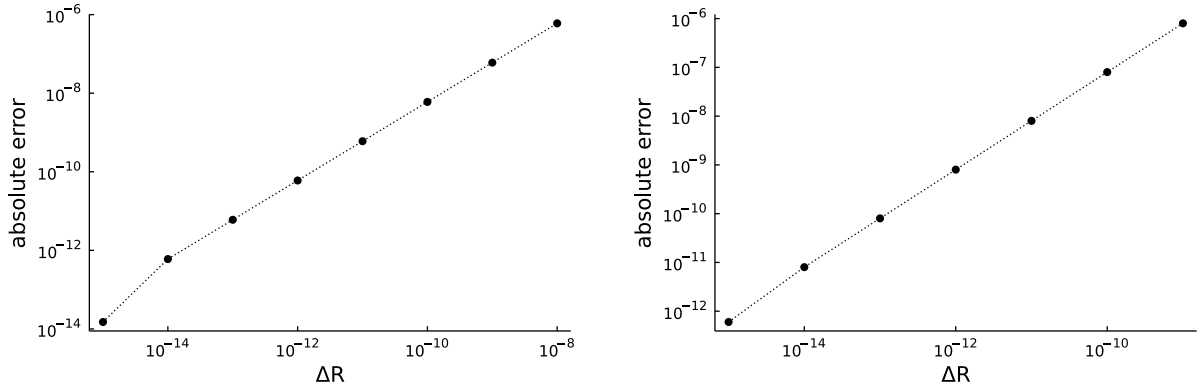

(a) $\beta = 1.1$ (b) $\beta = 1.68$

Figure 3.15: Plot of the absolute error between analytic solution to the problem in (3.13) with indicated β and a numerical solution computed using a radius value perturbed by the values on the x-axis.

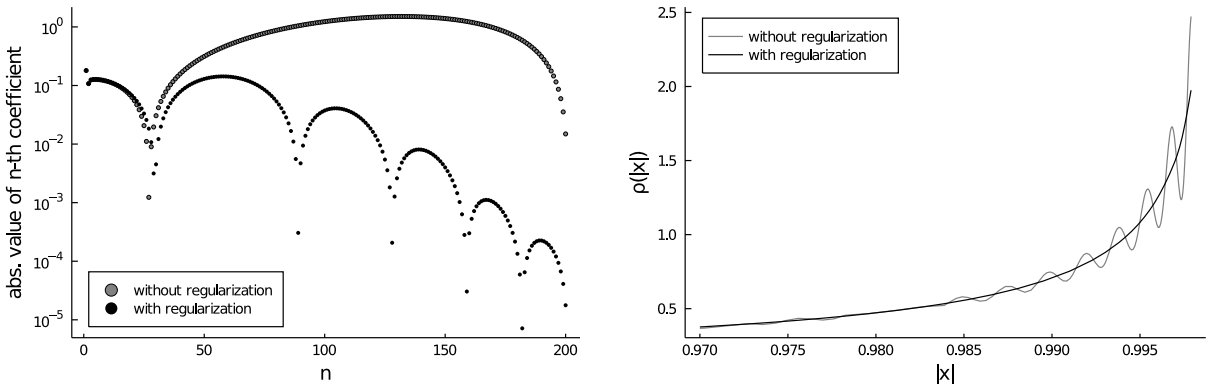

(a) (b)

Figure 3.16: (a) shows the absolute value of the n-th approximation coefficient in the numerical solution obtained for the problem in Figure 3.13(b) with and without Tikhonov regularization on a semi-logarithmic scale. (b) shows how regularization corrects incorrect oscillations near the boundary. Note that the measures plotted in (b) are normalized to the unit ball, such that 1 represents the boundary.

Void formation for high repulsive powers

A primary motivation for the development of this method was the possibility to explore the void formation phenomenon observed in discrete particle simulations in a continuous context. In Figure 3.17 we plot two examples in $d = 2$ computed using 1000 particles in which we can observe the later stages of void formation which include a large void around the origin and for high parameter ranges even an apparent collapse to a ring. Unfortunately, particle simulations converge at extremely slow rates in the initial void formation ranges, making it near impossible to study the range of powers at which the void begins to form. This problem is only further exacerbated by the increased degrees of freedom in higher dimensions, requiring particle numbers well beyond reasonable computing capacity.

Using our method the boundary between compactly supported measures and those with a void can be explored to arbitrary precision, possibly contributing to future analytic understanding of this phenomenon. In one dimension we may study both the pre and post void formation measures using the two interval method described in Section 3.6. For higher dimensions, while we may still explore the void formation boundary, the post void formation measures cannot be directly investigated unless future research finds a way to use similar methods for hyperspherical annuli which is work-in-progress.

In Figure 3.18 we show contour plots of the void formation boundary in dimension $d = 2$ and $d = 3$. Note that the boundaries observed in Figure 3.18 may be made arbitrarily smooth by decreasing the stepsizes at which we probe for void formation.

3.11 Discussion

In this chapter we have introduced, to the best of the knowledge of the author, the first continuous numerical method to solve power law equilibrium measures. The method can be used for the case of one or two intervals of support in one dimension or for arbitrary dimensional problems supported on balls, while scaling favorably with the dimension due to the radial symmetry of the problem. This contrasts with the particle swarm simulation approach

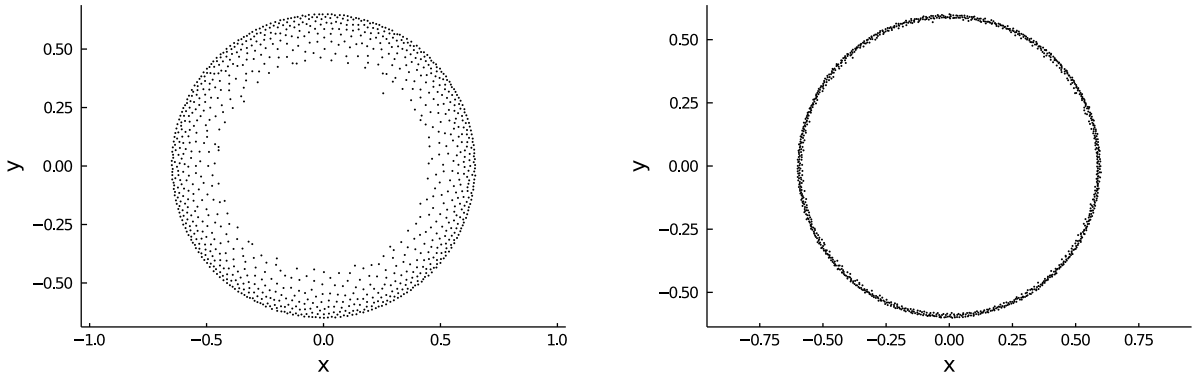

(a) $\alpha = 4.18, \beta = 0.86$ (b) $\alpha = 3.88, \beta = 1.23$

Figure 3.17: Plot of converged particle simulation for the attractive-repulsive equilibrium measure problem for 1000 particles in two dimensions with indicated parameters. In these high (relative to d, cf. Figure 3.18) parameter ranges we observe that in (a) a void begins to form around the origin which as seen in (b) for further increased repulsive powers eventually leads to collapse to a ring.

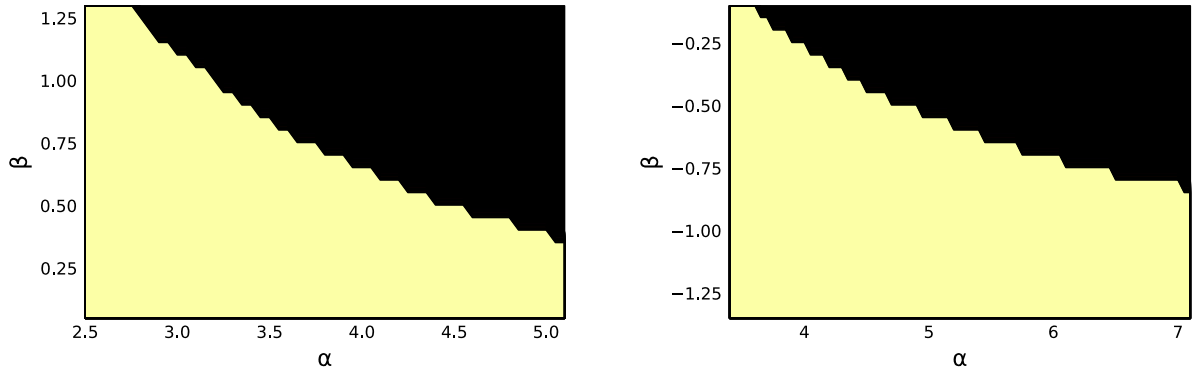

(a) $d = 2$ (b) $d = 3$

Figure 3.18: Contour plots of void formation boundary for $d = 2$ and $d = 3$. Light regions indicate existence of non-negative ball support equilibrium measure while black regions indicate that no such solutions exist. Data underlying contour plots was generated with a stepsize of 0.05 in α and β. The observed qualitative behavior is the same in other dimensions.

to equilibrium measure problems which have so far been the only way to explore equilibrium measures outside the range of analytically known solutions. As these particle simulations scale very poorly with dimension as well as the number of particles and additionally show very poor convergence to the equilibrium near the parameter ranges of interest, our method provides an opportunity to explore previously poorly understood parameter ranges such as the neighborhood of the void formation boundary, and in the original publication in [48] predicted uniqueness properties later proved to be true in [27].

Chapter 4

Conclusion

4.1 Summary of thesis achievements

In this thesis, I have extended the range of problems that banded spectral methods using orthogonal polynomials may be used for to include general kernel linear Volterra integral equations (VIEs) of first and second kind, general kernel nonlinear and integro-differential Volterra equations (VIDEs) and equilibrium measure problems involving the computation of power law kernel integrals (Riesz potentials) in one and higher dimensions.

The introduced method for Volterra integral and integro-differential equations is to the best knowledge of the author the first sparse spectral method for these equations which is not restricted to convolution-type kernels. For the problem of equilibrium measures the introduced methods are unique in that, to the best knowledge of the author, they represent the first numerical analysis contribution to the *continuous* equilibrium measure problem as opposed to the alternative of extraordinarily costly particle swarm simulations and is also the first computational method to explore the continuous void formation behavior, as well as the uniqueness of solutions in certain parameter regions which are out of reach of current analytic methods.

4.2 Outlook and future research

Several interesting questions for future research arise from the results discussed in Chapter 2 and 3.

For Volterra integral equations, we observed reasonable results without any additional work or regularization for problems involving certain kernel singularities which may be rewritten into one type of so-called third kind Volterra equations – it is worth exploring third kind equations further to find or improve the extent of applicability for methods based on multivariate orthogonal polynomials. Many natural applications of Volterra integral and integro-differential equations also involve systems of equations, for which the discussed sparse methods may readily be adapted by linearizing the system followed by an application of Newton's method. Lastly, while we proved convergence for first and second kind Volterra integral equations, similar proofs for Volterra integro-differential equations are expected to hold but so far remain conjecture.

Many open questions regarding equilibrium measures were already addressed in Chapter 3, primarily relating to the void formation phenomenon at high parameter ranges. While the two interval method in one dimension shines some light on the form of the post-void formation measures, similar methods in higher dimension remain out of reach for lack of equally powerful recurrence relationships on annular or hyperspherical shell domain polynomial bases. Beyond the immediate applicability to equilibrium measures, many of the recurrence relationships derived in Chapter 3 may also find use in solving fractional differential equations featuring the Riesz potential or the fractional Laplacian – their potential in this area has yet to be fully explored and is work in progress. Furthermore, while Tikhonov regularization remains the standard approach to improving the stability of first kind problems, it may be worthwhile to investigate the existence of more specialized regularization schemes for this problem type. On the analytic side, the numerical experiments performed using these methods hint at various as of yet unproven uniqueness and existence results and may also help in forming conjectures about the analytic nature of the void formation boundary as a function of the attractive and repulsive powers as well as dimension of the problem. Finally, equilibrium measure problems of interest in applications are not limited to logarithmic and power law kernel type, with some other kernels of interest such as Morse kernels being discussed in e.g. [26, 24]. No numerical methods to work with these types of

kernels in the continuous problem are known as of now.

Bibliography

[1] ApproxFun.jl, October 2021. Julia Package, v0.13.0, accessed: 2021-12-25, github.com/JuliaApproximation/ApproxFun.jl.

[2] ClassicalOrthogonalPolynomials.jl, December 2021. Julia Package, v0.5.1, accessed: 2021-12-25, github.com/JuliaApproximation/ClassicalOrthogonalPolynomials.jl.

[3] ContinuumArrays.jl, November 2021. Julia Package, v0.10.0, accessed: 2021-12-25, github.com/ JuliaApproximation/ContinuumArrays.jl.

[4] FastTransforms, December 2021. C library, v0.5.1, accessed: 2021-12-25, github.com/ MikaelSlevinsky/FastTransforms.

[5] FastTransforms.jl, December 2021. Julia Package, v0.13.2, accessed: 2021-12-25, github.com/JuliaApproximation/FastTransforms.jl.

[6] MultivariateOrthogonalPolynomials.jl, October 2021. Julia Package, v0.2.4, accessed: 2021-12-28, github.com/ JuliaApproximation/MultivariateOrthogonalPolynomials.jl.

[7] QuasiArrays.jl, October 2021. Julia Package, v0.9.0, accessed: 2021-12-25, github.com/ JuliaApproximation/QuasiArrays.jl.

[8] B. Aharmim, E. H. Amal, E. W. Fouzia, and A. Ghanmi. Generalized Zernike polynomials: operational formulae and generating functions. *Integral Transform. Spec. Funct.*, 26(6):395–410, 2015. doi:10.1080/10652469.2015.1012510.

[9] S. S. Allaei, Z. Yang, and H. Brunner. Existence, uniqueness and regularity of solutions to a class of third-kind Volterra integral equations. *J. Integral Equ. Appl.*, 27(3):325–342, 2015. doi:10.1216/JIE-2015-27-3-325.

[10] S. S. Allaei, Z. Yang, and H. Brunner. Collocation methods for third-kind VIEs. *IMA J. Num. Ana.*, 37(3):1104–1124, 2017. doi:10.1093/imanum/drw033.

[11] I. Area, D. K. Dimitrov, and E. Godoy. Recursive computation of generalised Zernike polynomials. *J. Comput. Appl. Math.*, 312:58–64, 2017. doi:10.1016/j.cam.2015.11.017.

[12] K. E. Atkinson and W. Han. *Theoretical Numerical analysis: A Functional Analysis Framework*. Number 39 in Texts in applied mathematics. Springer, Dordrecht ; New York, 3rd ed edition, 2009.

[13] G. Bachman and L. Narici. *Functional Analysis*. Dover Publications, Mineola, N.Y, 2000.

[14] D. Balagué, J.A. Carrillo, T. Laurent, and G. Raoul. Dimensionality of local minimizers of the interaction energy. *Arch. Ration. Mech. An.*, 209(3):1055–1088, 2013.

[15] A. L. Bertozzi, T. Kolokolnikov, H. Sun, D. Uminsky, and J. von Brecht. Ring patterns and their bifurcations in a nonlocal model of biological swarms. *Commun. Math. Sci.*, 13(4):955–985, 2015. doi:10.4310/CMS.2015.v13.n4.a6.

[16] J. Bezanson, A. Edelman, S. Karpinski, and V. B. Shah. Julia: A fresh approach to numerical computing. *SIAM Rev.*, 59(1):65–98, 2017. doi:10.1137/141000671.

[17] A. Böttcher and B. Silbermann. *Introduction to Large Truncated Toeplitz Matrices*. Springer, New York, 1999.

[18] A. Böttcher, B. Silbermann, and A. Karlovich. *Analysis of Toeplitz Operators*. Springer monographs in mathematics. Springer, Berlin, 2. ed edition, 2006.

[19] H. Brunner. On the numerical solution of nonlinear Volterra integro-differential equations. *BIT Numerical Mathematics*, 13(4):381–390, 1973. doi:10.1007/BF01933399.

[20] H. Brunner. *Collocation Methods for Volterra Integral and Related Functional Differential Equations*. Cambridge Monographs on Applied and Computational Mathematics. Cambridge University Press, 2004. doi:10.1017/CBO9780511543234.

[21] H. Brunner. *Volterra Integral Equations: An Introduction to Theory and Applications*. Cambridge Monographs on Applied and Computational Mathematics. Cambridge University Press, 2017. doi:10.1017/9781316162491.

[22] J. A. Cañizo, J. A. Carrillo, and F. S. Patacchini. Existence of compactly supported global minimisers for the interaction energy. *Arch. Ration. Mech. Anal.*, 217(3):1197–1217, 2015. doi:10.1007/s00205-015-0852-3.

[23] J. A. Carrillo, Y-P. Choi, and S. P. Perez. A Review on Attractive–Repulsive Hydrodynamics for Consensus in Collective Behavior. In Nicola Bellomo, Pierre Degond, and Eitan Tadmor, editors, *Active Particles, Volume 1 : Advances in Theory, Models, and Applications*, pages 259–298. Springer International Publishing, Cham, 2017. doi:10.1007/978-3-319-49996-3_7.

[24] J. A. Carrillo, M. R. D'Orsogna, and V. Panferov. Double milling in self-propelled swarms from kinetic theory. *Kinet. Relat. Models*, 2(2):363, 2009. doi:10.3934/krm.2009.2.363.

[25] J. A. Carrillo and Y. Huang. Explicit equilibrium solutions for the aggregation equation with power-law potentials. *Kinet. Relat. Models*, 10(1):171, 2017. doi:10.3934/krm.2017007.

[26] J. A. Carrillo, S. Martin, and V. Panferov. A new interaction potential for swarming models. *Phys. D Nonlinear Phenom.*, 260:112–126, 2013. doi:10.1016/j.physd.2013.02.004.

[27] J. A. Carrillo and R. Shu. From radial symmetry to fractal behavior of aggregation equilibria for repulsive-attractive potentials. *arXiv preprint, arxiv:2107.05079v1*, 2021.

[28] R. Choksi, R. C. Fetecau, and I. Topaloglu. On minimizers of interaction functionals with competing attractive and repulsive potentials. *Annales de l'Institut Henri Poincare (C) Non Linear Analysis*, 32(6):1283–1305, 2015. doi:10.1016/j.anihpc.2014.09.004.

[29] O. Christensen. *An Introduction to Frames and Riesz Bases*. Applied and Numerical Harmonic Analysis. Birkhäuser Boston, Boston, MA, 2003. doi:10.1007/978-0-8176-8224-8.

[30] C. W Clenshaw. A note on the summation of Chebyshev series. *Math. Comput.*, 9(51):118–120, 1955.

[31] P. Deift. *Orthogonal polynomials and random matrices: a Riemann-Hilbert approach*, volume 3. American Mathematical Soc., 1999.

[32] T. A. Driscoll. Automatic spectral collocation for integral, integro-differential, and integrally reformulated differential equations. *J. Comput. Phys.*, 229(17):5980–5998, 2010. doi:10.1016/j.jcp.2010.04.029.

[33] T. A Driscoll, N. Hale, and L. N. Trefethen. *Chebfun Guide*. Pafnuty Publications, 2014. URL: http://www.chebfun.org/docs/guide/.

[34] M. Dubiner. Spectral methods on triangles and other domains. *J. Sci. Comput.*, 6(4):345–390, 1991.

[35] C. F. Dunkl and Y. Xu. *Orthogonal polynomials of several variables*. Number 155 in Encyclopedia of mathematics and its applications. Cambridge University Press, Cambridge, second edition edition, 2014.

[36] B. Dyda, A. Kuznetsov, and M. Kwaśnicki. Fractional Laplace operator and Meijer G-function. *Constr. Approx.*, 45(3):427–448, 2017. doi:10.1007/s00365-016-9336-4.

[37] E. D. Fackerell and R. A. Littler. Polynomials biorthogonal to Appell's polynomials. *Bull. Aust. Math. Soc.*, 11(2):181–195, 1974. doi:10.1017/S0004972700043781.

[38] M. Fasondini, S. Olver, and Y. Xu. Orthogonal polynomials on planar cubic curves. *Found. Comput. Math.*, pages 1–31, 2021.

[39] R. C. Fetecau, Y. Huang, and T. Kolokolnikov. Swarm dynamics and equilibria for a nonlocal aggregation model. *Nonlinearity*, 24(10):2681, 2011.

[40] R. L. Frank. Minimizers for a one-dimensional interaction energy. *Nonlinear Anal.*, 216:112691, 2022.

[41] W. Gautschi. *Orthogonal polynomials: computation and approximation*. Numerical mathematics and scientific computation. Oxford University Press, Oxford; New York, 2004.

[42] J Górski. Méthode des points extrémaux de résolution du problème de dirichlet dans l'espace. In *Annales Polonici Mathematici*, volume 1, pages 418–429. Instytut Matematyczny Polskiej Akademii Nauk, 1955.

[43] J. J. Grobler, L. E. Labuschagne, and M. Möller, editors. *Operator Algebras, Operator Theory and Applications*. Birkhäuser Basel, Basel, 2010. doi:10.1007/978-3-0346-0174-0.

[44] T. S. Gutleb. SparseVolterraExamples.jl, December 2020. Julia Package, v0.1.1, accessed: 2022-01-12, github.com/TSGut/SparseVolterraExamples.jl. doi:10.5281/zenodo.4382253.

[45] T. S. Gutleb. A fast sparse spectral method for nonlinear integro-differential Volterra equations with general kernels. *Adv. Comput. Math.*, 47(3):42, 2021. doi:10.1007/s10444-021-09866-7.

[46] T. S. Gutleb, J. A. Carrillo, and S. Olver. 1D Power Law Equilibrium Measure Transition from Single to Two Interval Support. *figshare*, 2020. 10.6084/m9.figshare.13095821.v3.

[47] T. S. Gutleb, J. A. Carrillo, and S. Olver. Computation of power law equilibrium measures on balls of arbitrary dimension. *arXiv preprint, arXiv: 2109.00843*, 2021.

[48] T. S. Gutleb, J. A. Carrillo, and S. Olver. Computing equilibrium measures with power law kernels. *Math. Comput.*, 91(337):2247–2281, 2022. doi:10.1090/mcom/3740.

[49] T. S. Gutleb and S. Olver. A sparse spectral method for Volterra integral equations using orthogonal polynomials on the triangle. *SIAM J. Numer. Anal.*, 58(3):1993–2018, 2020. doi:10.1137/19M1267441.

[50] M. F. Hagan and D. Chandler. Dynamic pathways for viral capsid assembly. *Biophys. J.*, 91(1):42–54, 2006. doi:10.1529/biophysj.105.076851.

[51] R. Hagen, S. Roch, and B. Silbermann. *C*-Algebras and Numerical Analysis*. Number 236 in Chapman & Hall/CRC Pure and Applied Mathematics. CRC Press, Taylor & Francis Group, New York, 2001.

[52] N. Hale. An ultraspherical spectral method for linear Fredholm and Volterra integro-differential equations of convolution type. *IMA J. Numer. Anal.*, 39(4):1727–1746, 2019. doi:10.1093/imanum/dry042.

[53] N. Hale and A. Townsend. An algorithm for the convolution of Legendre series. *SIAM Journal on Scientific Computing*, 36(3):A1207–A1220, 2014.

[54] M. H. Heydari, M. R. Hooshmandasl, F. Mohammadi, and C. Cattani. Wavelets method for solving systems of nonlinear singular fractional Volterra integro-differential

equations. *Commun. Nonlinear Sci. Numer. Simul.*, 2014. doi:10.1016/j.cnsns.2013.04.026.

[55] Y. Huang. Explicit Barenblatt profiles for fractional porous medium equations. *Bull. Lond. Math. Soc.*, 46(4):857–869, 2014. doi:10.1112/blms/bdu045.

[56] T. Koornwinder. Two-variable analogues of the classical orthogonal polynomials. In *Theory and Application of Special Functions*, pages 435–495. Elsevier, 1975.

[57] M. Kwaśnicki. Ten equivalent definitions of the fractional Laplace operator. *Fract. Calc. Appl. Anal.*, 20(1):7–51, 2017. doi:10.1515/fca-2017-0002.

[58] F Leja. Une méthode élémentaire de résolution du problème de dirichlet dans le plan. *Ann. Soc. Math. Polon*, 23(230-245):1–19, 1950.

[59] U. Lepik. Haar wavelet method for nonlinear integro-differential equations. *Appl. Math. Comput.*, 176, 2006. doi:10.1016/j.amc.2005.09.021.

[60] J. Lindenstrauss and L. Tzafriri. *Classical Banach Spaces*. Classics in mathematics. Springer, Berlin, 1996.

[61] O. Lopes. Uniqueness and radial symmetry of minimizers for a nonlocal variational problem. *Commun. Pure Appl. Anal.*, 18(5):2265, 2019. doi:10.3934/cpaa.2019102.

[62] A. Loureiro and K. Xu. Volterra-type convolution of classical polynomials. *Math. Comput.*, 2019.

[63] V. N. Mahajan. Zernike circle polynomials and optical aberrations of systems with circular pupils. *Appl. Opt.*, 33(34):8121, 1994. doi:10.1364/AO.33.008121.

[64] C. Milici, G. Drăgănescu, and J. T. Machado. *Introduction to Fractional Differential Equations*. Springer, Cham, Switzerland, 2019.

[65] K. S. Miller and B. Ross. *An Introduction to the Fractional Calculus and Fractional Differential Equations*. Wiley, New York, 1993.

[66] J. Molina and R. M. Slevinsky. A rapid and well-conditioned algorithm for the Helmholtz–Hodge decomposition of vector fields on the sphere. *arXiv preprint, arXiv:1809.04555*, 2018.

[67] G. Munschy and P. Pluvinage. Résolution de l'équation de Schrödinger des atomes à deux électrons. II. Méthode rigoureuse. États s symétriques. *J. Phys. Radium*, 18(3):157–160, 1957. doi:10.1051/jphysrad:01957001803015700.

[68] J. Muscat. *Functional Analysis An Introduction to Metric Spaces, Hilbert Spaces, and Banach Algebras*. Springer International Publishing, 2014.

[69] D. R. Myrick. A generalization of the radial polynomials of F. Zernike. *SIAM J. Appl. Math.*, 14(3):476–489, 1966. doi:10.1137/0114042.

[70] M. T. Nair. *Linear Operator Equations: Approximation and Regularization*. World Scientific, Singapore ; Hackensack, NJ, 2009.

[71] B. Neggal, N. Boussetila, and F. Rebbani. Projected Tikhonov regularization method for Fredholm integral equations of the first kind. *J. Inequal. Appl.*, 2016(1):195, 2016. doi:10.1186/s13660-016-1137-6.

[72] R. J. Noll. Zernike polynomials and atmospheric turbulence. *J. Opt. Soc. Am.*, 66(3):207–211, 1976. doi:10.1364/JOSA.66.000207.

[73] F.W.J. Olver, A.B.O. Daalhuis, D.W. Lozier, B.I. Schneider, R.F. Boisvert, C.W. Clark, B.R. Miller, and B. V. Saunders (eds.). NIST Digital Library of Mathematical Functions. Release 1.1.3, 2021. URL: http://dlmf.nist.gov.

[74] S. Olver. Computation of equilibrium measures. *J. Approx. Theory*, 163(9), 2011. doi:10.1016/j.jat.2011.03.010.

[75] S. Olver. Computing the Hilbert transform and its inverse. *Math. Comput.*, 80(275):1745–1767, 2011. doi:10.1090/S0025-5718-2011-02418-X.

[76] S. Olver, R. M. Slevinsky, and A. Townsend. Fast algorithms using orthogonal polynomials. *Acta Numer.*, 29:573–699, 2020. doi:10.1017/S0962492920000045.

[77] S. Olver, A. Townsend, and G. Vasil. A sparse spectral method on triangles. *SIAM J. Sci. Comput.*, 41(6):A3728–A3756, 2019. doi:10.1137/19M1245888.

[78] S. Olver, A. Townsend, and G. M. Vasil. Recurrence relations for a family of orthogonal polynomials on a triangle. In *Spectral and High Order Methods for Partial Differential Equations ICOSAHOM 2018*, pages 79–92. Springer, 2020.

[79] S. Olver and Y. Xu. Orthogonal Structure on a Wedge and on the Boundary of a Square. *Found. Comput. Math.*, 19(3):561–589, 2019. doi:10.1007/s10208-018-9393-0.

[80] S. Olver and Y. Xu. Orthogonal polynomials in and on a quadratic surface of revolution. *Math. Comput.*, 89(326):2847–2865, 2020. doi:10.1090/mcom/3544.

[81] S. Olver and Y. Xu. Orthogonal structure on a quadratic curve. *IMA J. Numer. Anal.*, 41(1):206–246, 2021. doi:10.1093/imanum/draa001.

[82] J. K. Parrish and W. M. Hamner, editors. *Animal Groups in Three Dimensions: How Species Aggregate*. Cambridge University Press, Cambridge, 1997. doi:10.1017/CBO9780511601156.

[83] G. Ia. Popov. Some properties of classical polynomials and their application to contact problems. *J. Appl. Math. Mech.*, 27(5):1255–1271, 1963. doi:10.1016/0021-8928(63)90066-2.

[84] J. Proriol. Sur une famille de polynomes á deux variables orthogonaux dans un triangle. *Comptes rendus hebdomadaires des seances de l academie des sciences*, 245(26):2459–2461, 1957.

[85] A. P. Prudnikov, Yu. A. Brychkov, and O. I. Marichev. *Integrals and Series, Volume 1: Elementary Functions*. Gordon and Breach Science Publishers, 1986.

[86] A. P. Prudnikov, Yu. A. Brychkov, and O. I. Marichev. *Integrals and Series, Volume 2: Special Functions*. Gordon and Breach Science Publishers, 1986.

[87] A. P. Prudnikov, Yu. A. Brychkov, and O. I. Marichev. *Integrals and Series, Volume 3: More Special Functions*. Gordon and Breach Science Publishers, 1990.

[88] J. Prüss. *Evolutionary Integral Equations and Applications*. Modern Birkhäuser classics. Springer, Basel ; New York, 2012.

[89] K. M. Rocha, L. Vabre, F. Harms, N. Chateau, and R. R. Krueger. Effects of Zernike wavefront aberrations on visual acuity measured using electromagnetic adaptive optics technology. *J. Refract. Surg.*, 23(9):953–959, 2007. doi:10.3928/1081-597X-20071101-17.

[90] N. A. Roddier. Atmospheric wavefront simulation using Zernike polynomials. *Opt. Eng.*, 29(10):1174–1180, 1990. doi:10.1117/12.55712.

[91] B. Rubin. One-dimensional representation, inversion, and certain properties of the Riesz potentials of radial functions. *Mathematical notes of the Academy of Sciences of the USSR*, 34(4):751–757, 1983. doi:10.1007/BF01157392.

[92] B. Rubin. A method of characterization and inversion of Bessel and Riesz potentials. *Izv. Vyssh. Uchebn. Zaved. Mat.*, (in Russian), 1986. URL: http://mi.mathnet.ru/eng/ivm7555.

[93] B. Rubin. Fractional integrals and weakly singular integral equations of the first kind in the n-dimensional ball. *Journal d'Analyse Mathématique*, 63(1):55–102, 1994. doi:10.1007/BF03008419.

[94] B. Rubin. *Fractional integrals and potentials*. Number 82 in Pitman monographs and surveys in pure and applied mathematics. Longman, Harlow, Essex, 1996.

[95] E. B Saff and V. Totik. *Logarithmic potentials with external fields*, volume 316. Springer Science & Business Media, 2013.

[96] P. K. Sahu and S. Saha Ray. Legendre wavelets operational method for the numerical solutions of nonlinear Volterra integro-differential equations system. *Appl. Math. Comput.*, 2015. doi:10.1016/j.amc.2015.01.063.

[97] R. M. Slevinsky. Conquering the pre-computation in two-dimensional harmonic polynomial transforms. *arXiv preprint, arXiv:1711.07866*, 2017.

[98] R. M. Slevinsky. Fast and backward stable transforms between spherical harmonic expansions and bivariate fourier series. *Appl. Comput. Harmon. Anal.*, 47(3):585–606, 2019.

[99] B. Snowball and S. Olver. Sparse spectral and -finite element methods for partial differential equations on disk slices and trapeziums. *Stud. Appl. Math.*, 145(1):3–35, 2020. doi:10.1111/sapm.12303.

[100] H. Song, Z. Yang, and H. Brunner. Analysis of collocation methods for nonlinear Volterra integral equations of the third kind. *Calcolo*, 56(1):1–29, 2019. doi:10.1007/s10092-019-0304-9.

[101] L. N. Thibos, R. A. Applegate, J. T. Schwiegerling, R. Webb, and VSIA Standards Taskforce Members. Standards for Reporting the Optical Aberrations of Eyes. In *Vision Science and its Applications*, Santa Fe, New Mexico, 2000. OSA. doi:10.1364/VSIA.2000.SuC1.

[102] A. N. Tikhonov. On the Solution of Ill-posed Problems and the Method of Regularization. In *Doklady Akademii Nauk*, volume 151, pages 501–504. Russian Academy of Sciences, 1963.

[103] A. N. Tikhonov. Regularization of Incorrectly Posed Problems. *Soviet Mathematics Doklady*, 4, 1963.

[104] C. M. Topaz, A. L. Bertozzi, and M. A. Lewis. A nonlocal continuum model for biological aggregation. *Bull. Math. Biol.*, 68(7):1601, 2006. doi:10.1007/s11538-006-9088-6.

[105] A. Torre. Generalized Zernike or disc polynomials: An application in quantum optics. *J. Comput. Appl. Math.*, 222(2):622–644, 2008. doi:10.1016/j.cam.2007.12.009.

[106] L. N. Trefethen. *Approximation Theory and Approximation Practice, Extended Edition*. SIAM, 2019.

[107] T.D. Trogdon and S. Olver. *Riemann-Hilbert Problems, Their Numerical Solution, and the Computation of Nonlinear Special Functions*. Number 146 in Other titles in applied mathematics. SIAM, Society for Industrial and Applied Mathematics, Philadelphia, 2016.

[108] G. Vasil, K. J. Burns, D. Lecoanet, S. Olver, B. P. Brown, and J. S. Oishi. Tensor calculus in polar coordinates using Jacobi polynomials. *J. Comput. Phys.*, 325:53–73, 2016. doi:10.1016/j.jcp.2016.08.013.

[109] V. Volterra. *Sulla inversione degli integrali definiti: nota*. Reale Accademia dei Lincei, 1896.

[110] J. H. von Brecht, D. Uminsky, T. Kolokolnikov, and A. L. Bertozzi. Predicting pattern formation in particle interactions. *Math. Models Methods Appl. Sci.*, 22(suppl. 1):1140002, 31, 2012. doi:10.1142/S0218202511400021.

[111] J. H. Von Brecht, D. Uminsky, T. Kolokolnikov, and A. L. Bertozzi. Predicting pattern formation in particle interactions. *Math. Models Methods Appl. Sci.*, 22, 2012.

[112] D. Wallis, C. J. Solomon, A. T. Kearsley, G. Graham, and N. McBride. Modelling radially symmetric impact craters with Zernike polynomials. *Int. J. Impact Eng.*, 27(4):433–457, 2002. doi:10.1016/S0734-743X(01)00148-8.

[113] A. Wazwaz. *Linear and Nonlinear Integral Equations: Methods and Applications*. Higher Education Press; Springer, Beijing, Heidelberg, New York, 2011.

[114] A. Wazwaz and R. Rach. Two reliable methods for solving the Volterra integral equation with a weakly singular kernel. *J. Comput. Appl. Math.*, 302:71–80, 2016. doi:10.1016/j.cam.2016.02.004.

[115] A. Wünsche. Generalized Zernike or disc polynomials. *J. Comput. Appl. Math.*, 174(1):135–163, 2005. doi:10.1016/j.cam.2004.04.004.

[116] K. Xu and A. Loureiro. Spectral approximation of convolution operators. *SIAM J. Sci. Comput.*, 40(4):A2336–A2355, 2018. doi:10.1137/17M1149249.

[117] F. Zernike. Beugungstheorie des Schneidenverfahrens und seiner verbesserten Form, der Phasenkontrastmethode. *Physica*, 1(7):689–704, 1934. doi:10.1016/S0031-8914(34)80259-5.

[118] F. Zernike and H. Brinkman. Hypersphärische Funktionen und die in sphärische Bereichen orthogonalen Polynome. In *Proc. Akad. Wet. Amsterdam*, volume 38, pages 161–170, 1935.